VOLUME 34 NOVEMBER 1956 NUMBER 11

Canadian Journal of Physics

Published by THE NATIONAL RESEARCH COUNCIL
OTTAWA CANADA

CANADIAN JOURNAL OF PHYSICS

(Formerly Section A, Canadian Journal of Research)

Under the authority of the Chairman of the Committee of the Privy Council on Scientific and Industrial Research, the National Research Council issues THE CANADIAN JOURNAL OF PHYSICS and six other journals devoted to the publication, in English or French, of the results of original scientific research. Matters of general policy concerning these journals are the responsibility of a joint Editorial Board consisting of: members representing the National Research Council of Canada; the Editors of the Journals; and members representing the Royal Society of Canada and four other scientific societies.

Manuscripts for publication should be submitted to Dr. Léo Marion, Editor-in-Chief, Canadian Journal of Physics, National Research Council, Ottawa 2, Canada.
(For instructions on preparation of copy, see **Notes to Contributors** (inside back cover).)

Proof, correspondence concerning proof, and orders for reprints should be sent to the Manager, Editorial Office (Research Journals), Division of Administration, National Research Council, Ottawa 2, Canada.

Subscriptions, renewals, requests for single or back numbers, and all remittances should be sent to Division of Administration, National Research Council, Ottawa 2, Canada. Remittances should be made payable to the Receiver General of Canada, credit National Research Council.

The journals published, frequency of publication, and prices are:

Canadian Journal of Biochemistry and Physiology	Bimonthly	$3.00 a year
Canadian Journal of Botany	Bimonthly	$4.00 a year
Canadian Journal of Chemistry	Monthly	$5.00 a year
Canadian Journal of Microbiology	Bimonthly	$3.00 a year
Canadian Journal of Physics	Monthly	$4.00 a year
Canadian Journal of Technology	Bimonthly	$3.00 a year
Canadian Journal of Zoology	Bimonthly	$3.00 a year

The price of single numbers of all journals is 75 cents.

Canadian Journal of Physics

Issued by THE NATIONAL RESEARCH COUNCIL OF CANADA

VOLUME 34 NOVEMBER 1956 NUMBER 11

THE REFLECTION OF SLOW ELECTRONS FROM TANTALUM AND COPPER[1]

BY J. P. HOBSON

ABSTRACT

Targets of tantalum and copper on tantalum have been bombarded by electrons with energy 0–40 ev., and the ratio of the number of back-scattered to incident electrons measured. Particular emphasis has been placed on the range 0–10 ev. of primary energy where elastic reflection is dominant. The reflection coefficient for tantalum in this range was found to decrease monotonically as the primary energy fell, approaching a value less than 0.05 as the energy approached zero. This result differs from that of Warnecke below 3.7 ev. The reflection coefficient of copper was found to contain maxima and minima below primary energies of 25 ev. in general agreement with the results of Farnsworth.

INTRODUCTION

The scattering of very slow electrons (0–10 ev.) by the surface of a metal has been investigated in several ways.

Nottingham (1936) and Hutson (1955) have measured deviations from a Maxwell–Boltzmann velocity distribution of thermionically emitted electrons from tungsten and have proposed that electrons crossing the surface barrier of tungsten suffer reflection according to the law $r = e^{-E/0.19}$. (E is the kinetic energy in electron volts of the electrons outside the metal, and r is the ratio of the number of electrons reflected from the barrier to the number incident on the barrier and is called the reflection coefficient.)

Work on the periodic deviations from the Schottky effect (Juenker 1955) gives a reflection coefficient $r \approx 0.2$ for the refractory metals in the thermionic range of electron energy.

The reflection coefficient of a metal can also be measured directly by bombardment of a sample by an electron beam. Since the back-scattered electrons from a metal consist of elastically reflected primaries for primary energies below a few volts (Harrower 1956), much of the early work on secondary electron emission gives a measure of the reflection coefficient in the low primary energy range. The secondary emission of tantalum was measured by Warnecke (1934) and that of copper by Farnsworth (1925, 1929), who found distinct maxima in the secondary emission for copper. The more recent results of Gimpel and Richardson (1943) and also of Myers (1952) on copper show no such behavior. The experimental difficulties in these measurements are listed

[1]Manuscript received July 3, 1956.
Contribution from Electron Physics Group, Microwave Section, Division of Radio and Electrical Engineering, National Research Council, Ottawa. Issued as N.R.C. No. 4098.

by Gimpel and Richardson (1943) and seem likely to be responsible for the divergent results.

Theoretical studies by MacColl (1951) on a one-dimensional model of a metal surface yield a reflection coefficient of $r \approx 0.05$ which falls with increasing energy, except when a diffraction band occurs near zero energy when r can approach unity.

The experiment to be described, in which a large target is bombarded by an electron beam, was performed in an attempt to clarify this general situation and as a first step in a more detailed program of experimental study of the interaction of very slow electrons with metals. It is thought that such experiments, if successfully carried out, will give direct data on the electronic band structure of these metals.

Concurrent related experiments by Shelton* and Lange* on single-crystal tantalum were recently reported together with the present work.*

APPARATUS

Fig. 1 shows the tube used, which is similar in principle to one used by Farnsworth and Goerke (1930). The electron gun delivers a space charge limited current from a tungsten hairpin cathode at about 2500° K. The target

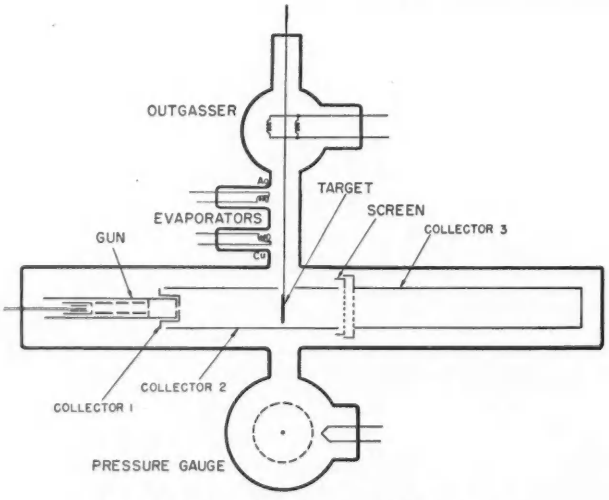

FIG. 1. Schematic of electron reflection tube.

can slide by gravity into a side arm where the operations denoted can be carried out. When the target is withdrawn the primary beam falls on a tungsten screen of 91% transparency and then on a similar screen attached to collector 3. These screens were not used as anticipated and played no essential role in the measurements. Reflected electron currents were normally measured on collectors 1 and 2, connected together. All tube parts were tantalum. A pressure of

*Report on Sixteenth Annual Conference on Physical Electronics, M.I.T., 1956.

10^{-9} mm. Hg was obtained as a lower limit of measured pressure, with 10^{-7} mm. when the outgasser was operating. The primary beam currents striking the target were 10^{-8} to 10^{-9} amp., while the smallest measurable reflected current was 10^{-11} amp. All currents were direct and were measured with a vibrating reed electrometer.* The target was a 1 cm. disk of 0.020 in. tantalum sheet with a 1 mm. hole at the center, which was used to check beam alignment.

The whole tube was sealed off and was rotatable inside a pair of Helmholtz coils which were used to cancel the earth's field or to supply an axial magnetic field up to 5 gauss.

METHOD OF MEASUREMENT

The reflection coefficient measured in this experiment is the ratio of the total current scattered back from the target to that incident on the target. No attempt was made to analyze the energies of the back-scattered component. The geometry (Fig. 2) was designed to provide a quantitative check on the fraction of the primary beam missing the target and being measured erroneously as reflected current.

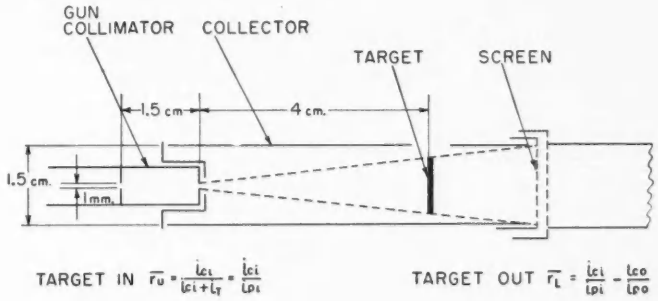

FIG. 2. Experiment geometry.

i_{c_i} and i_{c_o} are the collected or reflected currents with target in and out respectively. Provided the primary beam trajectories are unaltered by the presence or absence of the target they both contain any primary current missing the target, while i_{c_i} contains also the current reflected from the target and i_{c_o} that reflected from the screen and collector 3. i_{p_i} and i_{p_o} are the total currents entering the system with target in and out respectively and are normally equal. i_t is the target current. Provided a negligible fraction of the reflected beam escapes through the entrance hole, $i_{c_i} \geqslant$ true reflected current from the target, while $i_{c_o} \geqslant$ primary current missing the target. Hence the relations given below Fig. 2 may be written, where $\bar{r}_u$ and $\bar{r}_L$ are upper and lower bounds on the reflection coefficient averaged over the thermal distribution. The difference between $\bar{r}_u$ and $\bar{r}_L$ is measured with target out and hence is not a function of the target surface.

*Applied Physics Corporation, Model 30.

An axial magnetic field was applied to hold the primary beam on the target against the diverging effects of space charge repulsion and the overconvergent lens at the exit of the gun.

After the contact potential of the target had been measured, the target and collector potentials were set to give zero field between them, so that primary trajectories were unaltered by removal of the target, and the energy of the incident electrons was controlled by varying the common potential. At a certain value of this common potential, i.e. at a certain incident energy, the gun collimator voltage was varied until a minimum of $\overline{r_u}$ was obtained. This was chosen as the final value of $\overline{r_u}$ representing the best focus of the primary beam on the target.

MEASUREMENT OF CONTACT POTENTIAL OF TARGET

The gun collimator was set at the lowest voltage delivering a convenient current to the measuring system. This gave a thermal beam of lowest energy about 4 ev. Quotations of energy in this paper refer to the lowest energy of the thermal distribution. A retarding field curve with the target out gave the result of Fig. 3(*a*) where the system represents collectors 1, 2, 3, and screen joined. The system voltage was then set at the value marked X, and the target reinserted. The target voltage was varied and the target current and $\overline{r_u}$ were obtained. Typical curves are shown in Fig. 3(*b*).

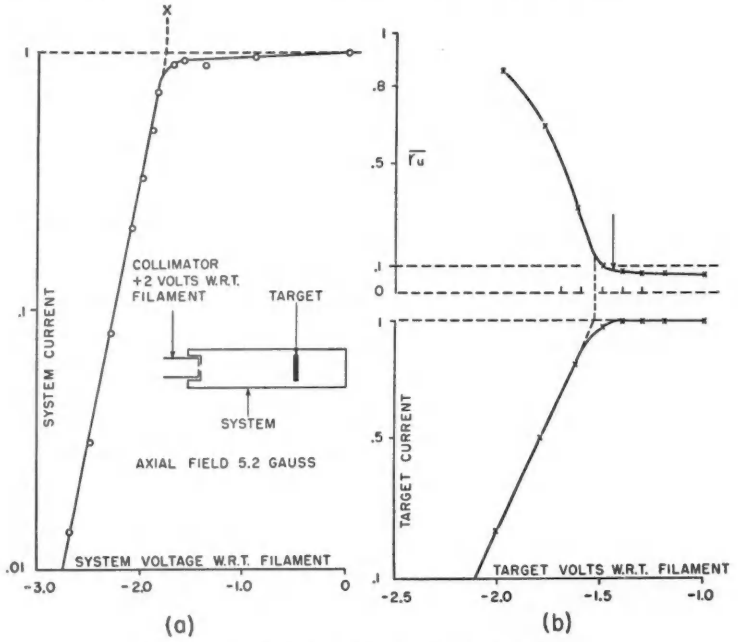

FIG. 3. Measurement of contact potential of target.

$\bar{r}_u$ falls rapidly to a constant value. The onset of this value, which is taken as an upper limit on the zero energy reflection coefficient, is displaced from the break in the retarding field curve of target current by 0.1 to 0.15 ev. The main part of this displacement has been assigned to the patch effect of the target, although some may be due to a divergence from a Maxwellian energy distribution of the incident electrons. The contact potential of the target is set at the onset of the constant reflection region (see arrow in Fig. 3(*b*)).

On occasion a drop in the sum of collector and target currents (measured sequentially) was observed when the target voltage was in the zero energy region, suggesting the possible escape of reflected electrons through the incident hole. This drop was not present when two meters were used simultaneously to measure collected and target currents, nor was it reproducible when one meter was used. The curve of $\bar{\ }$ was however reproducible. It is concluded that no significant fraction of the reflected beam escaped through the incident hole.

However, all doubt on this point can be eliminated if no axial magnetic field is necessary. It is planned to eliminate this field in future reflection tubes.

RESULTS

The main objective of the measurements has been the investigation of the primary energy range 0–10 ev. Measurements have been made however out to 40 ev. in order better to compare results with those of other workers. Above about 5 ev. the reflected current contains an increasing fraction of true secondaries but no attempt was made to separate these from the elastically reflected primaries.

The results obtained for tantalum are shown in Fig. 4. The curve below 6 ev. was examined on several occasions with reproducible results. Measurements on the tantalum target which had not been outgassed for two months give $\bar{r}_u$ 5% higher than shown at 6 ev., with no essential change at 0 ev. The curve for $\bar{r}_L$ was not measured above 6 ev. because $\bar{r}$ presumably approaches $\bar{r}_u$ above this range. Also shown in Fig. 4 is a curve giving the main features of Warnecke's (1934) results on tantalum.

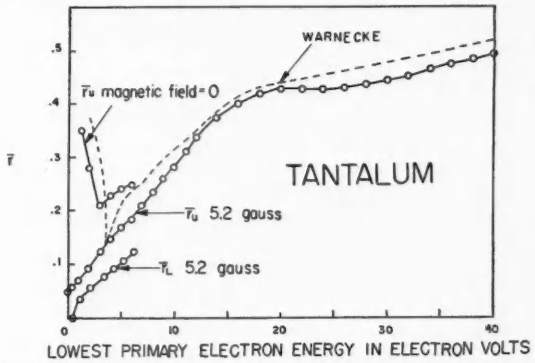

FIG. 4. Reflection coefficient of tantalum. Outgassed 10 min. at 1850°K. before measurement; $\bar{r}_L \leqslant \bar{r} \leqslant \bar{r}_u$.

The results for copper films on tantalum are shown in Fig. 5. No precise measure of film thickness was available but a calculation based on geometry and an estimated copper temperature gave the standard layer as approximately 10 monolayers. The films were homogeneous but crystalline in appearance. $\bar{r}_L$ is omitted from Fig. 5 for clarity. It is displaced from $\bar{r}_u$ by the same amount as in Fig. 4, the displacement being independent of the target surface.

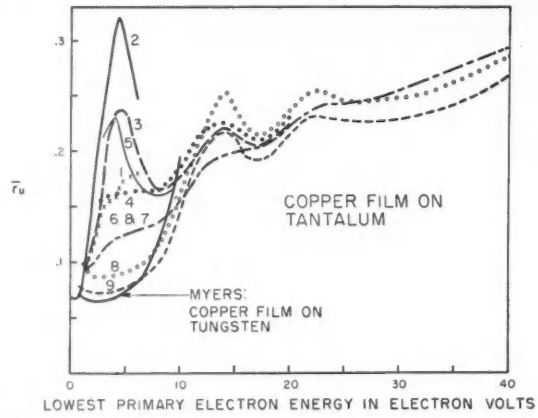

FIG. 5. Reflection coefficient of copper film on tantalum.
1. Clearly visible layer of Cu on Ta outgassed at 1600°K. for 5 min. prior to evaporation.
2. Standard layer about three times as thick as 1 on top of 1 measured immediately.
3. Second measurement of 2—15 min. later.
4. Third measurement of 2—15 hr. later.
5. Layer on top of 4 measured immediately.
6. Second measurement on 5—one week later.
7. Layer on top of 6 measured immediately.
8. All previous layers evaporated. Then layer on Ta outgassed at 1850°K. for 10 min. measured immediately.
9. Layer on top of 8 measured immediately.

No results were obtained for silver films because of failure of the silver evaporator.

DISCUSSION

(1) A reflection coefficient of the form $r = e^{-E/0.19}$ would yield a value of $\bar{r} = 0.5$ at 0 ev. falling to 0.1 at 0.3 ev. for a source at 2500°K. The interpretation placed on the measurements gives no such result for the targets of tantalum and copper on tantalum used. Rather $\bar{r}$ had a value less than 0.1 at 0 ev. for both targets, with a general tendency to remain unchanged or to increase slowly with energy in the thermionic region.

(2) The measurement of $\bar{r}$ for tantalum shows no minimum at 3.7 ev. as reported by Warnecke (1934) but instead shows a monotonic decrease through 3.7 ev. to 0 ev. Between 3.7 ev. and 40 ev. essential agreement with Warnecke is obtained. However, with no axial field our results generally agree with Warnecke in the region below 5 ev. (see Fig. 4). But our measurements with the target out in this region indicate that, with no axial field, a significant

fraction of the primary beam misses the target, and hence that the results with no axial magnetic field are in error. A field of 5 gauss is not expected to influence the reflection process.

(3) All the results on copper exhibit maxima in the same range as those found by Farnsworth (1925, 1929), although no detailed correlation in position with his results is evident. Curves 8 and 9 of Fig. 5 also show agreement with Myers over his range of measurement, although curves 1–7 have a peak of variable height at about 4.5 ev. It is evident that although peak height generally decreases with time after evaporation, the main characteristics of a layer are maintained for long periods. However, the reason for the lack of reproducibility of the peak at 4.5 ev. for standard fresh layers (curves 2, 5, 7, 8, 9) while the peaks at 14 ev. and 22 ev. show essential reproducibility is not clear. It seems possible that we are unable to control the average crystal orientation of the films and that the presence or absence of a peak is correlated with this orientation, since Farnsworth (1929) has correlated the maxima in the reflection coefficient of a single crystal of copper with diffraction beams. If this interpretation is correct, then the correlation between our results with the peak at 4.5 ev. present and a calculated density of states curve for copper from Rudberg and Slater (1936) is of interest (Fig. 6). There appears to be a maximum in the reflection coefficient where there is a minimum in the density of states.

On the other hand the time required for taking a complete curve was comparable with the time for deposition of a monolayer of gas on the target

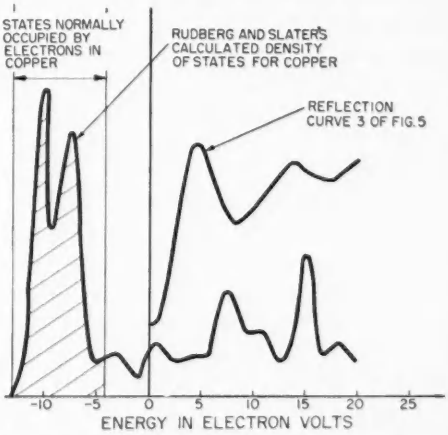

FIG. 6. Comparison of Cu results with calculated density of states for Cu from Rudberg and Slater (1936).

surface and this gas might be responsible for the results obtained. It is planned to check both these possibilities with single-crystal targets at better pressures, in an experiment similar to that of Davission and Germer (1927).

None of our results show agreement with Gimpel and Richardson (1943).

(4) Herring and Nichols (1949) present a summary of the theories of the reflection of slow electrons from metals. In general, they predict a reflection coefficient falling with increasing primary energy in contrast to the trend of our results. However, even the most advanced of these theories (MacColl 1951) is one dimensional but does predict the possibility of diffraction maxima in the reflection coefficient at low energies. More definitive experiments and a general theory for the diffraction of very slow electrons by a metal surface are requ ired to establish the connection between the diffraction of external electrons and the internal electronic band structure of a metal.

ACKNOWLEDGMENTS

The author wishes to express his thanks to P. A. Redhead for suggesting the problem and for continual active assistance in the execution of the program. Thanks are also due to M. G. Armstrong and J. J. Coupal for their part in construction of the apparatus.

REFERENCES

DAVISSON, C. J. and GERMER, L. H. 1927. Phys. Rev. **30**: 705.
FARNSWORTH, H. E. 1925. Phys. Rev. **25**: 42.
——— 1929. Phys. Rev. **34**: 679.
FARNSWORTH, H. E. and GOERKE, V. H. 1930. Phys. Rev. **36**: 1190.
GIMPEL, I. and RICHARDSON, O. 1943. Proc. Roy. Soc. A, **182**: 17.
HARROWER, G. A. 1956. Phys. Rev. In press.
HERRING, C. and NICHOLS, M. H. 1949. Revs. Mod. Phys. **21**: 185.
HUTSON, A. R. 1955. Phys. Rev. **98**: 889.
JUENKER, D. W. 1955. Phys. Rev. **99**: 1155.
MACCOLL, L. A. 1951. Bell System Tech. J. **30**: 888.
MYERS, H. P. 1952. Proc. Roy. Soc. A, **215**: 329.
NOTTINGHAM, W. B. 1936. Phys. Rev. **49**: 78.
RUDBERG, E. and SLATER, J. C. 1936. Phys. Rev. **50**: 150.
WARNECKE, R. 1934. J. phys. radium, **5**: 267.

PRODUCTION AND PROPERTIES OF C^{15} [1]

By R. A. Douglas,[2] B. R. Gasten, and Ambuj Mukerji[3]

ABSTRACT

Uniform thin C^{14} targets on 2500 Å nickel backings were prepared in a discharge tube containing acetylene (enriched to 28.8% C^{14}). A NaI(Tl) crystal was used to measure the yield of C^{15} (2.25±0.05 sec. half life) from $C^{14}(d, p)C^{15}$ from E_d = 1.3 to 3.0 Mev. A 7.5±1.5 sec. activity was also observed, presumably N^{16} produced by $C^{14}(d, \gamma)N^{16}$. The C^{15} gamma-ray spectrum indicates only a 5.3-Mev. transition. A plastic scintillator was used to measure the C^{15} beta spectrum. End-point energies of 9.5±0.3 and 4.5±0.2 Mev. with a branching ratio of 4 to 1 favoring the lower energy component were observed. The results are consistent with a spin and parity assignment of 1/2(+) for the C^{15} ground state.

I. INTRODUCTION

The unusual stability of C^{14} provides an opportunity to study the $T = 3/2$ nuclide C^{15} by means of the $C^{14}(d, p)C^{15}$ reaction. Previous information about C^{15} has come from the measurement of the C^{15} beta decay end point (Hudspeth *et al.* 1950) and from an analysis of the excitation function of $C^{14}(d, p)C^{15}$ (Rickard *et al.* 1954). Q values for this reaction resulting from the above data and analysis are 0.0±0.5 and 0.15±0.15 Mev., respectively. In addition Rickard *et al.* (1954) report a private communication from Spearman giving a Q value of +0.12±0.05 Mev. from direct measurement of the proton energy. A search with an electrostatic analyzer (Douglas *et al.* 1956) failed to detect the protons corresponding to a Q value of 0.0±0.3 Mev. The cross section for such a reaction was found to be less than 0.05 mb./ster. at 135° and E_d = 1.8, 1.9, and 2.1 Mev. However, a group of protons from the $C^{14}(d, p)C^{15}$ reaction was detected corresponding to a Q value of −1.007±0.001 Mev. If this Q value corresponds to the ground state reaction, then a threshold is expected at a deuteron energy of 1.15 Mev. Previous measurements (Rickard *et al.* 1954) had shown appreciable yield down to E_d = 0.6 Mev. The present measurements were undertaken to investigate this apparent discrepancy.*

II. PREPARATION OF C^{14} TARGETS

$BaCO_3$ with a 28.8% C^{14} isotopic abundance was obtained from the A.E.C.[4] It was converted by a standard procedure[5] (Monat *et al.* 1950) to acetylene with an over-all efficiency of 95%. The acetylene was deposited by means of a high frequency discharge in the apparatus shown in Fig. 1. Target backings

[1]Manuscript received May 23, 1956.

Contribution from the Department of Physics, University of Wisconsin, Madison, Wisconsin. Work supported in part by the U.S. Atomic Energy Commission and by the Graduate School from funds supplied by the Wisconsin Alumni Research Foundation.

[2]Now at State University of Iowa, Iowa City, Iowa.

[3]On leave from Tata Institute of Fundamental Research, Bombay.

[4]U.S. Atomic Energy Commission, Oak Ridge, Tenn.

[5]The authors are indebted to Dr. C. Heidelberger and Dr. K. Maller of the McArdle Memorial Institute for their assistance in suggesting this procedure and the use of their facilities in carrying it out.

*Note added in proof.—Professor S. K. Allison (private communication) reports a $C^{14}(d, p)C^{15}$ Q value of -1.06 ± 0.05 Mev. based on measurements by his group of the $Be^9(Li^7, p)C^{15}$ reaction Q value.

were copper-backed 2500 Å nickel foils[6] (Bashkin and Goldhaber 1951) spot-welded to 5-mil nickel washers and supported on the ends of the nickel electrodes by flat springs. Mycalex pieces which covered the sharp corners directed the discharge to the smooth central region of the foil where a uniform deposit would form. The acetylene pressure used was approximately 0.6 cm. of mercury. Power was supplied by a Tesla coil for two minutes, producing two

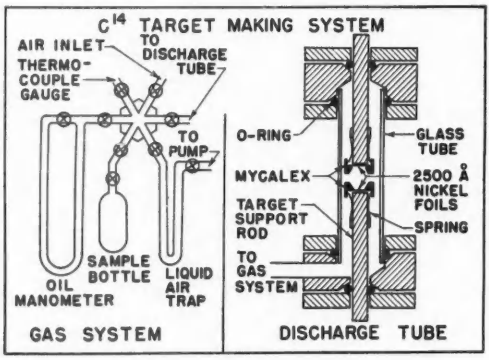

FIG. 1. Apparatus for making C^{14} targets.

targets of 25 kev. thickness to 1 Mev. deuterons. Following the discharge the copper backing was removed by means of a solution of 100 gm./liter of trichloroacetic acid and 100 ml./liter of ammonium hydroxide. The solution was handled with a dropper rather than the target being immersed, to prevent contamination or deterioration of the target.

An indication that the most important deposition process in the discharge is a polymerization of the acetylene is gained from the following evidence. The pressure in the system decreases to a low value during the discharge, indicating that little free hydrogen is produced. The deposit has a brownish color, but turns black after a few minutes of beam bombardment. Possibly the hydrogen is then driven off leaving elemental carbon.

III. APPARATUS

Figure 2 shows the target arrangement. A $1\frac{3}{4}$ in. diameter by 2 in. NaI(Tl) crystal was used for gamma detection and a $1\frac{1}{2}$ in. diameter by 2 in. plastic scintillator for beta detection. DuMont 6292 or RCA 5819 photomultipliers with linear, non-overloading amplifiers and scalers were used. Pulse height distributions were analyzed with a single channel analyzer.

Duration of irradiations was controlled by a "leaky" integrator (Snowdon 1950) in which the condenser was paralleled by a resistor so that the time constant matched the decay time of the radioactivity being studied. When the charge on the condenser reached a predetermined value, a solenoid shutter was activated which stopped the beam at a point 10 ft. from the target.

[6]Obtained from Chromium Corp. of America, Waterbury 90, Conn.

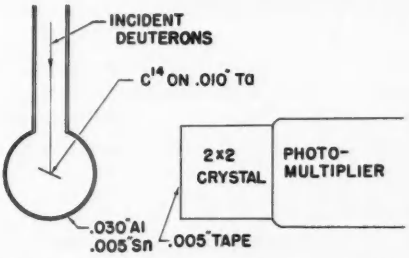

FIG. 2. Target mounting for beta and gamma ray counting. The target, consisting of C^{14} deposited on 2500 Å nickel, was attached to the 0.010 in. tantalum beam stop. Absorbers were placed in front of the crystal to discriminate between beta and gamma rays.

A magnetic oscillograph (Brush Development Co., Model BL-212) was used on the cascade output of the scalers to record the decay of induced activities after irradiation of the C^{14} targets. The target and detector crystal were placed in a lead house with a 2 in. wall. Slits and the shutter were shielded from the crystal by additional lead and water-filled cans.

IV. PROCEDURE

(*a*) *Yield Curves*

The following schedule was followed in obtaining the C^{15} yield curve.

1. The "start" button on the integrator was pushed, causing the solenoid to remove the shutter from the beam path and starting the irradiation.

2. When the charge on the leaky integrator condenser had reached a predetermined value, the shutter was automatically interposed. The size of the condenser was chosen so that the irradiation time was approximately two seconds.

3. A delay of one second was used to allow the 25 millisec. B^{12} activity (from $C^{14}(d, \alpha)B^{12}$) to decay.

4. Scalers were turned on for a period of three seconds.

5. A waiting period of 13 sec. was introduced to allow longer period activities to decay (e.g., 7.4 sec. N^{16}, see later discussion).

6. The above cycle was repeated until the desired total number of counts was obtained.

At certain energies the irradiation time was governed by the integrator, but the scalers counted continuously and fed into the Brush recorder. In this way data concerning longer period activities (e.g., 7.4 sec. N^{16}) were obtained. These longer period activities were also used to correct the observed yield in order to obtain the C^{15} component (2.25 sec.).

Since the X-ray background from the electrostatic generator made it difficult to follow the decays to low counting rates, it was desirable to eliminate the generator voltage while the decay was being recorded. If the spray voltage was simply decreased to zero, the generator voltage dropped slowly and hence gave a decaying background with a half life of a few seconds which was even

more undesirable. However, if the spray voltage was quickly increased until a spark was produced and then decreased to zero, the background was reduced to a very small value in a fraction of a second, and an accurate decay of possible longer period activities in the target could be observed.

For the decay curves a NaI(Tl) crystal was used with discriminator bias set to count only pulses corresponding to an energy loss in the crystal greater than 2.5 Mev.

(*b*) *Gamma Spectrum*

The C^{15} gamma spectrum was obtained with a NaI(Tl) crystal. A 1.27 cm. thick aluminum absorber was used to stop the betas. The procedure was the same as that described above except that the counting period was six seconds instead of three seconds. Because the termination of the run was governed by the "leaky" integrator it was difficult to coordinate a generator spark with the end of the irradiation. Hencé the generator was not sparked for these runs and the background was large, especially at lower pulse heights. It was measured by taking runs in which there was no irradiation but the scalers counted for a timed interval. As these were interposed with runs involving irradiations, any activity of longer half life than a few minutes would also be subtracted out with the generator background.

The NaI (Tl) scintillation spectrometer was calibrated by means of the 2.615 Mev. (Hollander *et al.* 1953) gamma ray from ThC″. It was produced by a source consisting of RdTh and its radioactive daughters. Other radiations from this source are low energy gamma and beta rays which were removed by absorption.

The linearity of the amplifier response was checked with a calibrated pulser, and corrections made both to the pulse height and to the channel width for non-linearities present. No corrections were necessary for output pulses less than 55 volts.

(*c*) *Beta Spectrum*

The beta spectrum was obtained with the plastic scintillator. A 2.5 cm. lucite absorber was used to measure the gamma-ray background. The correction for gamma-ray absorption in the lucite was found to be very small and so was neglected. The schedule of irradiations, etc., was the same as for the gamma-ray spectrum measurement.

For the plastic scintillator, pulse height calibration was accomplished with the RdTh source, taking the Compton edge as 2.36 Mev. Also the beta spectrum from Pr^{144} was observed under two sets of experimental conditions. The first set duplicated the conditions in which the C^{15} beta spectrum was obtained. The second set replaced the 0.010 in. Ta source backing with very thin rubber hydrochloride and eliminated the target chamber. The Pr^{144} end-point energy obtained from the latter experiment using the RdTh calibration was 3.05 ± 0.10 Mev. in good agreement with the published value, 2.98 ± 0.02 Mev. (Emmerich *et al.* 1954). The results of the Pr^{144} work permitted an experimental evaluation of absorption and back scattering for the C^{15} beta spectrum.

V. RESULTS AND ANALYSIS

(*a*) *Identification of 2.25 Sec. Activity*

The following tests were made to establish the reaction which produced the 2.25 sec. activity (Fig. 3). C^{12} targets were made in the same manner as the C^{14} targets, both starting from $BaCO_3$. Since only the C^{14} targets showed this 2.25 sec. activity it was concluded that neither the C^{12} nor contaminants on

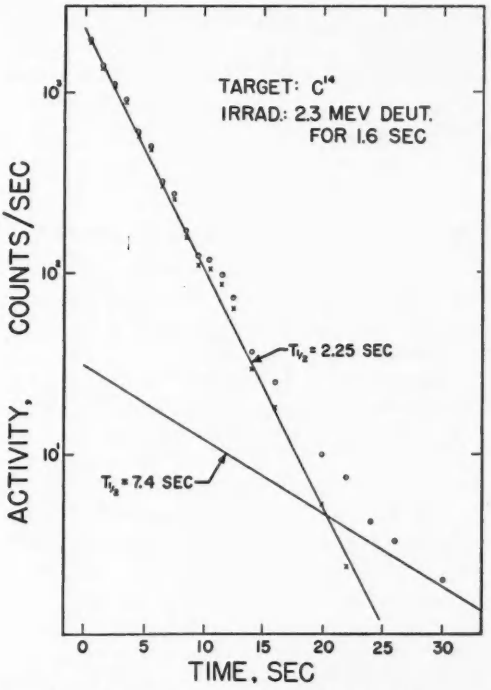

FIG. 3. Decay following the irradiation of C^{14} with 2.3-Mev. deuterons. Activities of 2.25 and 7.4 sec. are observed.

the target were responsible for the activity. However, C^{14} produces much higher energy neutrons by the (d, n) process than C^{12}, so the activity could be fast-neutron induced. To eliminate this possibility lithium and nitrogen targets, both of which produce high energy neutrons, were irradiated. No 2.25 sec. activity was observed in either bombardment. From a knowledge of the half lives of nuclides in this region it was concluded that the activity must be that of C^{15}.

(*b*) *Identification of the 7.5 Sec. Activity*

The identification of the 7.5 ± 1.5 sec. activity shown in Fig. 4 is not quite as definite as that of the 2.25 sec. component. However, an examination of

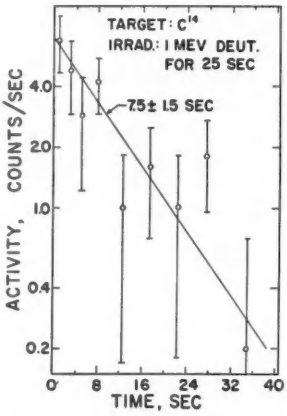

FIG. 4. Decay following the irradiation of C^{14} with 1.0-Mev. deuterons. Only a weak 7.5-sec. activity is observed.

the half lives of nuclides shows that this activity is almost certainly N^{16}. It could be produced by the following reactions: $C^{14}(d, \gamma)N^{16}$, $O^{18}(d, \alpha)N^{16}$, $N^{15}(d, p)N^{16}$, and $O^{16}(n, p)N^{16}$.

The following experiment sets a limit on the relative contributions of the above reactions to the observed yield. The relative amount of oxygen on a C^{14} and N^{14} target is known from surveys with the spherical electrostatic analyzer (Douglas *et al.* 1956) observing the yield from the elastic scattering of protons and deuterons. The decay following irradiation of the N^{14} target at 2 Mev., without sparking the electrostatic generator, showed no detectable 7.4 sec. component. By placing an upper limit on the magnitude of this component, it can be concluded that less than half of the 7.4 sec. activity observed with the C^{14} target was produced by the $O^{18}(d, \alpha)N^{16}$ and $O^{16}(n, p)N^{16}$ reactions. The contribution of the $N^{15}(d, p)N^{16}$ reaction must be extremely small since the activity was not observed for the nitrogen target.

Total cross sections (good to perhaps a factor of two) may be calculated from the data. At a bombarding energy of 2 Mev. the $C^{14}(d, p)C^{15}$ cross section is 0.03 barn.[7] If all the 7.4 sec. activity were ascribed to the $C^{14}(d, \gamma)N^{16}$ reaction the required (d, γ) cross section would be 0.0006 barn. If all of this activity were ascribed to $O^{18}(d, \alpha)N^{16}$ the required (d, α) cross section would be 2 barns. However, the lack of 7.4 sec. activity following the deuteron bombardment of the nitrogen target (which contained approximately 10% oxygen) limits the $O^{18}(d, \alpha)N^{16}$ cross section to 1 barn. This upper limit is to be com-

[7]This cross section is computed from:

(1) the number of C^{14} atoms per cm.^{2} from data on weighings before and after target deposition (1.7×10^{18}),

(2) the number of C^{15} atoms produced per second by a deuteron beam of known intensity. The number of C^{15} disintegrations per second is found by integrating under the curve of the beta spectrum, assuming the beta detection efficiency to be 100%. From these data, the known irradiation time, and the counter geometry (0.23 steradians) it was found that a beam current of 0.17 microamperes of deuterons produced 5.5×10^5 C^{15} atoms per sec.

pared with typical (d, α) cross sections of a few tenths of a barn (for example, $C^{13}(d, \alpha)B^{11}$, $\sigma = 0.15$ barn (Marion and Weber 1956) at $E_d = 2.2$ Mev.). No deuteron radiating capture cross sections have been previously reported (Allan and Sarma 1955). However, the $C^{14}(d, \gamma)N^{16}$ cross section appears to be of the same order of magnitude as that observed for (p, γ) cross sections (Cohen 1955).

(*c*) *C^{15} Yield Curves*

A yield of C^{15} as a function of deuteron energy is shown in Fig. 5. The broken curve represents the results of the University of Texas (Rickard *et al.* 1954). The two curves are normalized at 1.8 Mev. Decays taken with the Brush

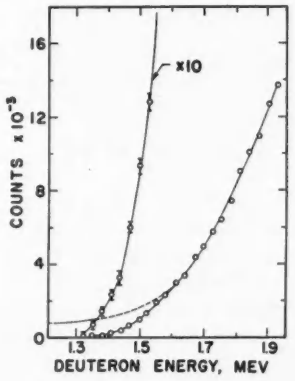

FIG. 5. Yield of C^{15} as a function of deuteron bombarding energy for the $C^{14}(d, p)C^{15}$ reaction. Indicated experimental points are the results of the present experiment. University of Texas data (Rickard *et al.* 1954) are represented by the broken curve which is normalized to our data at $E_d = 1.8$ Mev.

recorder at 2.3 and 1.0 Mev. are given in Figs. 3 and 4, respectively. These graphs show the presence of a weak 7.5 sec. component in both irradiations but the 2.25 sec. activity is present only in the higher energy irradiation. The absence of the C^{15} activity at $E_d = 1.0$ Mev. is in disagreement with the published work of Rickard *et al.* (1954). Bostrom *et al.* (1956) now think that the activity reported by Rickard for $E_d < 1.3$ Mev. was the 7.5 sec. N^{16} activity produced by the deuteron bombardment of O^{18}. [Also see *Note added in proof*.]

Fig. 6 shows the C^{15} yield curve up to a deuteron energy of 3 Mev. The dot dash curve represents the results of Rickard *et al.* (1954) and the crosses the results of Hudspeth *et al.* (1950). Their data are normalized to the present results at 1.8 Mev. The smooth broken curve is assumed to represent the nonresonant contribution to our cross sections. Subtraction of this from the observed curve gives the resonant contributions which are shown at the bottom of the graph. They indicate resonances at 2.0, 2.45, and 2.7 Mev. bombarding energies with total widths (in the center of mass system) of 270, 190, and 165 kev., respectively. This would correspond to resonances at 12.2, 12.6, and

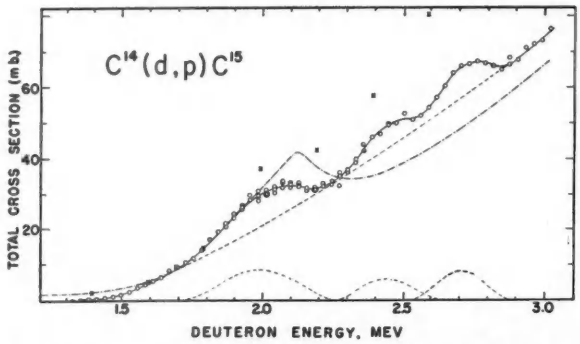

FIG. 6. Total cross section for the reaction $C^{14}(d, p)C^{15}$ as a function of deuteron bombarding energy. Circles are the present data; the crosses are the results of Hudspeth *et al.* (1950), and the dot dash curve the results of Rickard *et al.* (1954). The upper dashed curve represents the assumed non-resonant contribution to the cross section. The lower dashed curves indicate the resonant contributions obtained by subtraction of the non-resonant yield from the observed yield.

12.8 Mev. excitation in N^{16}, assuming the N^{16} mass defect to be 10.40 Mev. (Wapstra 1955).

An attempt was made to analyze the non-resonant portion of the C^{15} yield curve near threshold in order to obtain some information on the spin and parity of C^{15}. Predictions of 1/2(+) and 5/2(+) have been made on the basis of the shell model (Mayer 1950). The most important difference between these alternatives is that the 1/2(+) prediction includes the contribution from *s*-wave in and *s*-wave out, while the 5/2(+) does not. The energy dependence of the lower *l*-value combinations was computed using the explicit energy dependence and coulomb penetrabilities (Sharp *et al.* 1955) according to the formula

$$\sigma_{ll'} = B(E_p/E_d)^{\frac{1}{2}}(1/A_l^2)(1/A_{l'}^2),$$

where: $\sigma_{ll'}$ is the contribution to the cross section from *l*-wave in and *l'*-wave out.

B includes all constants, statistical factors, and reduced widths. It is assumed to be a constant.

E_p, E_d are proton and deuteron energies in center of mass coordinates.

$A_l^2 = F_l^2 + G_l^2$, where F_l and G_l refer to the regular and irregular coulomb functions. The l and l' refer to the incident deuteron and emitted proton angular momenta respectively.

The results of these calculations are shown in Fig. 7, where the energy dependence of the ratio of calculated cross section component to yield is shown. The $l = 0$, $l' = 0$ assumption comes closest to fitting the experimental yield function. Inclusion of higher *l*-values makes the fit worse. However, since this is a (d, p) reaction, it is expected that the stripping mechanism would contribute appreciably to the cross section. By extracting the factors with the strongest energy dependence from the Huby (1953) formula for stripping, the following approximation is obtained:

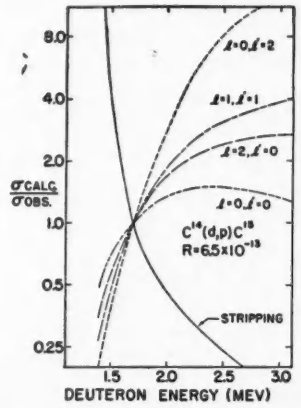

FIG. 7. Analysis of energy dependence of the C^{15} yield. The curve labelled stripping refers to the stripping mechanism in nuclear reactions. Curves labelled by l and l' refer to the compound nucleus mechanism with l-wave in and l'-wave out.

$$\sigma = C(E_d/E_p)^{\frac{1}{2}}$$

where: C is assumed to be independent of energy,

E_d, E_p are center of mass energies of the deuteron and proton.

The ratio of this cross section to the experimental yield is also plotted in Fig. 7. Hence by assuming the right admixture of stripping and compound nucleus formation it is certainly possible to fit the yield curve with various incoming and outgoing l's. Thus no conclusions concerning C^{15} spin can be made from the yield data.

(d) N^{16} Yield Curve

The N^{16} yield as a function of deuteron energy is shown in Fig. 8. The large uncertainties reflect the difficulty of subtracting this weak activity from the intense C^{15} activity.

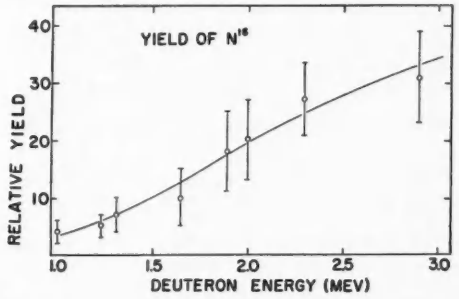

FIG. 8. Yield of N^{16} as a function of deuteron bombarding energy. At $E_d = 2$ Mev. the cross section is 0.6 mb. if the N^{16} is produced principally by the $C^{14}(d, \gamma)N^{16}$ reaction.

(*e*) *Beta Spectrum*

The beta spectrum of Pr^{144} has been observed (Emmerich *et al.* 1954) to produce a Kurie plot which is nearly linear above 0.4 Mev. Fig. 9 shows our

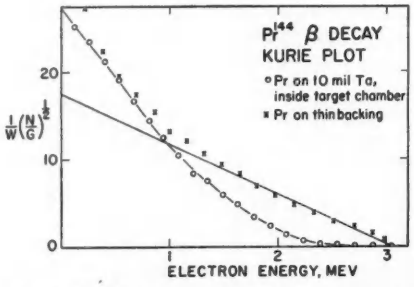

FIG. 9. Kurie plot of the Pr^{144} beta spectrum. The circles were taken under conditions duplicating the C^{15} target arrangement (Fig. 2). The crosses were taken with the Pr^{144} mounted on a thin rubber hydrochloride backing and no target chamber present.

data presented as a Kurie plot, calculated using published values of the Fermi function (Siegbahn 1955). When a thin backing is used fair linearity is achieved down to 1.5 Mev. The departure from linearity at the lower energies on the part of the Kurie plot for Pr^{144} on thin backing may result from the following processes:

1. Betas would be back-scattered (Bothe 1949) from the face of the scintillator.

2. As there was no collimator between the source and the scintillator some particles could pass through the corner of the crystal.

3. Betas could be scattered by the lead house before entering the crystal.

The additional distortion of the Kurie plot corresponding to the Pr^{144} source in the C^{15} experimental arrangement is due to the effect of the tantalum back-scattering and the absorption of the target chamber. The following procedure was used to obtain a corrected Kurie plot from data taken in the C^{15} target arrangement.

(i) The observed end-point energy is corrected for absorption.

(ii) A second point on the straight line Kurie plot is obtained by taking a value of the ordinate at zero energy equal to 0.65 of the ordinate of the uncorrected plot. (The empirical value of 0.65 comes from the Pr^{144} data of Fig. 9.)

Figs. 10 and 11 show the analysis of the C^{15} beta spectrum using the following steps:

1. The energy scale of the Pr^{144} Kurie plot from the C^{15} target arrangement was multiplied by the factor 3.6 so as to match the end points.

2. The ordinates of the above Pr^{144} Kurie plot were normalized to fit the higher energy portion of the C^{15} curve.

3. The straight line Kurie plot was drawn using the procedure outlined above (i.e. steps (i) and (ii)).

4. The higher energy component of the C^{15} beta decay was subtracted out under the assumption that the expanded and normalized Kurie plot of Pr^{144}

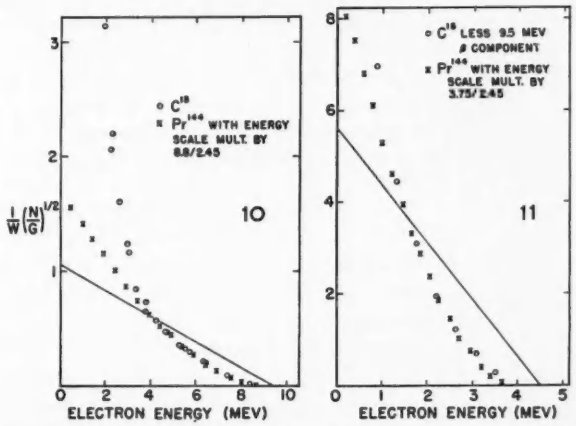

FIG. 10. Analysis of C^{15} beta spectrum I. The circles give an uncorrected Kurie plot of the C^{15} spectrum. The crosses are an uncorrected but normalized Kurie plot of the Pr^{144} in which the target conditions duplicated the C^{15} conditions but whose energy scale has been expanded to make the end points correspond. The straight line is the corrected Kurie plot for the higher energy component of the C^{15} betas.

FIG. 11. Analysis of C^{15} beta spectrum II. The circles give the appropriate difference between the circles and crosses of Fig. 10. The crosses are an uncorrected but normalized Kurie plot of the Pr^{144} in which the target conditions duplicated the C^{15} conditions, but whose energy scale has been expanded to match the end point of the lower energy component. The straight line is the corrected Kurie plot for the lower energy component of the C^{15} beta spectrum.

(crosses in Fig. 10) should have the same shape as the high energy C^{15} component.

5. The results of Fig. 4 are plotted (circles in Fig. 11), and the above procedure repeated.

6. The straight line Kurie plots of Figs. 10 and 11 are converted to the spectra of Fig. 12 where the branching ratio is determined from relative areas.

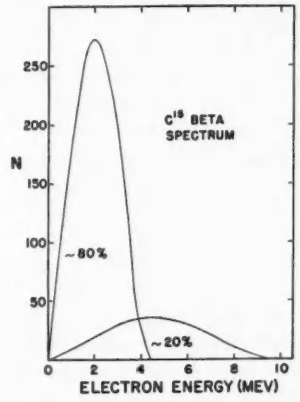

FIG. 12. C^{15} beta spectrum. The spectra were obtained from the assumed straight line Kurie plots of Figs. 10 and 11. The branching ratio is given by the relative areas under the curves.

The fit of the residual C^{15} curve (circles, Fig. 11) to the expanded and normalized Pr^{144} curve (crosses, Fig. 11) after the first subtraction was remarkably close. Hence one infers that there are only two important components to the beta spectrum so the subtraction procedure was not carried further. The validity of the method rests on the assumption that the scattering and energy loss of the electrons are independent of the energy over the range being considered. The reasonableness of this assumption is illustrated by the approximate linearity of the range–energy curve in this energy region (Katz and Penfold 1952).

This analysis gives end-point energies of 9.5±0.3 Mev. and 4.5±0.2 Mev. From the areas under the spectral plots of Fig. 12 a 4 to 1 intensity ratio favoring the 4.5-Mev. component is obtained. Still lower energy components are not observed and it is difficult to set upper limits on their possible intensities because of the nature of the beta-spectrum analysis. The resolution of the experiment is not sufficient to differentiate between beta transitions to the doublet levels of N^{15} at 5.276 and 5.305 Mev. (Malm and Buechner 1950).

(f) Gamma-ray Spectrum

Figure 13 shows the gamma-ray spectrum obtained from the C^{15} decay. The pulse height has been normalized to give the energy loss in Mev. of the electrons produced by a gamma ray. This is a typical spectrum corresponding

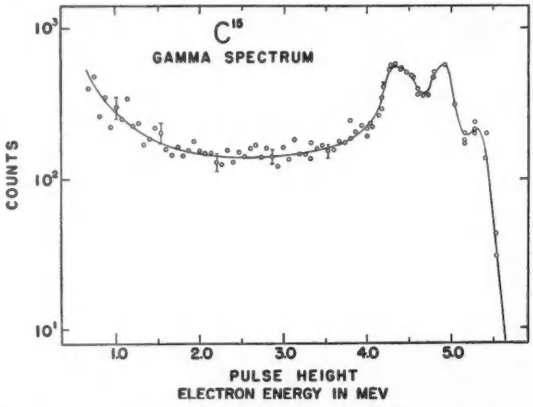

FIG. 13. C^{15} gamma-ray spectrum. The abscissa has been normalized to give the energy loss in Mev. of the electrons produced by a gamma ray. A $1\frac{3}{4}$ in. diameter by 2 in. NaI(Tl) crystal with a 1.27 cm. aluminum absorber (to stop the betas) was used for these data.

to 5.3-Mev. gamma radiation incident on a crystal this size. Within the statistics obtained, there is no evidence for the presence of any other gamma rays. Upper limits on possible intensities are 5% for all energies greater than 5.3 Mev. and 10% for a 1.9-Mev. gamma.

The gamma-ray spectrum confirms the existence of the strong beta transition to the 5.3-Mev. levels, which again are not resolved. The 7.16-Mev. level of N^{15} is known to decay (Campion and Bartholomew 1956; Bent *et al.* 1955;

Thompson 1954) to the 5.3-Mev. levels with the emission of a 1.9-Mev. gamma. Thus the intensity of the beta transition to the 7.16-Mev. level is less than 10% of the transition to the 5.3-Mev. levels.

(*g*) *Decay Scheme*

If one assumes that the C^{15} decay has a 20% component to the ground state and an 80% component to one of the two levels at 5.3 Mev. the log *ft* values are 6.1 and 3.7 respectively. If one assumes there is a 20% component to the ground state and a 40% component to each of the doublet levels at 5.3 Mev. then the log *ft* values are 6.1, 4.0, and 4.0 respectively. The presence of additional components consistent with the previous limits would increase each log *ft* value by less than 0.1. Fig. 14 shows the C^{15} decay scheme together with other pertinent information.

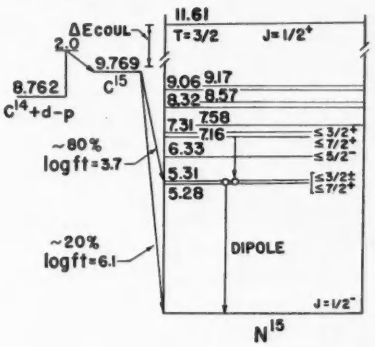

FIG. 14. C^{15} decay scheme. ΔE_{coul} indicates the C^{15}–N^{15} energy difference due to the coulomb interaction and neutron–proton mass difference.

The existence of superallowed or favored transitions in $N-Z = 3$ nuclei has been noted by King (1955). A calculation of the Gamow–Teller matrix elements has been performed by Feenberg (1955). The low log *ft* value (less than 4.1) for the transition to one of the 5.3-Mev. levels indicates that it belongs to this class. By comparison with the listing of Mayer *et al.* (1951) the transition to the ground state would be classified as first forbidden. These designations result in $\Delta J = 0, \pm 1$, no parity change, and $\Delta J = 0, \pm 1$, yes, respectively, for the above transitions.

VI. OTHER EXPERIMENTAL EVIDENCE

Unfortunately the *J*-values and parities of the excited states of N^{15} are not known. However, there is experimental evidence which limits the possible assignments.

The angular distributions of the proton groups from $N^{14}(d, p)N^{15}$ have been observed at M.I.T. (Sharp and Sperduto 1955). The protons resulting from the transition to the 5.305-Mev. level have an isotropic distribution indicating the absence of a contribution from the stripping mechanism. Lane (Sharp and

Sperduto 1955) has suggested the shell model configuration $(1s)^3(1p)^{12}$ for this level, which has zero width for breakup into $N^{14}(1s)^4(1p)^{10}$ and a neutron. This speculation requires an assignment of $1/2(+)$ for this level.

The angular correlations in the $N^{14}(d, p\gamma)N^{15*}$ have been measured at the Cavendish laboratory (Stanley 1954). In this experiment the 5.276- and 5.305-Mev. levels were not resolved, but the gamma transition from this doublet to the ground state was found to be dipole. Since the ground state has spin 1/2 and odd parity, the level or levels contributing to this gamma radiation are $J = 1/2$ or $3/2$ with either parity.

The recent Chalk River data on $N^{14}(n, \gamma)N^{15}$ (Campion and Bartholomew 1956) are in agreement with the Rice data (Bent *et al.* 1955; Thompson 1954) on $N^{14}(d, p\gamma)N^{15}$ which indicates that the 7.16-Mev. level of N^{15} decays to one or both of the 5.3-Mev. levels rather than the ground state. The 6.33-, 7.31-, and 8.32-Mev. levels in N^{15} are observed to decay to the ground state.

A study of the reactions $C^{14}(p, \gamma)N^{15}$ and $C^{14}(p, n)N^{14}$ at Chalk River (Bartholomew *et al.* 1955) has particular pertinence to the C^{15} decay. At $E_p = 1.5$ Mev. (11.61-Mev. excitation in N^{15}) a level is reported with properties which are explained by a $T = 3/2$, $J = 1/2(+)$ assignment. When the $C^{15}-N^{15}$ difference in coulomb energies and the neutron–proton mass difference have been allowed for, the C^{15} ground state corresponds to 11.83-Mev. excitation in N^{15}, which suggests that the ground state of C^{15} is the isobaric analogue of the 11.61-Mev. level. Hence one would expect the ground state of C^{15} to be $J = 1/2$ and even parity. See also Bartholomew *et al.* (1956).

The above experimental data (see Fig. 14) enable one to present a consistent picture. If C^{15} is $1/2(+)$ then one has a first forbidden beta transition to the ground state of N^{15} ($\Delta J = 0, \pm 1$, yes) and a favored transition to one of the doublet levels at 5.3 Mev. ($\Delta J = 0, \pm 1$, no). This requires one of these levels to be $1/2(+)$ or $3/2(+)$ which is consistent with all the preceding evidence. The beta transition to the 6.33-Mev. level is at least first forbidden because of the parity change. Beta components to higher levels, if allowed, would not be observed because of the smaller probability resulting from the lower beta end-point energies.

VII. CONCLUSIONS

1. The C^{15} yield curve with careful discrimination of half lives confirmed that the $C^{14}(d, p)C^{15}$ Q value measured with the electrostatic spherical analyzer pertained to the ground state reaction.

2. The end points of the beta spectra (9.5±0.3 Mev. and 4.5±0.2 Mev.) were in agreement with the above Q-value determination.

3. The gamma-ray spectrum indicated a single 5.3-Mev. gamma ray.

4. There is considerable evidence for a spin and parity assignment of $1/2(+)$ for the C^{15} ground state. A $3/2(+)$ assignment would conflict only with the Chalk River data on the assumed analogous level at 11.61 Mev. excitation in N^{15}. A $5/2(+)$ assignment would produce a second forbidden beta transition to the ground state which contradicts observations. A negative parity for C^{15}

contradicts the Chalk River result. Also, one would expect to see the transition to the negative parity state at 6.33 Mev. in N^{15}. A spin of 5/2 and negative parity would require a second forbidden transition to the ground state.

ACKNOWLEDGMENTS

We wish to thank Professor H. T. Richards for his continued guidance. The scintillators and associated equipment were supplied by Professor D. A. Lind who also assisted with the experiment. Messrs. Jan Broer, Ren Chiba, and J. Downey helped in taking data.

REFERENCES

ALLAN, H. R. and SARMA, N. 1955. Proc. Phys. Soc. (London), A, **68**: 535.
BARTHOLOMEW, G. A., BROWN, F., GOVE, H. E., LITHERLAND, A. E., and PAUL, E. B. 1955. Can. J. Phys. **33**: 441.
BARTHOLOMEW, G. A., LITHERLAND, A. E., PAUL, E. B., and GOVE, H. E. 1956. Can. J. Phys. **34**: 147.
BASHKIN, S. and GOLDHABER, G. 1951. Rev. Sci. Instr. **22**: 112.
BENT, R. D., BONNER, T. W., MCCRARY, J. H., RANKEN, W. A., and SIPPEL, R. F. 1955. Phys. Rev. **99**: 710.
BOSTROM, N. A., HUDSPETH, E. L., and MORGAN, I. L. 1956. Bull. Am. Phys. Soc. **1**: 94.
BOTHE, W. 1949. Z. Naturforsch. **4a**: 542.
CAMPION, P. J. and BARTHOLOMEW, G. A. 1956. Bull. Am. Phys. Soc. **1**: 28.
COHEN, B. L. 1955. Phys. Rev. **100**: 206.
DOUGLAS, R. A., BROER, J. W., CHIBA, R., HERRING, D. F., and SILVERSTEIN, E. A. 1956. Phys. Rev. In press.
EMMERICH, W. S., AUTH, W. J., and KURBATOV, J. D. 1954. Phys. Rev. **94**: 110.
FEENBERG, E. 1955. Phys. Rev. **99**: 71.
HOLLANDER, J. M., PERLMAN, I., and SEABORG, G. T. 1953. Revs. Mod. Phys. **25**: 469.
HUBY, R. 1953. Progr. Nuclear Phys. **3**: 177.
HUDSPETH, E. L., SWANN, C. P., and HEYDENBURG, N. P. 1950. Phys. Rev. **80**: 643.
KATZ, L. and PENFOLD, A. S. 1952. Revs. Mod. Phys. **24**: 28.
KING, R. W. 1955. Phys. Rev. **99**: 67.
MALM, R. and BUECHNER, W. W. 1950. Phys. Rev. **80**: 771.
MARION, J. B. and WEBER, G. 1956. Bull. Am. Phys. Soc. **1**: 94 and private communication.
MAYER, M. G. 1950. Phys. Rev. **78**: 16.
MAYER, M. G., MOSZKOWSKI, S. A., and NORDHEIM, L. W. 1951. Revs. Mod. Phys. **23**: 315.
MONAT, S., ROBBINS, C., and RONZIO, A. R. 1950. AECU672 (LADC-736). An analytic study of the conversion of barium carbonate to acetylene.
RICKARD, J. A., HUDSPETH, E. L., and CLENDENIN, W. W. 1954. Phys. Rev. **96**: 1272.
SHARP, W. T., GOVE, H. E., and PAUL, E. B. 1955. Table of Coulomb Functions, TPI–70, A.E.C.L. No. 268. Chalk River, Ont.
SHARP, R. D. and SPERDUTO, A. May, 1955. M.I.T. Annual Progress Report. Unpublished.
SIEGBAHN, K. 1955. Beta and gamma ray spectroscopy. North-Holland Publ. Co., Amsterdam.
SNOWDON, S. C. 1950. Phys. Rev. **78**: 299.
STANLEY, A. G. 1954. Phil. Mag. **45**: 807.
THOMPSON, L. C. 1954. Phys. Rev. **96**: 369.
WAPSTRA, A. H. 1955. Physica, **21**: 367.

A MICROWAVE WAVEGUIDE TROMBONE PHASE SHIFTER[1]

By Albert W. Adey[2] and Joyce Britton[3]

ABSTRACT

A microwave phase shifter is described which is based on the sliding principle of the trombone and which involves the telescoping together of two snugly-fitting sections of rectangular waveguide of different cross-sectional dimensions. Quarter-wave transformers are used to reduce the reflection at the change of waveguide cross-section. An attempt is made to increase the bandwidth of the instrument by making the transformers of different lengths. A phase change of several wavelengths is possible with an error of approximately plus or minus one degree.

INTRODUCTION

The trombone principle, involving the telescoping together of two sections of transmission line of different cross-section, has been widely used in the design of coaxial line phase shifters or line stretchers (King 1952). But no results for a waveguide instrument appear to have been discussed in the literature, although one of the present authors has reported using one at a wavelength of 3 cm. (Adey 1955). Telescoping sections have been used as a temperature-compensating device (Rzymowski and Edwards 1952) in 3 cm. waveguide and the authors who describe this apparatus have also discussed a method of cutting the waveguide transformers—a method very well known (Huxley 1947) but not much used—on which the design of the transformers used in the phase shifters reported here was based.

It is the purpose of the present paper to describe a 2 cm. phase shifter and to present some phase shift and reflection coefficient results obtained at several frequencies and for a number of combinations of transformer lengths. The less extensive results for the 3 cm. phase shifter reported elsewhere (Adey 1955) are included merely for comparison.

CONSTRUCTION

The 2 cm. instrument is shown in Fig. 1 and the details of the transformer section in Fig. 2. The fixed part of the trombone is formed of standard 0.702×0.391 in. O.D. brass waveguide with 0.040 in. walls. The U-shaped part is of brass and comprises two straight sections which telescope with the fixed sections and which are connected by a 180 degree turn. Each of the straight guides of the moving part was milled as a slot in a brass block to the outside dimensions of the fixed guides and a cover plate was screwed over the milled slot. The guide forming the 180 degree turn was milled in the form of a circular slot of rectangular cross-section in the end of a cylindrical block of brass, the slot being half the required guide depth. The cylinder was then slit along a

[1]Manuscript received July 11, 1956.
Contribution from the Radio Physics Laboratory, Defence Research Telecommunications Establishment, Defence Research Board, Ottawa, Ontario.
Issued as Radio Physics Laboratory Project Report 5–1–1, PCC. D48–95–11–04, January 6, 1956.
[2]Now at Radio Physics Laboratory, Defence Research Board, Ottawa, Ontario.
[3]Now at University of Toronto, Toronto, Ontario.

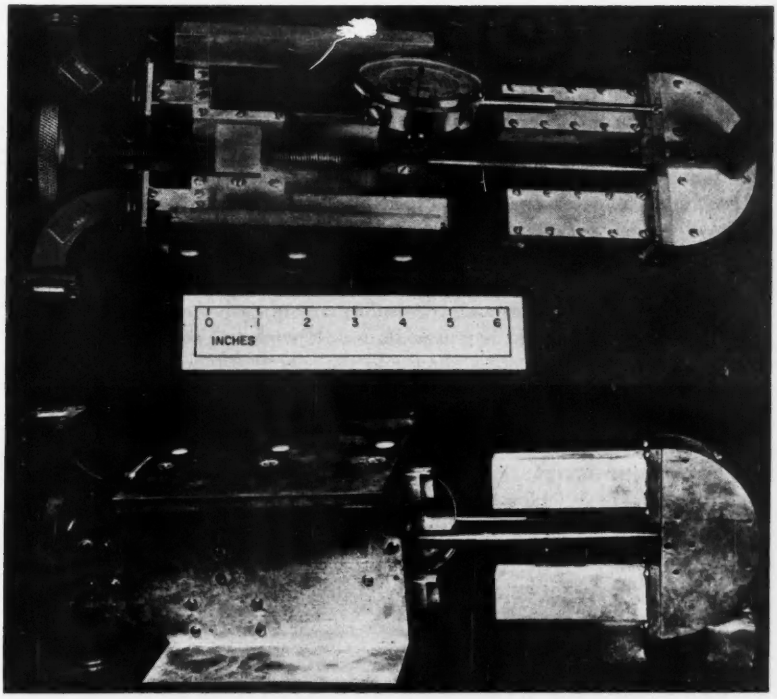

FIG. 1. Upper and lower views of 2 cm. trombone phase shifter.

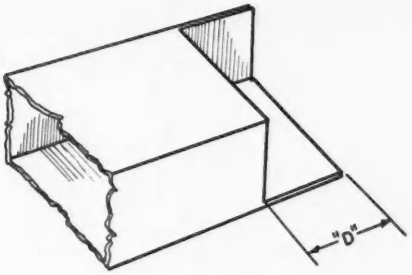

"D" @ 9375 Mc = 0.423"

"D" @ 15000 Mc = 0.246"

FIG. 2. Waveguide transformer section.

diameter, the two pieces aligned over each other by pins, and then screwed together. All the surfaces were finally silver-plated.

The 3 cm. instrument differed from the one described above in one respect. At that wavelength use was made of the fortuitous circumstance that the two standard British waveguides of 0.90×0.40 in. I.D. and O.D. respectively can be made to form a telescoping junction with a manipulation of the dimensions corresponding to the guide manufacturing tolerances.

The transformer can be constructed by cutting away two adjacent walls of the smaller guide for a quarter wavelength in the resulting intermediate size guide. The characteristic impedance of this guide is very nearly the geometric mean of the characteristic impedance of the two telescoping guides. Such a design neglects the discontinuity susceptance produced when a guide changes a cross-section dimension. This will be inductive for a change in the broad dimension and capacitive for a change in the narrow dimension (for the usual H_{01} mode). A consideration of these susceptances involves changing the length of the transformers from that of a quarter wavelength (Cohn 1955).

The slide is driven by a screw with a 1 mm. pitch and its position is indicated on a 0.01 mm. Ames gauge.

EXPERIMENTAL PROCEDURE

The equipment as set up for the VSWR measurements is shown in Fig. 3. Microwave power, square-wave modulated at 1000 c.p.s., was obtained from a Varian Type X-12 klystron which was driven from either a Hewlett-Packard

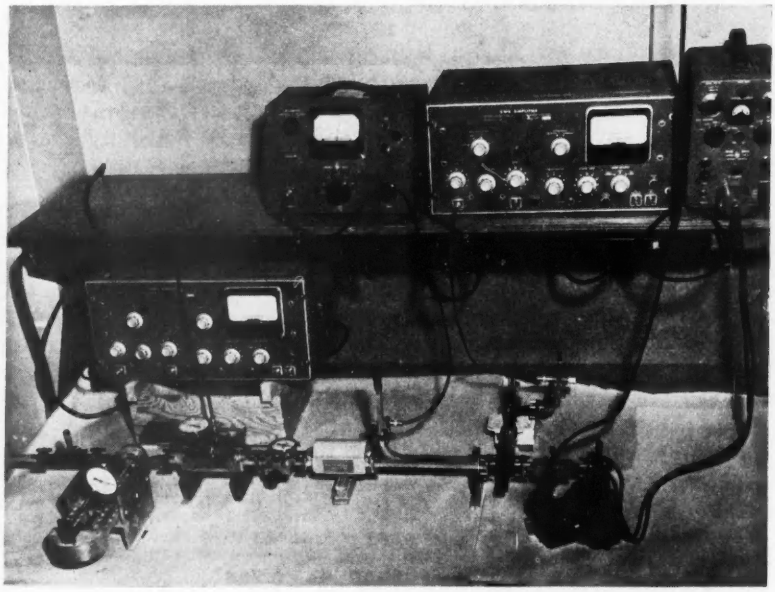

FIG. 3. Setup for VSWR tests.

Type 715A or an F-R Machinery Type Z815A stabilized power supply, matched to the waveguide by a slide-screw tuner. Frequency and power monitors were excited by signals taken off through 20 db. directional couplers. Isolation of the klystron and monitors from the measuring circuits was provided by an attenuator and a Uniline. Line voltage for all the circuit was supplied through a Sorensen Type 2000-S regulator.

For the VSWR measurements the phase shifter was preceded by a standing wave detector and terminated by a commercial load and a slide-screw tuner, the combination being matched to better than 1.005. The VSWR was measured with a Browning amplifier and standing wave indicator Type TAA-16B, which had been calibrated previously by standard mismatches determined by the Weissfloch–Feenberg method (Barlow and Cullen 1950; Marcuvitz 1951).

The phase measurements were made using a Magic-T in a bridge circuit. With the H-arm excited, one side arm was loaded by a section of waveguide approximately equal in length to the mean length of the phase shifter and terminated in a movable short circuit. The inclusion of this waveguide section made the bridge less sensitive to frequency variations. The phase shifter, terminated by a calibrated short circuit with a 0.01 mm. micrometer head, loaded the other side arm. A matched crystal holder feeding a 0–1 μamp. galvanometer was coupled to the E-arm. The T and the crystal holder could be matched to a VSWR of 1.02. The bridge was balanced initially with the slide in a reference position (with the guides overlapping by approximately a half inch). The slide was then moved in a distance of 0.5 mm., the movement being indicated by the Ames gauge. The bridge was rebalanced by moving the calibrated short circuiting plunger terminating the phase shifter, balance being indicated by a null reading on the galvanometer. For increased accuracy a bridging method was used to determine the balance position of the plunger, which could be reproduced to 0.005 mm.

The phase shifter error E for each slide position was then calculated from the relation

$$E_\phi = 2\pi\left(\frac{2P}{\lambda_p} - \frac{S}{\lambda_s}\right) \text{ radians}$$

$$= \frac{360}{\lambda_s}\left(\frac{2P\lambda_s}{\lambda_p} - S\right) \text{ degrees}$$

where P = slide displacement,

S = short circuit plunger displacement,

λ_s = guide wavelength in the short circuit,

λ_p = guide wavelength in the straight section of the slide.

λ_s was determined at each frequency from the short circuiting plunger displacement between two adjacent balance points of the bridge for a fixed value of P. λ_p was calculated from the wavemeter reading and the measured broad inside dimension of the straight guide of the slide by the usual waveguide wavelength formula.

EXPERIMENTAL RESULTS

The first measurements on the 2 cm. instrument were for transformers 0.246 in. long, as shown in Fig. 2. The VSWR results of Fig. 4 indicate, however, that the optimum frequency was somewhat lower than the design fre-

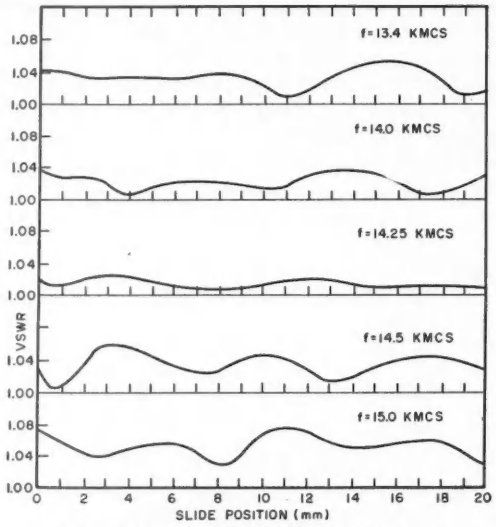

FIG. 4. VSWR for transformers 0.246 in. long.

quency of 15 kMc./sec. Thus it would appear that a neglect of the discontinuity susceptance results in a transformer that is too long. Since the magnitude of a simple, small discontinuity susceptance is approximately proportional to the ratio of the discontinuity of the dimension in which the discontinuity occurs, one would probably expect the susceptance at each end of a transformer of the type being considered here to be capacitive. A transmission line analysis of a transformer between two waveguides of different characteristic impedance (Huxley 1947) indicates the necessity of making the transformer shorter than a quarter wavelength.

However, if the total discontinuity at each end of the transformer is considered to be the combination of two simple discontinuities extending completely across the broad and narrow dimensions respectively, the predicted magnitude of the shortening of the transformer, based on data for simple inductive and capacitive discontinuities (Marcuvitz 1951), is less than that indicated by the results of Fig. 4. No data seem to be available for the type of discontinuity encountered here and it is probable that this composite asymmetrical discontinuity cannot be broken down so simply.

In an attempt to increase the optimum frequency and possibly the bandwidth of the phase shifter, one step was shortened by 0.005 in. The VSWR results indicated a little improvement. Two regions of low VSWR now existed, one corresponding to the matching frequency of each transformer.

When the transformer lengths were changed to 0.241 and 0.231 in. respectively, the VSWR behavior indicated a further improvement in the bandwidth, but with a higher VSWR between the two minima. Finally the two transformers were cut to 0.226 in. The VSWR results showed that the optimum band was now centered at approximately 15 kMc./sec., the transformer having been shortened by 0.020 in. from the length corresponding to the design neglecting the step susceptances.

The phase error was measured at several frequencies and for only two sets of transformers, because of the time involved in rematching the Magic T whenever the frequency was changed. Some of the results are presented in Fig. 5. One notes that a large mismatch results in a large phase error, but that the phase peaks occur, in the main, for those regions of slide position corresponding to the maxima in the rate of change of VSWR.

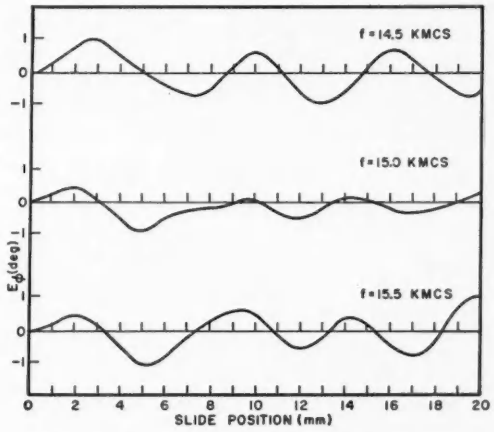

FIG. 5. Phase error for transformers 0.226 in. long.

From the error results shown it would appear that a phase accuracy of approximately plus or minus one degree could be achieved with this instrument in a narrow band about an optimum frequency. More satisfactory results in the direction of increased bandwidth could probably be obtained by the use of multisection transformers (Cohn 1955; Collin 1955), although a lack of data for the susceptances might still necessitate a large degree of cut-and-try in the design.

All the measurements were made with the phase shifter terminated by 90 degree, H-plane bends, to enable the instrument to be inserted in a line with no resulting change of transmission direction. The bends were found to have a negligible reflection coefficient. They can be eliminated in the present instrument by use of a second, smaller-diameter nut on the drive screw, whenever a reversal of transmission can be tolerated.

3 CM. PHASE SHIFTER

Results for this instrument are available for only one frequency and one set of transformers. This instrument was referred to in a previous publication (Adey 1955) and the results are shown in Fig. 6 for comparison with those

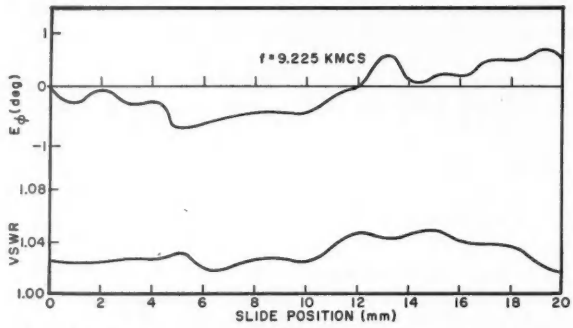

FIG. 6. VSWR and phase error for 3 cm. trombone phase shifter. Transformer length 0.423 in.

presented above.* For the measurements the phase shifter was terminated in sections tapering from 1×0.5 in. to 0.9×0.4 in. I.D. The results do not necessarily represent the optimum obtainable for the transformers used, since they were taken for only one frequency.

CONCLUSIONS

The paper has presented phase and VSWR results which indicate that the trombone principle can provide a useful basis for the design of a microwave waveguide phase shifter. Such an instrument can be fairly easily constructed, possesses ruggedness, and can provide phase shifts of several wavelengths. The bandwidth could undoubtedly be improved by use of multisection transformers.

ACKNOWLEDGMENTS

The authors wish to thank Mr. D. Faire of the Radio Physics Laboratory for his assistance in the mechanical design of the phase shifter and Sgt. Maj. Elder of the Canadian Army Signals Experimental Establishment for its construction.

REFERENCES

ADEY, A. W. 1955. Can. J. Phys. **33**: 407.
BARLOW, H. M. and CULLEN, A. L. 1950. Microwave measurements. Constable & Co., Ltd., London.
COHN, S. B. 1955. I.R.E. MTT-**3**: 16.
COLLIN, R. E. 1955. Proc. I.R.E. **43**: 179.
HUXLEY, L. G. H. 1947. A survey of the principles and practice of wave guides. The MacMillan Co. of Canada, Ltd., Toronto.
KING, D. D. 1952. Measurements at centimeter wavelengths. D. Van Nostrand Company, Inc., New York.
MARCUVITZ, N. 1951. Wave guide handbook. Rad. Lab. Ser. Vol. 10. McGraw-Hill Book Company, Inc., New York and London.
RZYMOWSKI, E. and EDWARDS, P. 1952. ASRE Tech. Note R3–52–2.

*The results of Fig. 6 were obtained by Dr. R. E. Collin, formerly of Imperial College of Science and Technology, London, England, and now of Canadian Armament Research and Development Establishment, Valcartier, Que., whose assistance is acknowledged.

INFLUENCE OF VIBRATION–ROTATION INTERACTION ON THE INTENSITIES OF PURE ROTATION LINES OF DIATOMIC MOLECULES[1]

By Robert Herman[2] and Robert J. Rubin[3]

ABSTRACT

The magnitude of the effect of the vibration–rotation interaction on the intensities of pure rotation lines of diatomic molecules has been calculated for two different molecular models, the anharmonic oscillator and the rotating Morse or Pekeris oscillator. The intensity correction for the anharmonic oscillator has been obtained by adapting the contact transformation formalism for calculating second-order corrections to the energy to the calculation of first-order corrections to the matrix elements of the electric moment as suggested by H. H. Nielsen. The correction to the line intensity for vibrationless transitions of the anharmonic oscillator is found to be

$$1+\frac{2\gamma^2}{\theta}\left[m^2-\frac{3k_3}{\gamma^{3/2}\omega_e}(v+\tfrac{1}{2})\right].$$

The results obtained here are also in complete agreement, to first order, with the results obtained earlier by Herman and Wallis for the 1–0 and 2–0 vibration–rotation line intensities. In the case of the Pekeris or rotating Morse oscillator the correction to the pure rotation line intensity is of the same form as above, namely,

$$1+\frac{2\gamma^2}{\theta}\left[m^2+\frac{1}{4\gamma\epsilon}+\frac{1}{48\epsilon^3}\right], \quad v=0,$$

but exhibits minor differences which can be explained in terms of the difference in the vibrational potential energy function in the two cases.

I. INTRODUCTION

The results of the study of intensities of individual lines in vibration–rotation bands and of integrated intensities of vibration–rotation bands of diatomic molecules have important applications. These applications arise, for example, in the spectroscopic determination of population distributions, in the study of line shape and width, and in the determination of the sign of the ratio of the effective charge to the dipole moment of a diatomic molecule.

The first calculation of the effect of vibration–rotation interaction on the line intensities was made by Kemble (1925) using the old quantum theory. Oppenheimer (1926) obtained the J-dependent correction factor to the intensity of a line in the fundamental vibration–rotation band of a diatomic molecule treated as a harmonic oscillator consisting of point charges. More recently there have been two additional calculations of the effect of vibration–rotation interaction on line intensities. Herman and Wallis (1955), using a conventional perturbation method, considered a more realistic model in which anharmonic corrections to the vibrational motion were included and in which the electric dipole moment was represented by a power series expansion in

[1]Manuscript received August 8, 1956.
Contribution from the Research Staff, General Motors Corporation, Detroit 2, Michigan, and the Department of Chemistry and Chemical Engineering, University of Illinois, Urbana, Illinois.

[2]Research Staff, General Motors Corporation, Detroit 2, Michigan.
[3]Department of Chemistry and Chemical Engineering, University of Illinois, Urbana, Illinois.

the normal coordinate. The perturbation calculation was carried out specifically for the intensity corrections for the 0–1, 1–2, and 0–2 transitions where the effect of anharmonicity can be expected to be small. Herman and Rubin (1955) calculated the matrix elements of the electric moment operator for a rotating Morse (or Pekeris) oscillator. These calculations are accurate for the Morse potential with not too large values of the rotational quantum number J.

The purpose of the present work is to calculate the vibration–rotation correction to the intensity of the pure rotation lines of a diatomic molecule. The correction is obtained for two different molecular models, the anharmonic oscillator treated by Herman and Wallis (1955) and the Pekeris oscillator treated by Herman and Rubin (1955). Following a recent suggestion by Nielsen,* the correction for the anharmonic oscillator has been obtained using an alternative but equivalent type of perturbation calculation to the one used by Herman and Wallis (1955). The calculation outlined here for the anharmonic oscillator is considerably shortened since we merely adapt an existing formalism for the calculation of second-order corrections to the energy to the calculation of first-order corrections to the matrix elements of the electric moment. The vibration–rotation corrections for the Pekeris oscillator for the $0,J \rightarrow 0,J'$ and $1,J \rightarrow 1,J'$ transitions are obtained by reducing the general formulae given by Herman and Rubin (1955) in these cases.

The intensity $I_{v,J}^{v',J'}$ of a line in a vibration–rotation band of a diatomic molecule associated with the transition $v,J \rightarrow v',J'$ is†

$$I_{v,J}^{v',J'} = \frac{8\pi^3 N_{v,J}}{3hc(2J+1)} \omega_{v,J}^{v',J'} \mathscr{S}_J^{J'} |\mathfrak{M}_{v,J}^{v',J'}|^2 \tag{1}$$

where $N_{v,J}$ is the number of molecules in the initial state, $\omega_{v,J}^{v',J'}$ is the frequency of the transition in wave numbers,

$$\mathscr{S}_J^{J'} = J\delta_{J',J-1} + (J+1)\delta_{J',J+1}$$

and $\mathfrak{M}_{v,J}^{v',J'}$ is the vibrational matrix element of the electric moment operator,

$$\mathfrak{M}_{v,J}^{v',J'} = \langle v, J|M(r)|v', J'\rangle, \text{ with } M(r) = \sum_{i=0} M_i(r-r_e)^i.$$

Thus the quantity which we wish to calculate is $\mathfrak{M}_{v,J}^{v',J'}$.

II. CALCULATION OF THE MATRIX ELEMENTS OF THE ELECTRIC MOMENT

The Anharmonic Oscillator

The quantum-mechanical form of the Hamiltonian for a rotating–vibrating diatomic molecule is‡

$$H = \frac{\mu}{2}(P_x^2 + P_y^2) + \frac{1}{2}\left(\frac{2\pi c\omega_e}{\hbar}\right)\mu^{\frac{1}{2}} p\mu^{-1} p\mu^{\frac{1}{2}} + U(q) \tag{2}$$

*A complete discussion of this method will be found in a paper entitled "Intensities of Rotation Lines in Absorption Bands" by H. Hanson, H. H. Nielsen, W. H. Shaffer, and J. Waggoner (J. Chem. Phys. In press.)

†See, for example, Herman and Rubin (1955).

‡See, for example, Darling and Dennison (1940), Herman and Shaffer (1948), and Wilson *et al.* (1955).

where P_x and P_y are angular momentum operators. The dimensionless normal coordinate q is

$$q = \left(\frac{2\pi c}{\hbar}\right)^{\frac{1}{2}} \omega_e^{\frac{1}{2}} (r - r_e) \rho^{\frac{1}{2}}$$

where ω_e is the vibration frequency in cm^{-1}, r and r_e are respectively the instantaneous and equilibrium internuclear distances in cm., and ρ is the reduced mass of the system. The symbol p represents the operator for the momentum conjugate to the normal coordinate q. The quantity μ is the reciprocal of the instantaneous moment of inertia,

$$\mu = \rho^{-1}(r_e + q/\alpha^{\frac{1}{2}})^{-2} \quad \text{where} \quad \alpha = 2\pi\rho c\omega_e/\hbar.$$

The potential energy $U(q)$ can be expressed in the form

$$U(q) = hc(\tfrac{1}{2}\omega_e q^2 + k_3 q^3 + \dots).$$

When the expression for μ in terms of the normal coordinate q is substituted in Eq. (2) and the indicated p-operations are performed, and when quantities of the form $(r_e + q/\alpha^{\frac{1}{2}})^t$ are expanded in powers of $q r_e^{-1}\alpha^{-\frac{1}{2}}$, the Hamiltonian assumes the form $H = H_0 + H_1 + \dots$ where H_0, the zeroth-order Hamiltonian, is

$$H_0 = \tfrac{1}{2}\rho r_e^{\,2}(P_x^{\,2} + P_y^{\,2}) + \tfrac{1}{2}hc\omega_e\left(\frac{p^2}{\hbar^2} + q^2\right), \tag{3}$$

and H_1, the first-order Hamiltonian, is

$$H_1 = -[\gamma^{3/2} hc\omega_e (P_x^{\,2} + P_y^{\,2})/\hbar^2]q + hck_3 q^3 \tag{4}$$

with $\gamma = \alpha^{-1} r_e^{-2} = 2B_e/\omega_e$. The terms comprising H_1 do not contribute to the energy in a first-order approximation. It is therefore convenient to transform H by a particular contact transformation (Johrdahl 1934; Kemble 1937; Shaffer, Nielsen, and Thomas 1939; Herman and Shaffer 1948) $THT^{-1} = H'$ such that the first-order Hamiltonian will be zero in the new representation. The evaluation of the energy to the second order of approximation is thus reduced to a first-order perturbation calculation in the transformed representation. The transformation function T can be represented by e^{iS} and T^{-1} by e^{-iS}. The function S is a sum of terms where each term removes a single term from H_1. Herman and Shaffer (1948) have tabulated the basic transformation functions S which will remove a given type of term from H_1. The function S which will remove the entire first-order Hamiltonian H_1 is

$$S = \gamma^{3/2}\hbar^{-2}(P_x^{\,2} + P_y^{\,2})p/\hbar - \frac{2k_3}{\omega_e}\left(\frac{p^3}{3\hbar^3} + \frac{qpq}{2\hbar}\right). \tag{5}$$

The operator $(P_x^{\,2} + P_y^{\,2})/\hbar^2$ in Eq. (5) can be treated as constant to the second order of approximation (Herman and Shaffer 1948) so that Eq. (5) can be rewritten as

$$S_J = \gamma^{3/2} J(J+1)p/\hbar - \frac{2k_3}{\omega_e}\left(\frac{p^3}{3\hbar^3} + \frac{qpq}{2\hbar}\right) \tag{6}$$

where J is the angular momentum quantum number.

The zero-order wave functions of $H' = H_0' + H_2' + \ldots$ are harmonic oscillator wave functions. These wave functions can be used to calculate the second-order energy corrections in a first-order perturbation calculation where H_2' is treated as the perturbation.

We are concerned here with the calculation of the vibrational matrix elements of the electric moment. This matrix element can be calculated in either the original or the transformed representation:

$$\begin{aligned}(7)\qquad \mathfrak{M}_{v,J}^{v',J'} &= \langle \bar{\psi}_{v,J} M(r) \psi_{v',J'} \rangle \\ &= \langle \bar{\psi}_{v,J} T_J^{-1} T_J M T_{J'}^{-1} T_{J'} \psi_{v',J'} \rangle \\ &= \langle \bar{\psi}'_{v,J} M' \psi'_{v',J'} \rangle\end{aligned}$$

where $\psi_{v,J}$ is an eigenfunction of H, $\psi'_{v,J} = T_J \psi_{v,J}$ is an eigenfunction of H', and $M' = T_J M T_J^{-1}$. For our purposes, it will be sufficient to assume that the expansion of the electric moment can be terminated after the second term. It can, moreover, be expressed in terms of the normal coordinate q as

$$(8)\qquad M \cong M_0 + \gamma^{\frac{1}{2}} r_e M_1 q.$$

In order to calculate the first-order corrections to the electric moment matrix element in either the original or the transformed representation, it is necessary to know the first-order corrections to the eigenfunctions. This requirement is trivial in the transformed representation since the eigenfunctions $\psi'_{v,J}$ are harmonic oscillator wave functions $\psi_{v,J}^{(0)'}$ to the first order of approximation. The first-order approximation for $\mathfrak{M}_{v,J}^{v',J'}$ can be written according to Eq. (7) as

$$(9)\qquad \mathfrak{M}_{v,J}^{v',J'} \cong \langle \bar{\psi}_{v,J}^{(0)'} M' \psi_{v,J}^{(0)'} \rangle$$

in which we use the appropriate e^{iS} transformation function (Herman and Shaffer 1948). Thus the first-order calculation of $\mathfrak{M}_{v,J}^{v',J'}$ has been reduced to the calculation of the matrix elements of

$$(10)\qquad M' = e^{iS_J}(M_0 + \gamma^{\frac{1}{2}} r_e M_1 q) e^{-iS_{J'}}$$

for a harmonic oscillator. The transformed electric moment operator M', correct to first order, can be obtained by expanding the exponential functions in Eq. (10) to give

$$(11)\qquad M' \cong M_0 + iM_0(S_J - S_{J'}) + \gamma^{\frac{1}{2}} r_e M_1 q + i\gamma^{\frac{1}{2}} r_e M_1 (S_J q - q S_{J'}),$$

where terms involving products of S's have been neglected. When we substitute Eq. (6) for S_J in Eq. (11), the resulting expression can be simplified. The simplification can be made with the aid of the commutation relations (Herman and Shaffer 1948)

$$p^3 q - q p^3 = -3i\hbar p^2 \quad \text{and} \quad qpq^2 - q^2 pq = -i\hbar q^2.$$

Equation (11) reduces finally to

$$\begin{aligned}(12)\qquad M' \cong M_0 &+ i\gamma^{3/2} M_0 [J(J+1) - J'(J'+1)] + \gamma^{\frac{1}{2}} r_e M_1 q \\ &+ i\gamma^2 r_e M_1 \left[J(J+1) \frac{pq}{\hbar} - J'(J'+1) \frac{qp}{\hbar} \right] - 2\gamma^{\frac{1}{2}} r_e M_1 \frac{k_3}{\omega_e} \left(\frac{p^2}{\hbar^2} + \frac{q^2}{2} \right).\end{aligned}$$

When we substitute M' from Eq. (12) in Eq. (9), the desired matrix element can be written*

$$\mathfrak{M}_{v,J}^{v',J'} = M_0\langle 1\rangle_{v,J}^{v',J'}+\gamma^{3/2}M_0[J(J+1)-J'(J'+1)]\langle ip/\hbar\rangle_{v,J}^{v',J'}+\gamma^{\frac{1}{2}}r_eM_1\langle q\rangle_{v,J}^{v',J'}$$

$$+\gamma^2r_eM_1\{J(J+1)\langle ipq/\hbar\rangle_{v,J}^{v',J'}-J'(J'+1)\langle iqp/\hbar\rangle_{v,J}^{v',J'}\} \tag{13}$$

$$-\frac{2k_3}{\omega_e}\gamma^{\frac{1}{2}}r_eM_1\{\langle p^2/\hbar^2\rangle_{v,J}^{v',J'}+\tfrac{1}{2}\langle q^2\rangle_{v,J}^{v',J'}\}.$$

As a check on the foregoing expression, we note that for the 0–1 and 0–2 transitions, we obtain the following results in agreement with Herman and Wallis (1955):

$$\mathfrak{M}_{0,J}^{1,J'} \cong \frac{M_1}{(2\alpha)^{\frac{1}{2}}}(1-2\gamma\theta m), \tag{14}$$

and

$$\mathfrak{M}_{0,J}^{2,J'} \cong \frac{M_1}{(2\alpha)^{\frac{1}{2}}}\frac{k_3}{\omega_e}\left(1-2\gamma^{3/2}\frac{\omega_e}{k_3}m\right), \tag{15}$$

where

$$m = \begin{cases} J+1, & R\text{-branch}, \\ -J, & P\text{-branch}, \end{cases}$$

and where $\theta = M_0/(M_1r_e)$. The higher order terms in the matrix elements $\mathfrak{M}_{0,J}^{1,J'}$ and $\mathfrak{M}_{1,J}^{2,J'}$ given by Herman and Wallis (1955) have been obtained in elegant fashion by means of a higher order contact transformation by Hanson *et al.*

For the vibrationless transition, $v,J \rightarrow v,J'$, the matrix element is found to be

$$\mathfrak{M}_{v,J}^{v,J'} \cong M_0\left\{1+\frac{\gamma^2}{\theta}\left[m^2-\frac{3k_3}{\gamma^{3/2}\omega_e}(v+\tfrac{1}{2})\right]\right\}, \tag{16}$$

in which k_3 is the coefficient of the cubic term in the potential function and where now since there is only an R-branch,

$$m = \begin{cases} J+1, & \text{absorption}, \\ -J, & \text{emission}. \end{cases}$$

The Pekeris Oscillator

The matrix element of the electric moment, given in Eq. (16), for the vibrationless transitions $0,J \rightarrow 0,J'$ and $1,J \rightarrow 1,J'$ of an anharmonic oscillator can be compared with the corresponding matrix elements for a Pekeris or rotating Morse oscillator. The general formula for $\mathfrak{M}_{v,J}^{v',J'}$ for a Pekeris oscillator has been given by Herman and Rubin (1955). For the transition $v,J \rightarrow v',J'$, their result for the matrix element of the first two terms of the electric moment expansion can be written as

$$\mathfrak{M}_{v,J}^{v',J'} = \left\{q_0\sum_{i=0}^{v}\sum_{j=0}^{v'}Q_{ij}\right\}M_0-\left\{q_0\sum_{i=0}^{v}\sum_{j=0}^{v'}Q_{ij}[\psi(\xi_{ij})-\ln(d_0+d_0')]\right\}\frac{M_1}{\beta}, \tag{17}$$

*A list of harmonic oscillator matrix elements is given in Wilson *et al.* (1955), Appendix 3.

where the quantities q_0, Q_{ij}, and ξ_{ij} are, respectively,

$$q_0 = \left[\Gamma(b)\,\Gamma(b')\binom{v+b}{v}\binom{v'+b'}{v'}\right]^{-\frac{1}{2}} \frac{(2d_0)^{b/2}(2d_0')^{b'/2}}{(d_0+d_0')^{(b+b')/2}},$$

$$Q_{ij} = (-1)^{i+j}\binom{v+b}{v-i}\binom{v'+b'}{v'-j}\frac{\Gamma(\xi_{ij})}{i!\,j!}\,\frac{(2d_0)^i(2d_0')^j}{(d_0+d_0')^{i+j}},$$

and

$$\xi_{ij} = \tfrac{1}{2}(b+b')+i+j.$$

The function $\Gamma(y)$ is the gamma function; the function $\psi(y)$ is the logarithmic deviate of the gamma function; and the symbol $\binom{m}{n}$ represents the binomial coefficient, $m!/[n!(m-n)!]$. The quantities d_0 and b are defined in terms of the spectroscopic constants and the parameters of the Morse potential, $U(r) = D_e[1-e^{-\beta(r-r_e)}]^2$. The definitions are as follows:

(18) $$d_0^2 = \epsilon^4\gamma^{-2}\{1+\gamma^2\epsilon^{-1}(3\epsilon-1)J(J+1)\},$$

and

(19) $$b = 2\epsilon^4\gamma^{-2}d_0^{-1}\{1+\gamma^2\epsilon^{-1}(3\epsilon-2)J(J+1)\},$$

where

$$\epsilon = (r_e\beta)^{-1}, \quad \beta = \left(\frac{2c\rho}{D_e\hbar}\right)^{\frac{1}{2}}\omega_e, \quad \frac{B_e}{D_e} = \frac{\gamma^2}{\epsilon^2},$$

and the other constants which appear have been defined earlier in this paper. A prime on d_0 or b denotes the replacement of J by J'.

If we set v equal to zero in Eq. (17), the matrix element $\mathfrak{M}_{0,J}^{0,J'}$ can be written as

(20) $$\mathfrak{M}_{0,J}^{0,J'} = \frac{\Gamma(\frac{1}{2}[b+b'])}{\Gamma^{\frac{1}{2}}(b)\,\Gamma^{\frac{1}{2}}(b')}\,\frac{(2d_0)^{b/2}(2d_0')^{b'/2}}{(d_0+d_0')^{(b+b')/2}} \times\left\{M_0-\left[\psi\left(\frac{b+b'}{2}\right)-\ln(d_0+d_0')\right]\frac{M_1}{\beta}\right\}.$$

In order to obtain Eq. (20) in a useful form, the quantities b, b', d_0, and d_0' which are defined in Eq. (18) and Eq. (19) must be substituted in Eq. (20) and the resulting expression must be expanded in a power series in γ. In carrying out the expansion, the factor in front of the braces in Eq. (20) can be shown to be equal to unity to the second order in γ. In obtaining this result, we have taken advantage of the fact that the dimensionless quantity b for most diatomic molecules is of the order of 50, and therefore we have used the asymptotic expansion of the Γ-function,

$$\Gamma(y+1) \sim y^y e^{-y}(2\pi y)^{\frac{1}{2}}\{1+1/(12y)\}.$$

The expression inside the braces can be similarly expanded in a power series in γ. In this expansion we have used the asymptotic expansion of the ψ-function,

$$\psi(y) \sim \tfrac{1}{2}\ln y(y+1)+\frac{1}{6}\left[\frac{1}{y}+\frac{1}{y+1}\right].$$

After a lengthy algebraic reduction, the matrix element $\mathfrak{M}_{0,J}^{0,J'}$ correct to the second power in γ is obtained

(21) $$\mathfrak{M}_{0,J}^{0,J'} \cong M_0\left\{1+\frac{\gamma^2}{\theta}\left[m^2+\frac{1}{4\gamma\epsilon}+\frac{1}{48\epsilon^3}\right]\right\}.$$

The matrix element for the $1,J \rightarrow 1,J'$ transition can be obtained in a similar manner. The final result is

$$\mathfrak{M}_{1,J}^{1,J'} \cong M_0\left\{1+\frac{\gamma^2}{\theta}\left[m^2+\frac{7}{4\gamma\epsilon}+\frac{61}{48\epsilon^3}\right]\right\}. \tag{22}$$

In the course of obtaining Eq. (22), we have used the following property of the ψ-function:

$$\psi(y+n) = \psi(y)+\sum_{i=0}^{n-1}\frac{1}{y+i}.$$

The electric moment matrix elements for the anharmonic and Pekeris oscillators for the $0,J \rightarrow 0,J'$ and $1,J \rightarrow 1,J'$ transitions are similar in form. The minor differences which do arise can be explained in terms of the difference in the vibrational potential energy function in the two cases.

III. CONCLUSION

The expressions for the matrix elements $\mathfrak{M}_{v,J}^{v,J'}$ given in Eqs. (14) to (16) and Eqs. (21) and (22) for the anharmonic and Pekeris oscillators, respectively, can be used in Eq. (1) to obtain the intensities of the various rotation lines. The results for the anharmonic oscillator have been obtained by adapting the contact transformation formalism as suggested by Nielsen to our needs. The results for the Pekeris oscillator were obtained from the general results of Herman and Rubin (1955). Equations (14) and (15) are in agreement with the results of Herman and Wallis (1955), but the intensity corrections obtained from Eqs. (16), (21), and (22) for pure rotation transitions are new. These latter results can also be used to determine $\theta = M_0/(M_1 r_e)$ as in the study of vibration–rotation line intensities.

It should be noted that the change in line intensity with J for pure rotation lines will be most evident for diatomic molecules having $\theta \ll 1$. The CO molecule is of such type since $\theta \cong 1/30$. In this case we estimate using the rigid rotor approximation that the fractional absorption per atmosphere for the line $J = 20$, using a 1 cm^{-1} slit, is $\sim 0.05\, l^{\frac{1}{2}}$, where l, the path length, is in cm. This means that one can measure changes in line intensity with J with a path length of $\sim$1 meter.

ACKNOWLEDGMENTS

We wish to thank Professor H. H. Nielsen for suggesting the approach employed for the anharmonic oscillator, for a number of stimulating discussions, and for his constant interest in our work.

REFERENCES

Darling, B. T. and Dennison, D. M. 1940. Phys. Rev. **57**: 128.
Hanson, H., Nielsen, H. H., Shaffer, W. H., and Waggoner, J. J. Chem. Phys. In press.
Herman, R. and Rubin, R. J. 1955. Astrophys. J. **121**: 533.
Herman, R. and Shaffer, W. H. 1948. J. Chem. Phys. **16**: 453.
Herman, R. and Wallis, R. F. 1955. J. Chem. Phys. **23**: 637.
Johrdahl, O. M. 1934. Phys. Rev. **45**: 87.
Kemble, E. C. 1925. Phys. Rev. **25**: 1.
——— 1937. Fundamental principles of quantum mechanics. McGraw-Hill Book Company, Inc., New York. pp. 237–240.
Oppenheimer, J. R. 1926. Proc. Cambridge Phil. Soc. **23**: 327.
Shaffer, W. H., Nielsen, H. H., and Thomas, L. H. 1939. Phys. Rev. **56**: 1051.
Wilson, E. B., Decius, J. C., and Cross, P. C. 1955. Molecular vibrations. McGraw-Hill Book Company, Inc., New York. Chap. 11.

ABSOLUTE PAIR PRODUCTION CROSS SECTION OF LEAD AT 2.76 MEV.[1]

By S. Standil and R. D. Moore

ABSTRACT

A value has been obtained for the absolute pair production cross section of lead for the 2.76 Mev. gamma rays of Na^{24}. A collimated beam of these gamma rays was made to fall on a specially constructed target and the positrons produced in the target were detected by counting two-quanta annihilation events by means of two scintillation spectrometers in coincidence. The strength of the Na^{24} source was measured by a coincidence counting technique and the counter detection efficiency for annihilation radiation was measured with a calibrated Na^{22} source. The effect of absorption of the 0.511 Mev. annihilation radiation in the target was measured in a separate experiment. The value obtained for the cross section was 2.38 ± 0.62 barns.

INTRODUCTION

This work was undertaken for two reasons:

(1) At the time at which the work was begun no absolute measurements had been made at low energy.

(2) The work of Motz (1955) on absolute bremsstrahlung cross sections at low energy shows large discrepancies with theory. Since this process is closely related to the pair production process theoretically, it was a matter of some interest to see if a similar discrepancy existed for the latter process.[2]

Theories of the pair production process have been given by Bethe and Heitler (1934) and Hulme and Jaeger (1936*a*, *b*). The former theory makes use of the Born approximation, i.e. assumes plane wave functions for the electrons, the latter of exact coulomb wave functions. Values of the total cross section calculated from the more accurate Jaeger and Hulme theory at low energies are higher than those obtained from the theory of Bethe and Heitler.

THE EXPERIMENT

The geometry of the experiment is shown in Fig. 1. A collimated beam of gamma rays from a Na^{24} source was directed at the target which was so constructed that most of the positrons produced in its lead portion annihilated before leaving the target. The detectors were a pair of scintillation spectrometers of standard design with their outputs fed into a coincidence mixer. Thus it was possible to detect two-quanta annihilation events occurring in the target by setting each spectrometer astride the 0.511 Mev. photopeak and counting coincidences between them. With the counters arranged coaxially as shown, the detection efficiency for the oppositely directed annihilation quanta is a maximum and the coincidence rate obtained is proportional to the pair production cross section of the material in the target. The detection

[1]Manuscript received June 25, 1956.
Contribution from the Department of Physics, University of Manitoba, Winnipeg, Man. This work was supported by the National Research Council of Canada.

[2]We are indebted to Dr. S. M. Neamtan of the Mathematical Physics Department (University of Manitoba) for pointing this out.

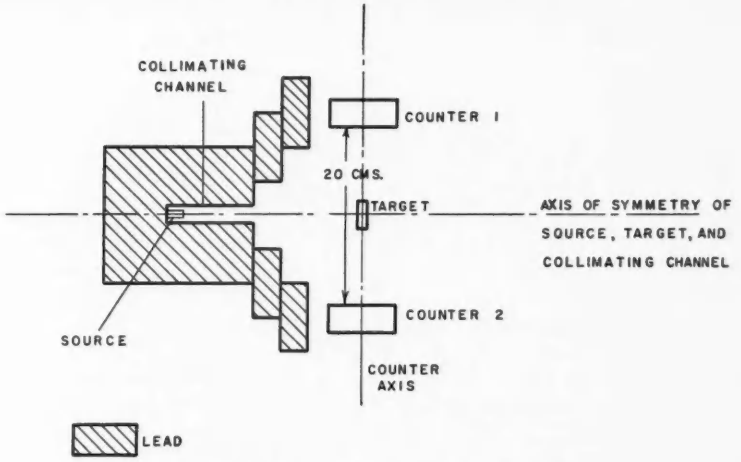

FIG. 1. Experimental arrangement (not to scale).

efficiency of the counting equipment for the annihilation radiation was determined making use of a calibrated Na^{22} source. The strength of the Na^{24} source was measured by a coincidence technique described below. Once this has been determined the photon flux at the target may be calculated from geometry. These data, suitably corrected, may be used to calculate the cross section.

Each of the spectrometers consisted of a cylindrical NaI(Tl) crystal, 9.6 cm. in diameter and 6.5 cm. long, mounted on a 5-in. photomultiplier tube (Dumont 6364). The resulting pulses were delay line clipped, amplified, and then sorted by a commercial differential pulse height analyzer (Dynatron Radio Co. Model N101). The output pulses of the pulse analyzers were fed into a gated beam tube coincidence mixer, a modification of the circuit of Fischer and Marshall (1952). The resolving time of this circuit was measured to be 3.5×10^{-7} sec. The equipment was calibrated during the experiment by running a coincidence spectrum of the annihilation radiation of Zn^{65}. The gates of the pulse height analyzers were then set so that the 0.511 Mev. photopeak lay within the acceptance channel. The position used for the analyzer gates may be seen in Fig. 2, which is a single channel gamma ray spectrum of the radiation from the target as seen by either of the spectrometers.

The target consisted of a lead disk, 1.75 cm. in diameter by 0.1 cm. thick, cemented to a graphite disk of the same diameter and 0.4 cm. thick. Since the mean energy of the positrons produced in the lead was about 1 Mev., a large percentage of them would pass out of the sensitive region of the counters before annihilating were it not for the presence of the graphite. The thickness of the graphite was sufficient to ensure that the most energetic positron entering it from the lead would annihilate before leaving it. Since most of the positrons produced in the lead are emitted in the forward direction as defined by the

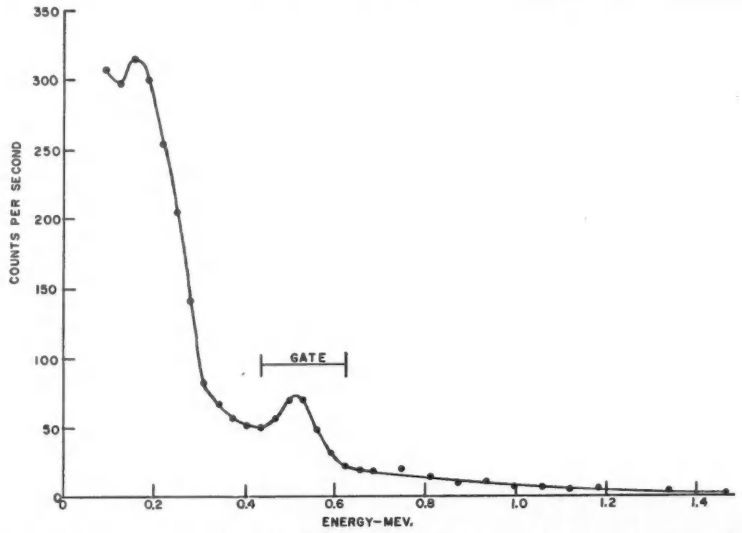

FIG. 2. Gamma ray spectrum of radiation from target taken with 25 kev. channel width.

photon beam, most of them annihilate in a small region over which the detection efficiency of the counting equipment is nearly constant. Positrons are also produced by the graphite. To account for these and hence to obtain the net coincidence rate due to the lead a carbon 'blank' of the same dimensions as the graphite portion of the target was used. The coincidence rate obtained with the blank was subtracted from that obtained with the target to get the net rate due to the lead. A correction for positrons which were emitted from the front face and around the edges of the disk, and thus not detected, was obtained by making use of a second target in which the lead disk was completely surrounded by 0.4 cm. of graphite. The correction for this effect was found to amount to 8%.

MEASUREMENT OF SOURCE STRENGTH

The decay scheme of Na^{24} is given by Hollander *et al.* (1953). Its gamma ray spectrum consists almost entirely of a pair of cascade gamma rays of 1.38 and 2.76 Mev. respectively. The half life is given by Tobaillem (1955) as 14.90 $\pm$0.05 hr.

Fig. 3 shows the arrangement of the counters for the source strength measurement. After calibration of both spectrometers one was set with a wide gate astride the 1.38 Mev. photopeak and the other on that at 2.76 Mev. (hereafter referred to as channel 1 and 2 respectively). Let Ω_1 and Ω_2 be the solid angles subtended at the source by counters 1 and 2 respectively. Let ϵ_1 be the probability that a 1.38 Mev. photon emitted into Ω_1 produces a pulse in the 1.38 Mev. photopeak, ϵ_3 be the probability that a 2.76 Mev. photon emitted into Ω_1 produces a pulse in the 1.38 Mev. photopeak, and ϵ_2 be the probability that a

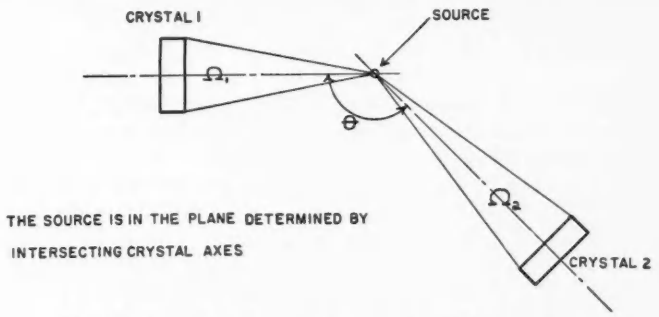

FIG. 3. Counter arrangement for source strength measurement.

2.76 Mev. photon emitted into Ω_2 produces a pulse in the 2.76 Mev. photopeak. The counting rates in channels 1 and 2, N_1 and N_2 respectively, will be given by

$$N_1 = N(\epsilon_1\Omega_1 + \epsilon_3\Omega_1) \tag{1}$$

and

$$N_2 = N\epsilon_2\Omega_2, \tag{2}$$

where N is the source strength, or

$$N_1 = N(\phi_1 + \phi_3) \tag{3}$$

and

$$N_2 = N\phi_2, \tag{4}$$

where $\phi_1 = \epsilon_1\Omega_1$, $\phi_2 = \epsilon_2\Omega_2$, and $\phi_3 = \epsilon_3\Omega_1$.

Since every 1.38 Mev. photon is accompanied by a time-coincident 2.76 Mev. photon there will be a real coincidence rate N_R given by

$$N_R = N\phi_1\phi_2 \tag{5}$$

neglecting angular correlation.

If we let

$$N_1' = N\phi_1, \tag{6}$$

then from (5), (6), and (4) we obtain:

$$N = N_1'N_2/N_R. \tag{7}$$

There will be a chance coincidence rate N_c given by:

$$N_c = 2\tau N_1N_2, \tag{8}$$

where τ is the resolving time of the coincidence mixer.

The total coincidence rate R is:

$$R = N_c + N_R. \tag{9}$$

It is necessary to obtain N_1' in order to calculate N. This was done graphically by extrapolating back the Compton distribution from the 2.76 Mev.

photons and subtracting the extrapolated curve from the 1.38 Mev. photopeak. It is estimated that in this way N_1' (found to be $0.6N_1$) is determined to 4% accuracy.

N_1, N_2, and R may be measured directly. N_c can then be calculated from (8) and N_R from (9). Having obtained N_1' as above, N may be calculated from (7).

Measurements of N were made over a period of five days during which the angle θ and the source to counter distances were varied. Since no dependence of N, as calculated above, on geometry was observed, the neglect of angular correlation in the derivation of (7) seems justified. These data were used to plot a decay curve for the Na^{24} source. From the slope of a least squares fit to these data a half life of 16.0 ± 1.6 hr. was obtained. This is in agreement with the value given by Tobaillem. Values of N for later calculations were obtained from a 14.90 hr. decay curve fitted to the experimental points.

MEASUREMENT OF DETECTION EFFICIENCY

A calibrated Na^{22} source loaned by Atomic Energy of Canada Ltd.[3] was used for this measurement. Na^{22} emits a 0.542 Mev. positron (Macklin *et al.* 1950) with 9.9% K-capture (Scherr and Miller 1954). The source was in the form of an aqueous solution of NaCl of known activity per unit volume. A small quantity of the solution was weighed out and sealed in the middle of a split lucite disk 1.75 cm. in diameter and 0.8 mm. thick. This ensured that all the positrons emitted by the Na^{22} annihilated before leaving the lucite. This arrangement thus constituted a source of annihilation radiation similar to that provided by the target.

Since both photons produced in a two-quanta annihilation process must enter the crystals in order that the event be counted, absorption of the annihilation photons by the material of the target lowers the detection efficiency for two-quanta annihilations in the target. Although such absorption in the graphite was very small, that taking place in the lead was not. The effect of the lead was determined experimentally. A number of targets similar to the one first described were made up with lead disks of various thicknesses. The apparatus was set up as shown in Fig. 1, using 50 mgm. of radium borrowed from the Manitoba Cancer Relief Institute as a gamma ray source. The coincidence rate for each of the targets was measured as before using a graphite blank. Neglecting absorption, the coincidence rate thus obtained is simply proportional to the mass of lead in the target. Thus in such a case a plot of coincidence rate against mass of lead would be a straight line through the origin. For each target the effect of absorption is to reduce the coincidence rate actually observed, the effect increasing with mass of lead. The experimental points should thus lie on a curve which is asymptotic to the above-mentioned straight line at the origin and falls farther below it for increasing mass of lead. This was found to be the case as is shown in Fig. 4. The vertical line in Fig. 4 cuts the mass axis at a point corresponding to the mass of lead in the original target. This leads to a target absorption correction factor of 1.67 ± 0.08.

[3]The co-operation of Dr. P. J. Campion (A.E.C.L.) is gratefully acknowledged.

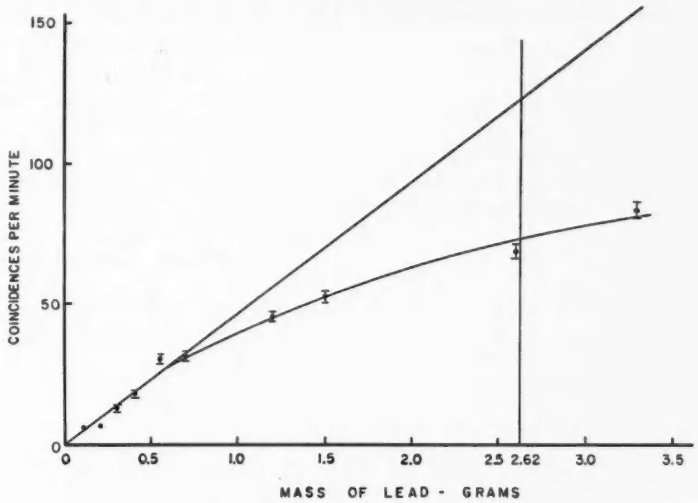

FIG. 4. Coincidence rate vs. mass of lead in target.

OTHER CORRECTIONS

(1) *Scattering from collimator.*—It is possible that small-angle Compton scattering near the surface of the collimating channel could result in a number of degraded photons, which were still energetic enough to produce pairs, striking the target. To check on this effect a small (1×1 in.) NaI(Tl) crystal mounted on a 2-in. photomultiplier tube was placed with its front face in the position previously occupied by the front face of the target. The 1-in. crystal was used because, of those available, it was closest to the target diameter. A single channel spectrum of the gamma radiation seen by the crystal was run with and without the collimator and from a comparison of the two curves the effect of such scattering was found to be negligible.

(2) *Contribution of the 1.38 Mev. gamma ray.*—The 1.38 Mev. gamma rays are energetic enough to produce pairs and hence contribute to the measured coincidence rate. Their effect was corrected for by using the data of West (1956) on the ratio of the pair production cross section at 2.76 Mev. to that at 1.38 Mev. (15.0±0.8).

(3) *Absorption of the primary photon beam in the lead disk.*—This results in two effects:

(i) The gamma ray flux seen by the graphite in the target is smaller than that seen by the blank. Hence the counting rate to be subtracted as the contribution of the graphite is slightly smaller than that obtained with the blank.

(ii) If the lead disk is thought of as divided into transverse layers the photon flux at a given layer will depend on its depth in the lead.

Corrections were calculated for these effects and applied where appropriate. In all cases these corrections were found to amount to less than 10%.

(4) *One and three quanta annihilation processes.*—It is possible for a positron to annihilate with the production of one or three quanta, events which this apparatus would not detect. The theoretical ratio of the rate of three to two quanta annihilation processes is given by Ore and Powell (1949) as 1/370. This figure has been experimentally verified for metals by De Benedetti and Siegel (1954). Hulme and Jaeger (1936*a*, *b*) calculate the ratio of one to two quanta annihilations in lead as 0.01, the ratio being even smaller for carbon. Thus both these processes are negligible in comparison to other errors in the experiment.

FINAL RESULTS

In the part of the experiment in which the target and blank were alternately irradiated with gamma rays from Na^{24}, 12,796 counts were obtained on the target and 8396 with the blank. Applying all the necessary corrections a value of $\sigma_{pair} = 2.38 \pm 0.62$ barns was obtained for the cross section.

DISCUSSION OF RESULTS

The value obtained for the cross section in this experiment is nearer the Bethe–Heitler value (2.8 barns) than the Jaeger–Hulme value (3.3 barns) although the experimental error is too large to assign any real significance to this.

During the course of this experiment, an experiment in which the same measurement was made was published by Schmid and Huber (1955). They give a value of σ_{pair} in lead of 3.12 ± 0.18 barns for 2.76 Mev. This represents an experimental error of about 6% as compared to some 25% in the present experiment. Their value is in agreement with that of Jaeger and Hulme.

Their experiment was similar to the present one in that Na^{22} was used to determine the detection efficiency, and the source strength was measured by a coincidence technique (this technique was not described in the paper but was presumably similar to that used in the present experiment). The method used by Schmid and Huber to produce and measure the pairs was, however, quite different. They made use of a "sandwich" consisting of a thin disk-shaped gamma ray source between two lead disks of the same diameter, the whole being housed in an aluminum "pill-box". This assembly was placed between a pair of scintillation counters in a coincidence circuit so that not only annihilation radiation but also primary photons from the source in large numbers entered the scintillators. Since liquid scintillators were employed, the background radiation could not readily be separated from the annihilation radiation by differential pulse height discrimination as was done in the present experiment. The net result was that annihilation radiation constituted only about 25% of the total coincidence rate. In calculating σ_{pair} it was necessary to make large theoretical corrections. Since the error given is primarily the statistical counting error, they have assumed that little error is implicit in these theoretical corrections.

REFERENCES

BETHE, H. and HEITLER, W. 1934. Proc. Roy. Soc., A, **146**: 83.
DE BENEDETTI, S. and SIEGEL, R. 1954. Phys. Rev. **94**: 955.
FISCHER, J. and MARSHALL, J. 1952. Rev. Sci. Instr. **23**: 417.
HOLLANDER, J. M., PERLMAN, J., and SEABORG, G. T. 1953. Revs. Mod. Phys. **25**: 469.
HULME, H. and JAEGER, J. 1936*a*. Proc. Roy. Soc. **153**: 443.
——— 1936*b*. Proc. Cambridge Phil. Soc. **32**: 158.
MACKLIN, P., LEDOFSKY, L., FELDMAN, L., and WU, C. S. 1950. Phys. Rev. **77**: 137.
MOTZ, J. W. 1955. Phys. Rev. **100**: 1560.
ORE, A. and POWELL, J. L. 1949. Phys. Rev. **75**: 1696.
SCHERR, R. and MILLER, R. H. 1954. Phys. Rev. **93**: 1076.
SCHMID, P. and HUBER, P. 1955. Helv. Phys. Acta, **28**: 369.
TOBAILLEM, J. 1955. J. phys. radium, **16**: 48.
WEST, H. J. 1956. Phys. Rev. **101**: 915.

ON FULLY DEVELOPED TURBULENT FLOW IN CURVED CHANNELS[1]

By A. W. Marris[2]

ABSTRACT

Formulae for the radial distribution of velocity and vorticity for the case of fully developed turbulent flow in the channel between concentric and infinitely long cylinders are developed on a similarity vorticity transfer theory, by postulating an Eulerian mixing length function dependent on both position and radius of curvature. The theoretical results obtained for the mean velocity distribution across the channel compare satisfactorily with existing experimental data when the curvature dependent parameters are given appropriate numerical values.

SUMMARY OF PRINCIPAL NOMENCLATURE

r = radius from center of curvature of annulus to representative point over which fluid flows.
θ = angular distance from fixed line to radius to representative point.
ρ = density of fluid, assumed constant.
$\tau_{r\theta}$ = turbulent shearing stress component at (r, θ).
ϵ_M = eddy diffusivity for momentum.
l_M = mixing length for momentum transfer.
V_θ = mean transverse velocity at radius r.
ζ = mean vorticity at (r, θ) in direction perpendicular to (r, θ) plane.
ϵ_V = eddy diffusivity for vorticity.
l_V = mixing length for vorticity transfer.
$\bar{P}$ = mean pressure at (r, θ).
R_1 = radius of internal boundary of channel.
R_2 = radius of external boundary of channel.
R = radius of cylindrical surface of separation of the two regions of channel.
$x_1 = r - R_1$.
$X_1 = R - R_1$.
$x_2 = R_2 - r$.
$X_2 = R_2 - R$.
ϕ_1, ϕ_2 = functions in mixing length hypothesis.
E_1, F_1, E_2, ζ_0, F_2 = parameters in theoretical velocity distribution.
V_{θ_m} = experimental mean velocity in channel.
E_1', F_1', E_2', ζ_0', $F_2' = E_1/V_{\theta_m}$, F_1/V_{θ_m}, E_2/V_{θ_m}, ζ_0/V_{θ_m}, F_2/V_{θ_m}, respectively.

1. INTRODUCTION

The mean velocity distribution in a curved channel is to be determined on a similarity theory of turbulence by postulating a mixing length of the form employed in the case of turbulent flow in a rectilinear channel but modified to allow for the effect of curvature and the resultant centrifugal forces.

[1]Manuscript received August 21, 1956.
Contribution from the Department of Civil Engineering, The University of British Columbia, Vancouver, British Columbia.
[2]Assistant Professor.

The channel considered will be the region between parallel concentric walls of constant radii R_1 and R_2. The channel will be of infinite depth. For flow in such a channel the centrifugal force created by the curvature will be in the direction of the mean velocity gradient $\partial V_\theta/\partial r$, and its effect will be manifested in the simplest possible way. For R_1 and R_2 infinite the case becomes that of flow in an infinite rectilinear channel.

The approach is a phenomenological one in that the mean velocity distribution resulting from the space-varying microscopic turbulent intensities, shears, and energy spectra of the fluctuating velocities is of prime interest rather than these complex microscopic parameters themselves. Present-day knowledge seems to be still insufficient for the formulation of a complete unarbitrary theory of a stable non-decaying fully developed turbulent field on the basis of these microscopic parameters, a fact which has been the reason for the recent intensive experimental work on turbulent microstructure (Eskinazi 1954; Laufer 1954). In this present work the microscopic transfer mechanism is regarded as being representable in an over-all way by a space-varying mixing length function.

Existing data are analyzed and for the problem under consideration the ideas of the vorticity transfer theory are chosen in favor of those of the momentum transfer theory.

2. BACKGROUND

Von Kármán (1930*a*, *b*; 1932; 1934*a*, *b*) in his original similarity theory of fully developed turbulent flow between rectilinear parallel planes assumed an Eulerian mixing length

$$l = k \frac{\partial u/\partial y}{\partial^2 u/\partial y^2} \tag{1}$$

where u is the longitudinal mean velocity (in x direction) at a distance y from the wall and k is a constant. It is seen that the mixing length depends on the velocity gradient and may be written

$$l = k \frac{\zeta}{\partial \zeta/\partial y} \tag{2}$$

where ζ is the vorticity in the z direction.

Goldstein (1937) applied this to both the momentum and vorticity transfer theories of the turbulent mechanism.

In the momentum transfer theory, the turbulent shearing stress is set, on the basis of Prandtl's hypothesis, as

$$\tau = \rho l^2 \left(\frac{\partial u}{\partial y}\right)^2 = \epsilon_M \frac{\partial u}{\partial y} \tag{3}$$

with l given by (1). In the vorticity transfer theory the rate M, at which x momentum is communicated to unit volume, is set in terms of l by

$$M = \rho l^2 \left(\frac{\partial u}{\partial y}\right)\left(\frac{\partial^2 u}{\partial y^2}\right) = \epsilon_V \frac{\partial^2 u}{\partial y^2} \tag{4}$$

where in each case l is given by equation (1). Goldstein found that the best agreement with the experimental work of Nikuradse (1929, 1932, 1933, etc.) was obtained on the momentum transfer theory.

Taylor (1937), in order to eliminate the singularities in l which von Kármán had to cut from the range of applicability of his equations, postulated

$$l = B(d-y) \tag{5}$$

where $2d$ is the distance between the parallel planes. On this somewhat arbitrary assumption* of l as a function of distance only over the whole half width of the channel he finds that the momentum and vorticity transfer theories give equally good agreement with experiment as far as the velocity distribution is concerned.

But it seems that it is impossible from the velocity distribution alone either to fix unambiguously the mixing length function or indeed to decide between the momentum and vorticity theories.

Such may not be the case for curved flow. Taylor (1935) has shown that for flow between concentric rotating cylinders the velocity distribution in the center 83.5% of the annulus is such as can be exactly explained on the vorticity transfer theory without having to make any assumption about the mixing length function, the theory immediately predicting the observed result of constant vorticity. This could only be explained on the momentum transfer theory under the assumption that no turbulent mixing takes place, a result immediately denied by the temperature distribution in a heat transfer experiment with the same set-up.

The reason why experimental data for this case can yield no information about the eddy diffusivity ϵ_V for vorticity is that the transverse pressure gradient in the annulus is zero.

On the modified vorticity transfer theory for statistically isotropic turbulence one has (Goldstein 1938*a*)

$$\overline{v\zeta' - w\eta'} = \epsilon_V\left(\frac{\partial\eta}{\partial z} - \frac{\partial\zeta}{\partial y}\right), \tag{6}$$

v, w, η', ζ' being the fluctuating components of turbulent velocity and vorticity in the y and z direction respectively. For the case of flow in concentric circles in a plane perpendicular to oz equation (6) yields

$$\overline{v_r\zeta'} = \epsilon_V(-\partial\zeta/\partial r) \tag{7}$$

where v_r is the radial component of the fluctuating turbulent velocity.

Again the rate of communication of momentum per unit volume is

$$M = \rho\overline{v_r\zeta'} = -\frac{\partial\bar{P}}{r\partial\theta}. \tag{8}$$

So that by (7) and (8)

$$\frac{1}{\rho}\frac{\partial\bar{P}}{r\partial\theta} = \epsilon_V\left(\frac{\partial\zeta}{\partial r}\right) = \epsilon_V\frac{\partial}{\partial r}\left(\frac{1}{r}\frac{\partial}{\partial r}(rV_\theta)\right), \tag{9}$$

V_θ being the transverse mean velocity at radius r.

*Author's comment on p. 506 (Taylor 1937).

It follows from (9) that if $\partial\bar{P}/r\partial\theta$ is zero then ζ is constant, as found experimentally, irrespective of the form of ϵ_V or the mixing length function.

Thus it seems that if the effect of curvature and associated centrifugal forces on the mixing length is to be investigated by correlation of theoretical and experimental velocity distributions, the case to be considered is that for turbulent flow in the curved channel described in the Introduction, for which case $\partial\bar{P}/r\partial\theta$ will not be zero, and the equations will be solvable for ϵ_V.

3. CHOICE OF VORTICITY TRANSFER THEORY

When the momentum transfer theory is applied to rectilinear fluid motion in which the mean velocity u is in the x direction and is a function of y only, the turbulent shearing stress τ_{xy} at any point in the fluid is given by

$$\tau_{xy}/\rho = \epsilon_M \, \partial u/\partial y \tag{10}$$

where ϵ_M is given by Prandtl's hypothesis

$$\epsilon_M = l^2|\partial u/\partial y|$$

and the mixing length l is decided upon as discussed above.

It is seen that whatever be the form of l the effect of the turbulence is to create an additional variable viscosity, and it has been indeed customary to assert that the turbulent mechanism is independent of, and unaffected by viscosity, so that the pressure equation is

$$\frac{1}{\rho}\frac{\partial\bar{P}}{\partial x} = \frac{\partial}{\partial y}\left[(\epsilon_M+\nu)\frac{\partial u}{\partial y}\right]. \tag{11}$$

When however the momentum transfer theory is applied to flow in circles the eddy diffusivity no longer appears merely as a turbulent viscosity.

For fully developed turbulent flow in a channel whose walls are concentric cylinders the turbulent shearing stress would, in the momentum transfer theory, be given by

$$\frac{\tau_{r\theta}}{\rho} = \epsilon_M\left(\frac{1}{r}\frac{\partial}{\partial r}(rV_\theta)\right), \tag{12}$$

Prandtl's hypothesis for ϵ_M now taking the form

$$\epsilon_M = \frac{l_M^{\,2}}{r}\left|\frac{\partial}{\partial r}(rV_\theta)\right|.$$

For purely laminar flow in the channel, on the other hand, one has for the viscous shearing stress

$$\frac{\tau_{r\theta}}{\rho} = \nu\left(\frac{\partial V_\theta}{\partial r}-\frac{V_\theta}{r}\right) = \nu\left(\frac{1}{r}\frac{\partial}{\partial r}(rV_\theta)-\frac{2V_\theta}{r}\right), \tag{13}$$

an equation which differs in form from equation (12).

The viscous shearing stress being very small in comparison with the turbulent stress, a basic criterion for the momentum transfer theory to be applicable to the case is that the stress function vanishes at

$$\partial V_\theta/\partial r = -V_\theta/r. \tag{14}$$

The experimental data of Wattendorf (1935) show that the turbulent stress does not vanish anywhere near $\partial V_\theta/\partial r = -V_\theta/r$, but about halfway

between $\partial V_\theta/\partial r = 0$ and $\partial V_\theta/\partial r = +V_\theta/r$, a result which casts grave doubt on the appropriateness of the momentum transfer theory to this kind of flow.

It has been mentioned above that the vorticity transfer theory holds in the closely related problem of flow between rotating cylinders, in which case the vorticity is sensibly zero over a large section of the annulus. For the case of channel flow Wattendorf finds that the vorticity is small over a large section of the flow, and that the slope of the vorticity distribution is continuously negative. The mean vorticity distribution is such that could well be created by transference through the turbulent fluctuations.

It is from these considerations that the vorticity transfer theory will be conditionally accepted to account for the turbulent mechanism.

4. THE MIXING LENGTH

Neglecting viscosity, the equation applicable to pressure flow in the curved channel envisaged is, on the vorticity transfer theory,

$$\frac{1}{\rho}\frac{\partial \bar{P}}{r\partial\theta} = \epsilon_V\left(\frac{\partial\zeta}{\partial r}\right) = \epsilon_V \frac{\partial}{\partial r}\left(\frac{1}{r}\frac{\partial}{\partial r}(rV_\theta)\right) \tag{9}$$

where on Prandtl's hypothesis

$$\epsilon_V = \frac{l_V^2}{r}\frac{\partial}{\partial r}(rV_\theta) = l_V^2\zeta. \tag{15}$$

So that equation (9) becomes

$$\frac{1}{\rho}\frac{\partial \bar{P}}{r\partial\theta} = l_V^2\zeta\frac{\partial\zeta}{\partial r} \tag{16}$$

and one can proceed no further without assumption concerning the mixing length l_V.

To allow for the differences in the effects of the convex inner surface and the concave outer surface on the flow, the annulus will be split up into two regions separated by a cylindrical surface $r = R$. Distances from the inner and outer

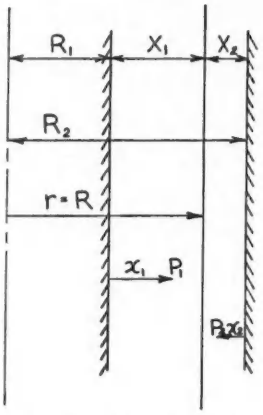

FIG. 1. Definition of variables.

cylindrical boundaries will be defined by x_1 and x_2 respectively as shown in Fig. 1; thus for

$$R_1 < r < R, \quad r = R_1 + x_1, \quad x_1 < R - R_1 = X_1, \tag{17}$$

and for

$$R < r < R_2, \quad r = R_2 - x_2, \quad x_2 < R_2 - R = X_2, \tag{18}$$

equation (16) now yields

$$\frac{1}{\rho}\frac{\partial \bar{P}}{r\partial\theta} = l_{V_1}{}^2 \zeta \frac{\partial \zeta}{\partial x_1} \quad \text{for } x_1 < X_1 \tag{16a}$$

and

$$\frac{1}{\rho}\frac{\partial \bar{P}}{r\partial\theta} = -l_{V_2}{}^2 \zeta \frac{\partial \zeta}{\partial x_2} \quad \text{for } x_2 < X_2 \tag{16b}$$

where it will be assumed that l_{V_1} is affected by R_1 only and l_{V_2} by R_2 only.

By analogy with von Kármán's hypothesis, for flow in a rectilinear channel, of a mixing length l given by

$$l = k\frac{\zeta}{\partial\zeta/\partial y}, \tag{2}$$

it seems logical to assume the mixing lengths l_{V_1} and l_{V_2} to be given by

$$l_{V_1} = \frac{\zeta}{\partial\zeta/\partial x_1}\phi_1\left(\frac{x_1}{r}\right), \tag{19}$$

$$l_{V_2} = \frac{\zeta}{\partial\zeta/\partial x_2}\phi_2\left(\frac{x_2}{r}\right), \tag{20}$$

such being dimensionally correct.

Wattendorf's experimental vorticity distribution indicates that $\partial\zeta/\partial r$ is not zero across the channel so that if the functions ϕ_1 and ϕ_2 are finite and continuous there are no singularities in the mixing length functions as there were for example in the case of flow in a rectilinear channel.

5. THE VELOCITY DISTRIBUTION

The forms of the functions $\phi_1(x_1/r)$ and $\phi_2(x_2/r)$ have to be determined by correlation with experiment. The functions and the vorticity and velocity distributions resulting from them will be considered in turn.

(*a*) *Inner Region*, $R_1 < r < R$

Take

$$\phi_1(x_1/r) = A_1(x_1/r)^{\frac{1}{2}} \tag{21}$$

where A_1 may involve the mean velocity, R_1, and perhaps R_2; then

$$l_{V_1} = \frac{A_1\zeta}{\partial\zeta/\partial x_1}\left(\frac{x_1}{r}\right)^{\frac{1}{2}}$$

and so, by (16*a*),

$$\frac{1}{\rho}\frac{\partial \bar{P}}{r\partial\theta} = \frac{A_1{}^2\zeta^3}{\partial\zeta/\partial x_1}\left(\frac{x_1}{r}\right). \tag{22}$$

On the assumption of fully developed flow, i.e. that the radial flow pattern is the same at each section, so that V_r is independent of θ, then $\partial P/\partial\theta$ is independent of r.*

Equation (22) may then be written

$$x_1 dx_1 = B_1\, d\zeta/\zeta^3 \tag{23}$$

or

$$x_1^2 = C_1/\zeta^2 + D_1, \tag{24}$$

and from Wattendorf's result it is noted that ζ is very large near $x_1 = 0$ so that D_1 may be taken as zero.

One obtains for the vorticity distribution in the inner region the rectangular hyperbolic form

$$x_1\zeta = E_1, \quad x_1 < X_1. \tag{25}$$

For the velocity distribution, one now has, from (25),

$$(r-R_1)\frac{1}{r}\frac{\partial}{\partial r}(rV_\theta) = E_1 \tag{26}$$

or

$$\begin{aligned} rV_\theta &= E_1 \int \frac{r\,dr}{r-R_1} \\ &= E_1(r+R_1\log(r-R_1)) + F_1 \end{aligned} \tag{27}$$

or finally

$$V_\theta = E_1\left(1+\frac{R_1\log(r-R_1)}{r}\right)+\frac{F_1}{r} \tag{28}$$

for $R_1 < r < R$, where the parameters E_1 and F_1 are likely to depend on the transverse pressure gradient, the mean flow velocity, and the radii of curvature of the channel walls.

(*b*) *Outer Region* $R < r < R_2$

In this region the vorticity function is regarded as the superposition of an effect due to the outer wall on a small vorticity already present as an invader from the inner region.

By the time x_1 has reached the value X_1, ζ is small and but slowly varying, so that very little error will be introduced by taking the invading vorticity as having a small positive constant value ζ_0.

If ζ then is total vorticity at x_2 in the outer region, equation (16*b*) may be taken as applying to the component $(\zeta-\zeta_0)$ since by equation (16) no transverse pressure gradient can be created by a radially constant vorticity

$$\frac{1}{\rho}\frac{\partial \bar{P}}{r\partial\theta} = -l_{V_2}{}^2(\zeta-\zeta_0)\frac{\partial(\zeta-\zeta_0)}{\partial x_2} = -l_{V_2}{}^2(\zeta-\zeta_0)\frac{\partial\zeta}{\partial x_2}. \tag{29}$$

Taking

$$\phi_2(x_2/r) = A_2(x_2/r)^{\frac{1}{2}} \tag{30}$$

as before, one has from (20)

*Wattendorf (1935), p. 577.

$$l_{v_2} = A_2\left(\frac{\zeta-\zeta_0}{\partial(\zeta-\zeta_0)/\partial x_2}\right)\left(\frac{x_2}{r}\right)^{\frac{1}{2}} = A_2\frac{(\zeta-\zeta_0)}{\partial\zeta/\partial x_2}\left(\frac{x_2}{r}\right)^{\frac{1}{2}} \tag{31}$$

and from (29)

$$\frac{1}{\rho}\frac{\partial\bar{P}}{r\partial\theta} = -A_2{}^2\frac{(\zeta-\zeta_0)^3}{\partial\zeta/\partial x_2}\left(\frac{x_2}{r}\right) \tag{32}$$

or since $\partial P/\partial\theta$ is independent of r

$$x_2dx_2 = B_2\frac{d\zeta}{(\zeta-\zeta_0)^3} \tag{33}$$

or

$$x_2{}^2 = \frac{C_2}{(\zeta-\zeta_0)^2}+D_2 \tag{34}$$

and the constant D_2 may be taken as zero since ζ is very large negative for x_2 small.

The vorticity distribution in the outer region is thus given by

$$x_2(\zeta-\zeta_0) = E_2, \qquad x_2 < X_2, \tag{35}$$

and E_2 is negative.

For the velocity distribution in the outer region, one has by (35)

$$(R_2-r)\left[\frac{1}{r}\frac{\partial}{\partial r}(rV_\theta)-\zeta_0\right] = E_2 \tag{36}$$

or

$$rV_\theta = \int\left(\frac{E_2r}{R_2-r}+\zeta_0r\right)dr$$

$$= -E_2(r+R_2\log(R_2-r))+\frac{\zeta_0r^2}{2}+F_2 \tag{37}$$

or finally

$$V_\theta = -E_2\left(1+\frac{R_2\log(R_2-r)}{r}\right)+\frac{\zeta_0r}{2}+\frac{F_2}{r} \tag{38}$$

where once again the parameters E_2, F_2, and ζ_0 are likely to depend on the transverse pressure gradient, the mean flow velocity, and the radii of curvature of the channel walls.

By continuity of vorticity at $r = R$ one obtains from equations (25) and (35) the relation

$$\frac{E_1}{R-R_1} = \frac{E_2}{R_2-R}+\zeta_0. \tag{39}$$

By continuity of velocity at $r = R$ one has from equations (28) and (38)

$$(E_1+E_2)R-\tfrac{1}{2}\zeta_0R^2+F_1-F_2+E_1R_1\log(R-R_1)+E_2R_2\log(R_2-R) = 0. \tag{40}$$

6. CORRELATION WITH EXPERIMENTAL RESULTS

It remains to see how the distributions given by (28) and (38) with the relations (39) and (40) between the parameters compare with available experimental data.

When Wattendorf's data* are examined for his two channels for which $R_1 = 20$ cm., $R_2 = 25$ cm. and $R_1 = 45$ cm., $R_2 = 50$ cm., it is noted that in both cases the function V_θ/V_{θ_m} seems to be independent of V_{θ_m} (the current nomenclature is used to denote transverse velocity).

It would seem then that the above parameters E_1, F_1, E_2, and F_2 merely contain V_{θ_m} as a multiplier, an idea which is supported by the dimensional form of equations (25) and (35).

One may in consequence write equations (28) and (38) in the forms

$$(28a)\quad \frac{V_\theta}{V_{\theta_m}} = E_1'\left(1+\frac{R_1\log(r-R_1)}{r}\right)+\frac{F_1'}{r} \quad \text{for inner region } R_1 < r < R,$$

$$(38a)\quad \frac{V_\theta}{V_{\theta_m}} = -E_2'\left(1+\frac{R_2\log(R_2-r)}{r}\right)+\frac{\zeta_0' r}{2}+\frac{F_2'}{r}$$

for outer region $R < r < R_2$,

with the continuity condition at $r = R$,

$$(39a)\qquad \frac{E_1'}{R-R_1} = \frac{E_2'}{R_2-R}+\zeta_0',$$

$$(40a)\quad (E_1'+E_2')\,R-\frac{\zeta_0' R^2}{2}+F_1'-F_2'+E_1'R_1\log(R-R_1)+E_2'R_2\log(R_2-R) = 0.$$

Except for a region near the inner (convex) wall, Wattendorf's velocity distribution can be fitted by equations of the form (28*a*) and (38*a*). One obtains, for the smaller channel ($R_1 = 20$ cm., $R_2 = 25$ cm.),

$$(41)\qquad \begin{cases} E_1' = 0.0766, \\ F_1' = 20.7, \\ E_2' = -0.0596, \\ \tfrac{1}{2}\zeta_0' = 0.02373, \\ F_2 = 9.20, \end{cases}$$

so that

$$(28b)\quad \frac{V_\theta}{V_{\theta_m}} = 0.0766+\frac{3.527}{r}\log_{10}x_1+\frac{20.7}{r}, \qquad R_1 < r < R,$$

$$(38b)\quad \frac{V_\theta}{V_{\theta_m}} = 0.0596+\frac{3.43}{r}\log_{10}x_2+0.02373r+\frac{9.20}{r}, \qquad R < r < R_2,$$

and for the larger channel ($R_1 = 45$ cm., $R_2 = 50$ cm.)

$$(42)\qquad \begin{cases} E_1' = 0.033, \\ F_1' = 48.7, \\ E_2' = -0.1061, \\ \tfrac{1}{2}\zeta_0' = 0.02566, \\ F_2 = -15.8, \end{cases}$$

*Wattendorf (1935), pp. 574, 575.

so that

$$(28c) \qquad \frac{V_\theta}{V_{\theta_m}} = 0.033+\frac{0.342}{r}\log_{10}x_1+\frac{48.7}{r}, \qquad R_1 < r < R,$$

$$(38c) \qquad \frac{V_\theta}{V_{\theta_m}} = 0.1061+\frac{12.217}{r}\log_{10}x_2+0.02566r-\frac{15.8}{r}, \qquad R < r < R_2.$$

The curves from equations (28b), (38b) and those from equations (28c), (38c) are shown respectively in Fig. 2 and Fig. 3, and the experimental points abstracted from the velocity distribution curves given in Wattendorf's paper are also given.

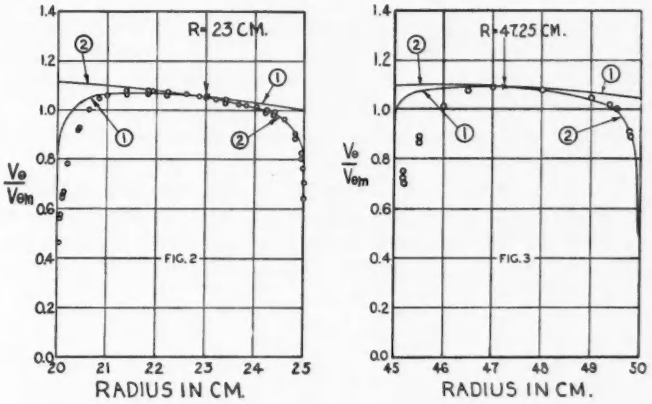

FIG. 2. Velocity distribution in channel with boundaries of radius $R_1 = 20$ cm. and $R_2 = 25$ cm.
1, theoretical curve $V_\theta/V_{\theta_m} = 0.0766+3.527\log_{10}(r-20)/r+20.7/r$.
2, theoretical curve $V_\theta/V_{\theta_m} = 0.0596+3.43\log_{10}(25-r)/r+0.02373r+9.20/r$.
Points shown as small circles are Wattendorf's experimental distribution for $V_{\theta_m} = 844$ cm./sec., $V_{\theta_m} = 1765$ cm./sec., and $V_{\theta_m} = 2500$ cm./sec.

FIG. 3. Velocity distribution in channel with boundaries of radius $R_1 = 45$ cm. and $R_2 = 50$ cm.
1, theoretical curve $V_\theta/V_{\theta_m} = 0.033+0.342\log_{10}(r-45)/r+48.7/r$.
2, theoretical curve $V_\theta/V_{\theta_m} = 0.1061+12.217\log_{10}(50-r)/r+0.02566r-15.8/r$.
Points shown as small circles are Wattendorf's experimental distribution for $V_{\theta_m} = 3100$ cm./sec., $V_{\theta_m} = 2500$ cm./sec., and $V_{\theta_m} = 1000$ cm./sec.

As stated above, a satisfactory fit is obtained except for the region near the inside wall of the channel, where the vorticity transfer theory may be expected to break down anyway.

From the points of intersection of the curves for the two regions of the channel the solution R of the equation (40a) is obtained graphically. One obtains $R = 23$ (approximately) for the smaller channel and $R = 47.25$ (approximately) for the larger channel.

Substituting the values of E_1', E_2', and ζ_0' in equation (39a) for continuity of vorticity of $r = R$, one obtains

$$(39b) \qquad \frac{0.0766}{R-20} = \frac{-0.0596}{25-R}+0.04746 \quad \text{for smaller channel,}$$

and

$$\frac{0.033}{R-45} = \frac{-1.061}{50-R} + 0.05132 \quad \text{for larger channel.} \tag{39c}$$

Setting $R = 23$ in equation (39*b*) one obtains the value 0.0255 for the left-hand side against 0.0177 for the right-hand side, and setting $R = 47.25$ in (34*c*) one obtains 0.0147 for the left-hand side against 0.0127 for the right-hand side.

Considering the fact of the small variation of velocity in the center region of the channel so that a relatively large change in the position of the intersection point R may not appreciably alter the form of the curves, and considering also the large number of parameters that can be adjusted to create a fit so that values of E_1', F_1', E_2', F_2', ζ_0' must at best be regarded as approximate, the equation (39*b*) can, it is felt, be considered as adequately satisfied. At least until further experimental evidence is obtained. It is remarked however that the values of R have been taken as distances from the channel boundaries; possibly they should be taken as distances from the boundaries of the region where the vorticity transfer theory holds.

With regard to the vorticity distribution across the channel, Wattendorf gives the experimental curve only for the smaller channel and the best fit to it the author was able to obtain was that given by the pair of rectangular hyperbolas

$$\zeta x_1 = 186, \tag{43}$$

$$(\zeta - 86)x_2 = -99, \tag{44}$$

with $R = 23$ cm. approximately.

Bearing in mind the smallness of the vorticity over the center region of the channel and then the fact of its steep slope nearer the channel walls (i.e. in the regions where the vorticity transfer theory is likely to break down) equations (43) and (44) must be regarded as very approximate.

Perhaps all that should be said is that with E_1' and ζ_0' positive and E_2' negative as found above they have the correct form.

Proceeding very tentatively however, one would have, from equations (43) and (44),

$$\begin{cases} E_1' V_{\theta_m} = 186, \\ E_2' V_{\theta_m} = -99, \\ \zeta_0' V_{\theta_m} = 86, \end{cases} \tag{45}$$

giving $E_1'/E_2' = 1.87$ as opposed to $E_1'/E_2' = 1.29$ as given by the velocity distribution, and $E_1'/\zeta_0' = 1.152$ as opposed to $E_1'/\zeta_0' = 1.255$ as given by the velocity distribution.

It is again remarked that the extraction of data from a vorticity curve constructed from such a slowly varying velocity distribution must be regarded as a questionable process.

Eskinazi (1954, Fig. 5) gives experimental data for the mean velocity distribution for air flow at Reynolds number 74,200 in a curved channel of the type envisaged with $R_1 = 27$ in. $= 58.58$ cm. and $R_2 = 30$ in. $= 76.2$ cm. In this work the dimensionless velocity function is obtained by dividing the local mean velocity by the maximum velocity rather than by the mean flow velocity, but the form of this distribution is very similar to that of Wattendorf for the larger channel. From the point of view of this theory the significant feature is the widening with increasing channel radius of the region adjacent to the inner wall of the channel over which the velocity is less than prophesied by the present vorticity transfer considerations.

7. COMMENTS AND CONCLUSION

The similarity vorticity transfer theory of flow in a curved channel, as given above, yields a velocity distribution which can be fitted to the limited experimental data available except for a region near the inner, convex, boundary. This is to be expected, firstly because of the existence of laminar and "semi-turbulent" layers immediately adjacent to the wall, and secondly on the basis that the vorticity transfer theory is known not to apply in the vicinity of solid boundaries (Taylor 1935).

The equations derived for V_θ/V_{θ_m} contain parameters to be determined by correlation with experiment. The parameters depend on curvature but apparently not on the mean transverse velocity V_{θ_m}. More comprehensive data are required if they are to be thoroughly checked and the nature of their dependence on curvature and transverse pressure gradient satisfactorily established.

A vorticity distribution in the form of a pair of rectangular hyperbolas was theoretically obtained, and this seemed to be the form of the single experimental vorticity distribution at the author's disposal.

Concerning the range of channel section over which the theoretical results seem to be valid, it is found that the width of the near-to-inner-wall region of disagreement is much greater in relation to the total channel width when the radius of curvature of the inner wall is 45 cm. than when it is 20 cm., showing that as the radius of curvature increases, the region over which this vorticity transfer theory holds becomes relatively less, and that for a very large radius of curvature it may not hold at all. In this connection of deducing whether the flow in a straight channel can be regarded as a limiting case of flow in a curved channel, it is remarked that a mixing length of an apparently analogous form to that used here, the velocity distribution straight channel flow, has best been obtained using the ideas of momentum transfer theory (Goldstein 1937). It is remarked too that while Wattendorf was able to obtain general correlation of experimental observed velocity distribution for his two different channels, he was unable to include the results for flow in a straight channel in the correlation (Wattendorf 1935). It would appear then that just as original instability seems to occur in a different way for a curved channel than for a straight channel so also may the mechanism of fully developed turbulent mixing be different (Goldstein 1938*b*).

In conclusion the need is again expressed for considerable experimental data of Wattendorf's type, but for channels of widely varying curvature, so that curvature dependent parameters of the type proposed may be more systematically investigated. Moreover, Wattendorf's experimental data were taken at rather high velocities. In this case one was able to eliminate V_{θ_m} from the parameters but one wonders whether this would still be possible at lower velocities.

ACKNOWLEDGMENT

This work was carried out under National Research Council of Canada Grant N.R.C. G.514.

REFERENCES

ESKINAZI, S. 1954. Report I–20. The Johns Hopkins University Mech. Eng. Dept. Internal Flow Research.
GOLDSTEIN, S. 1937. Proc. Roy. Soc. (London), A, **159**: 473.
——— 1938*a*. Modern developments in fluid dynamics. Oxford at the Clarendon Press. p. 214.
——— 1938*b*. Modern developments in fluid dynamics. Oxford at the Clarendon Press. p. 322.
KÁRMÁN, TH. VON. 1930*a*. Nachr. Ges. Wiss. Göttingen, 58.
——— 1930*b*. Proc. Third Intern. Congr. Appl. Mech., Stockholm, **1**: 83.
——— 1932. Hydromechanische Probleme des Schiffsantriebs. Hamburg. p. 63.
——— 1934*a*. J. Aeronaut. Sci. **1**: 1.
——— 1934*b*. Proc. Fourth Intern. Congr. Appl. Mech., Cambridge. p. 67.
LAUFER, J. 1954. Rept. 1174. N.A.C.A.
NIKURADSE, J. 1929. Forsch. Arb. Ing. Wes. No. 289.
——— 1932. Forschungsheft, No. 356.
——— 1933. Forschungsheft, No. 361.
TAYLOR, G. I. 1935. Proc. Roy. Soc. (London), A, **151**: 494.
——— 1937. Proc. Roy. Soc. (London), A, **159**: 496.
WATTENDORF, F. L. 1935. Proc. Roy. Soc. (London), A, **148**: 565.

FERMI DIAD 10^00 AND 02^00 OF NITROUS OXIDE[1]

By K. Narahari Rao and Harald H. Nielsen

ABSTRACT

Measurement of the fine structure of the bands ν_1 and $2\nu_2{}^0$ of nitrous oxide has led to an evaluation of the centrifugal stretching constants of the Fermi diad 10^00 and 02^00. It was found that as compared to the value in the ground state, the change in the centrifugal stretching constant of the 02^00 level is much more than in the 10^00 level. This result has been discussed in relation to the theory of Nielsen, Amat, and Goldsmith (1956). The following revised values have been obtained for some of the molecular constants of $N_2{}^{14}O^{16}$:

$$\Delta_0 = G_0(10^00) - G_0(02^00) = 100.2 \pm 3 \text{ cm}^{-1},$$
$$K = 42.3 \pm 3 \text{ cm}^{-1} \text{ or } W = 29.9 \pm 2.0 \text{ cm}^{-1},$$
$$\alpha_1 = 1.99 \times 10^{-3} \text{ cm}^{-1}, \alpha_2 = -0.56 \times 10^{-3} \text{ cm}^{-1}.$$

I. INTRODUCTION

During the past two years, there has been a renewal of interest in the role played by Fermi resonance in linear polyatomic molecules. The experimental studies by Courtoy and Herzberg (1955) and some work done in our own laboratory by Rossmann, France, Rao, and Nielsen (1956) have shown that in the case of the carbon dioxide molecule, the centrifugal stretching constants of levels perturbed by Fermi resonance are significantly different from the value in the ground state of the molecule. This result has prompted a re-examination of the theory on more rigorous lines, and the discussion of Nielsen, Amat, and Goldsmith (1956) relates to the general problem of anomalous centrifugal stretching constants in linear polyatomic molecules. For a satisfactory elucidation of this problem there is need to obtain experimental values of the centrifugal stretching constants in different molecular levels. It is proposed to present in this paper some information obtained in the case of the nitrous oxide molecule since it is of a different nature compared to the results in the carbon dioxide molecule.

To be sure, from a study of a number of the photographic infrared bands of nitrous oxide, G. Herzberg and L. Herzberg (1950) have shown that the effect of Fermi resonance between the levels 10^00 and 02^00 of nitrous oxide is much more important than has usually been realized. The later work of Thompson and Williams (1951, 1953), Douglas and Møller (1954), and Plyler *et al.* (1956) substantiated this conclusion. However, the data available for the bands ν_1 and $2\nu_2{}^0$ have been in a rather unsatisfactory state. Since the earlier work of Plyler and Barker (1931, 1932) these bands were studied again by Shaw, Oxholm, and Claassen (1952). But, as these latter authors confined their work only to the identification of solar spectra, their measurements did not extend to J values large enough for any evaluation of the rotational constants.

[1]Manuscript received July 18, 1956.
Contribution from the Physics Department, Ohio State University, Columbus, Ohio. Supported, in part, by The Office of Ordnance Research, U.S. Army, through contracts with The Ohio State University Research Foundation.
The results in this paper were reported at the Spectroscopy Symposium, The Ohio State University, June, 1956.

II. EXPERIMENTAL TECHNIQUES

Observations used in the present investigation were obtained with a prism grating infrared spectrometer of this University. As the grating was kept in a vacuum while measurements were being made, vacuum wave numbers of the spectral lines could be obtained directly without having to make any corrections for the index of refraction of the medium housing the grating. In measuring the bands ν_1 and $2\nu_2{}^0$, two main problems were encountered, viz. (i) wave length calibrations and (ii) interference due to "hot" bands of nitrous oxide. As regards wave length calibrations various methods are being critically examined in this laboratory by using "difference" bands of nitrous oxide. Results in the present paper are based on measurements made with reference to observations on the fundamental vibration–rotation band lines of the carbon monoxide molecule in higher orders of the grating in the manner described by Rossmann, Rao, and Nielsen (1956). It is realized that this is not the most precise method of determining the positions of infrared lines. Nevertheless, in view of our past experience* it is believed that the data obtained by this method lead to reasonably good results when used in the particular combination plots described in the next section. With regards to the second problem, viz. the "hot" bands, it was found desirable to minimize their interference by cooling the absorbing gas to dry ice temperatures. Indeed, one set of observations was obtained by circulating vapor of liquid nitrogen through a copper coil wrapped around the absorption cell. As can be seen from Fig. 1 the spectrum marked (*b*) obtained in this manner is practically free from "hot" bands. This procedure has enabled us to locate the centers of the rotational lines of ν_1 and $2\nu_2{}^0$ with better accuracy.

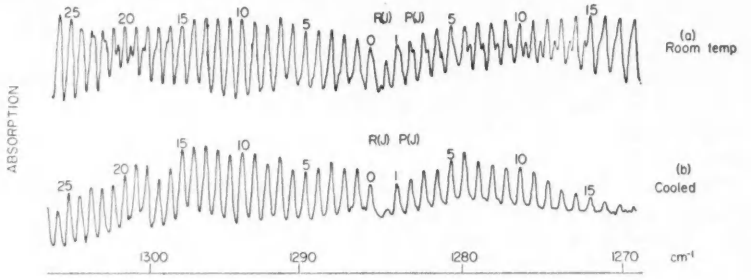

FIG. 1. ν_1 of nitrous oxide at 7.8 μ.

III. RESULTS

The absorption bands ν_1 and $2\nu_2{}^0$ have for their lower levels the ground state of the nitrous oxide molecule referred to as the 00^00 level.† The upper states involved in these transitions are the levels 10^00 and 02^00 which are perturbed

*Compare, for example, (*a*) combination plot of Fig. 2 by Rossmann, France, Rao, and Nielsen (1956) with appropriate results of Courtoy and Herzberg (1955) and (*b*) the ground state combination differences from measurement of ν_2 by Lakshmi, Rao, and Nielsen (1956) with similar values from the work of Douglas and Møller (1954).

†Most of the notation used here follows G. Herzberg, *Infrared and Raman Spectra of Polyatomic Molecules* (D. Van Nostrand Company, Inc., New York, 1945).

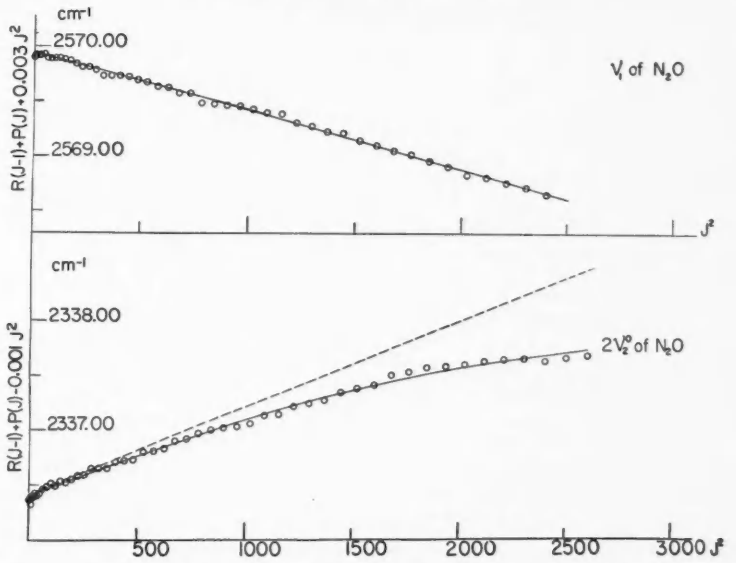

FIG. 2. Plot of $R(J-1)+P(J)$ against J^2 for ν_1 and $2\nu_2{}^0$ of $N_2{}^{14}O^{16}$.

by Fermi resonance. Fig. 2 shows the combination relation $R(J-1)+P(J)$ plotted against J^2 for these two bands. Since

$$R(J-1)+P(J) = 2\nu_0+2(B'-B'')J^2-2(D'-D'')J^2(J^2+1), \tag{1}$$

the deviation from linearity in this graph gives a measure of the deviation of the D_{10^00} or D_{02^00} value from the ground state value D_{00^00}. The striking result is that the $|D_{02^00}-D_{00^00}|$ value is much larger than the $|D_{10^00}-D_{00^00}|$ value. In other words, in nitrous oxide the average centrifugal stretching constant of the Fermi diad 10^00 and 02^00 is different from the ground state value. It is of interest to recall that in the case of the carbon dioxide bands the average centrifugal stretching constant of a Fermi diad is very nearly equal to the D_{00^00} value of the CO_2 molecule.

Table I summarizes the molecular constants obtained from the above combination plots and these results will form the basis for the discussion given in the remaining sections of this paper.

TABLE I

MOLECULAR CONSTANTS OF THE FERMI DIAD 10^00 AND 02^00 OF NITROUS OXIDE (CM^{-1})

$B_{10^00}-B_{00^00} = -0.0017_7 = -\alpha_1$ (perturbed)
$B_{02^00}-B_{00^00} = +0.0009_0 = -2\alpha_2$ (perturbed)
(a) $D_{10^00}-D_{00^00} < |1.5\times10^{-8}|$
$D_{02^00}-D_{00^00} = 5.4\times10^{-8}\pm1.5\times10^{-8}$
$\nu_1 = 1284.9_6$ $2\nu_2{}^0 = 1168.2_0$
(b) $\Delta = [G(10^00)-G(02^00)]_{\text{perturbed}} = 116.7_6$

(a) Actually a least squares solution up to $J = 50$ gave $D_{10^00}-D_{00^00} = -0.3\times10^{-8}$ cm^{-1} but the scatter still present in our data limits the accuracy of ΔD to $\pm1.5\times10^{-8}$ cm^{-1}.

(b) This value for Δ agrees with what has been derived from difference bands $(\nu_3-\nu_1)$ and $(\nu_3-2\nu_2{}^0)$ of N_2O measured by us (unpublished work).

IV. THEORY

Nielsen, Amat, and Goldsmith (1956) worked out formulae to represent the centrifugal stretching constants for levels of linear polyatomic molecules which are perturbed by Fermi resonance. As applied to the 10^00 and 02^00 levels of the nitrous oxide molecule they can be written as follows:

Level 10^00:

$$(2)\qquad (\Delta D)_{\nu_1} = D_{10^00}-D_{00^00} = -[B_{10^00}-B_{02^00}]^2\frac{\Delta^2-\Delta_0^2}{4\Delta^3}-\frac{q^2(\Delta_0-\Delta)}{\Delta(8X_{ll}-\Delta_0-\Delta)}$$

Level 02^00:

$$(3)\qquad (\Delta D)_{2\nu_2^0} = D_{02^00}-D_{00^00} = +[B_{10^00}-B_{02^00}]^2\frac{\Delta^2-\Delta_0^2}{4\Delta^3}+\frac{q^2(\Delta_0+\Delta)}{\Delta(8X_{ll}-\Delta_0+\Delta)}$$

where

$$(4)\qquad \Delta^2 = \Delta_0^2+2K^2,$$

Δ being the separation between the perturbed levels 10^00 and 02^00; Δ_0 is the separation for no perturbation and K is the Fermi interaction term which is the same as b in Dennison's discussion (1940) and $W\sqrt{2}$ in the nomenclature of Herzberg. q is the l-type doubling constant used exactly in the same way as defined by Herzberg and X_{ll} corresponds to g_{22} in Herzberg's notation. The rotational constants B occurring on the right-hand side of (2) and (3) are unperturbed values.

We shall return to the expressions (2)–(4) after considering the relation connecting the perturbed B values of the levels 10^00 and 02^00 with the unperturbed rotational constants of nitrous oxide. In this connection one has to solve the following secular determinant:

$$(5)\qquad \begin{vmatrix} G_0(10^00)+B_{10^00}J(J+1)-\epsilon & -K/\sqrt{2} \\ -K/\sqrt{2} & G_0(02^00)+B_{02^00}J(J+1)-\epsilon \end{vmatrix} = 0,$$

where ϵ is the perturbed term value and the other symbols have the meaning given earlier. After making use of the Maclaurin's series expansion appropriately it is easily seen that

$$(6)\qquad \epsilon = f(\text{vibrational term values})+\tfrac{1}{2}(B_{10^00}+B_{02^00})J(J+1)$$
$$\pm J(J+1)\{\Delta_0/2\sqrt{\Delta_0^2+2K^2}\}(B_{10^00}-B_{02^00}),$$

$$(\Delta B)_{\text{perturbed}} = [B_{10^00}-B_{02^00}]_{\text{perturbed}}$$
$$(7)\qquad = [B_{10^00}-B_{02^00}]_{\text{unperturbed}}\times(\Delta_0/\sqrt{\Delta_0^2+2K^2}).$$

Equations (4) and (5) should allow us to evaluate Δ_0 and K provided that $[B_{10^00}-B_{02^00}]_{\text{unperturbed}}$ can be calculated accurately.

An interesting and useful corollary follows from equation (7). It is necessary that

(8) $(\Delta B)_{\text{perturbed}}/(\Delta B)_{\text{unperturbed}}$ should be less than 1

in order that K may be real. The previously available rotational constants of N_2O have given for $(\Delta B)_{\text{unperturbed}}$ a value larger than $(\Delta B)_{\text{perturbed}}$ given in Table I, thus making K imaginary. The uncertainty in these earlier rotational constants was due to a lack of an accurate value for the constant α_2. We are now in a position to remove these uncertainties and therefore to evaluate the constants Δ_0 and K.

V. EVALUATION OF SOME MOLECULAR CONSTANTS

In the relation

$$B_{v_1v_2v_3} = B_e-\alpha_1(v_1+\tfrac{1}{2})-\alpha_2(v_2+1)-\alpha_3(v_3+\tfrac{1}{2}) \tag{9}$$

the constants B_e and α_3 are satisfactorily known from previous work (see Douglas and Møller (1954) for the latest values). The others are re-evaluated below:

α_2:

From the measurement of ν_2 of N_2O at 17 μ, Lakshmi, Rao, and Nielsen (1956) have derived that $B_{01^10}{}^{(d)}-B_{0000} = 0.16_4\times10^{-3}$ cm^{-1} $= -\alpha_2{}^{(PR)}$. This relation along with the $q_{010} = 0.79_2\times10^{-3}$ cm^{-1} obtained from the microwave work of Burrus and Gordy (1956) leads to a value of $\alpha_2 = -0.56\times10^{-3}$ cm^{-1} since

$$\alpha_2 = -\tfrac{1}{2}q_{010}+\alpha_2{}^{(PR)}. \tag{10}$$

α_1:

The value of $(\alpha_1+2\alpha_2)$ is not affected by Fermi resonance and, therefore, from the constants in Table I, we find that

$$\alpha_1+2\alpha_2 = +0.87\times10^{-3}\text{ cm}^{-1}.$$

Using the α_2 calculated above we obtain $\alpha_1 = 1.99\times10^{-3}$ cm^{-1}.

Incidentally, from the experimentally measured $(\alpha_1+2\alpha_2+\alpha_3)$ by Douglas and Møller (1954) we derive $\alpha_1+2\alpha_2 = 0.88\times10^{-3}$ cm^{-1} in good agreement with the present work.

Δ_0 and K:

From equation (9) it follows that

$$[B_{10^00}-B_{02^00}]_{\text{unperturbed}} = -\alpha_1+2\alpha_2.$$

Equations (7) and (11) and the $(\Delta B)_{\text{perturbed}}$ from Table I give

$$2.67\times10^{-3}/3.11\times10^{-3} = \Delta_0/\sqrt{\Delta_0{}^2+2K^2}. \tag{12}$$

From (4) we have

$$(116.76)^2 = \Delta_0{}^2+2K^2. \tag{13}$$

Equations (12) and (13) when solved for the two unknowns Δ_0 and K yield $\Delta_0 = 100.24$ cm^{-1} and $K = 42.32$ cm^{-1}. We believe that these constants are accurate to within ±3 cm^{-1}. It may be pointed out that Amat and Grenier-

Besson (1954) have attempted calculations of the vibrational constants of nitrous oxide taking account of Fermi resonance, and their estimate for $K \simeq 40$ cm^{-1} comes quite close to the value derived above. In order to introduce further refinement into these vibrational calculations it is necessary to have experimental data on more vibration–rotation bands. Appropriate infrared bands of nitrous oxide are being studied in this laboratory.

Centrifugal Stretching Constants and X_{ll} or g_{22}:

In the relations (2) and (3) one notices two separate terms contributing to the particular D value of the perturbed states. The first one is due to Fermi resonance and the second one is due to "l-type resonance". The l-type resonance is distinguished from l-type doubling in the respect that in l-type resonance the matrix elements $(l|l\pm2)$ which produce the interaction connect the non-degenerate sublevels of a state v_s with different values of $|l_s|$ whereas in l-type doubling the matrix elements connect the degenerate levels $l = +1$ and $l = -1$. This l-type resonance term contributes only to the D-values and does not affect the B values. As $(\Delta+\Delta_0)$ and $(\Delta-\Delta_0)$ respectively appear in the denominators of the l-type resonance term of the 10^00 and 02^00 levels, in nitrous oxide it is the smallness of $\Delta-\Delta_0$ $(=16$ cm$^{-1})$ as compared to $\Delta+\Delta_0$ $(=217$ cm$^{-1})$ that makes $|D_{02^00}-D_{00^00}|$ larger than $|D_{10^00}-D_{00^00}|$.

Using the observed $(\Delta D)_{2\nu_2{}^0}$ and equation (3), the constant X_{ll} has been calculated to be 0.78 cm^{-1}. We would like to emphasize that the value of X_{ll} (or g_{22}) determined in this manner gives only an order of magnitude to this constant. With the new data that are being obtained on other vibration–rotation bands of nitrous oxide it is anticipated that a better value can be derived for this constant.

ACKNOWLEDGMENT

Our thanks are due to Dr. G. Amat for useful discussions during the writing of this paper and to Mr. T. J. Coburn for his help in the experimental work.

REFERENCES

Amat, G. and Grenier-Besson, M. L. 1954. J. phys. radium, **15**: 591.
Burrus, C. A. and Gordy, W. 1956. Phys. Rev. **101**: 599.
Courtoy, C. P. and Herzberg, G. 1955. J. Chem. Phys. **23**: 975.
Dennison, D. M. 1940. Revs. Mod. Phys. **12**: 175.
Douglas, A. E. and Møller, C. K. 1954. J. Chem. Phys. **22**: 275.
Herzberg, G. and Herzberg, L. 1950. J. Chem. Phys. **18**: 1551.
Lakshmi, K., Rao, N. K., and Nielsen, H. H. 1956. J. Chem. Phys. **24**: 811.
Nielsen, H. H., Amat, G., and Goldsmith, M. 1956. To be published.
Plyler, E. K. and Barker, E. F. 1931. Phys. Rev. **38**: 1827.
——— 1932. Phys. Rev. **41**: 369.
Plyler, E. K., Tidwell, E. D., and Allen, H. C., Jr. 1956. J. Chem. Phys. **24**: 95.
Rossman, K., Rao, N. K., and Nielsen, H. H. 1956. J. Chem. Phys. **24**: 103.
Rossmann, K., France, W., Rao, N. K., and Nielsen, H. H. 1956. J. Chem. Phys. **24**: 1007.
Shaw, J. H., Oxholm, M. L., and Claassen, H. H. 1952. Astrophys. J. **116**: 554.
Thompson, H. W. and Williams, R. L. 1951. Proc. Roy. Soc. (London), A, **208**: 326.
——— 1953. Proc. Roy. Soc. (London), A, **220**: 435.

A METHOD TO DETECT THE PRESENCE OF IONIZED HYDROGEN IN THE OUTER ATMOSPHERE[1]

By L. R. O. Storey

ABSTRACT

The method proposed for the detection of ionized hydrogen in the outer atmosphere relies on the influence of the positive ions on the propagation of whistlers. If ionized hydrogen is the chief constituent of the atmosphere at great heights above the earth, then the relation between frequency and time in a whistler should depart at low audio frequencies from the form observed at higher frequencies. The departure is likely to be most marked in whistlers occurring at low magnetic latitudes. At magnetic latitude 45° the effect of the hydrogen ions should be detectable at frequencies below about 2 kc./sec.

1. INTRODUCTION

Whistlers are natural 'atmospherics' found in the audio-frequency band of the radio spectrum, where they normally appear as musical tones of falling pitch. They are now generally believed to consist of waves which originate as atmospheric 'clicks' from lightning strokes and then travel along the lines of magnetic force through the ionized outer atmosphere, where the clicks become dispersed into the whistling tones (Storey 1953). Since the waves require a certain minimum density of ionization to support their propagation, and since the lines of force rise to great heights, the existence of whistlers implies that the ionosphere must extend much further out from the earth than was formerly believed. Questions therefore arise as to how so much ionization comes to be present at great heights, and of what it may be composed.

If the ionization in the outer atmosphere is in equilibrium under gravity and formed from oxygen or nitrogen, the chief constituents of the lower ionosphere, then these gases would have to be very hot for their density far out from the earth's surface to be as great as the whistler observations suggest. To explain this density without invoking an unreasonably high temperature, either the assumption of gravitational equilibrium must be abandoned or the ionization must be supposed to be formed from some lighter gas. These considerations have led Dungey (1954*a*, 1955) to suggest that the outer atmosphere may consist chiefly of ionized hydrogen. The aim of the present paper is to consider how this hypothesis might be tested by further observations on whistlers.

In normal whistlers observed at middle latitudes the relationship between the instantaneous frequency f and the time t after the initiating click conforms quite closely to a simple law, according to which $f^{-\frac{1}{2}}$ is linearly proportional to t. Certain simplifying assumptions are made in deriving this dispersion law theoretically: both the electron gyro-frequency and the critical frequency of the medium are assumed to be much greater than the wave frequency at all points along the path, and no account is taken of the motion of the positive

[1]Manuscript received July 6, 1956.
Contribution from the Radio Physics Laboratory, Defence Research Board, Ottawa, Ontario. The work was performed under project PCC. No. D48-28-01-02.

ions in the electric field of the wave. The ions should begin to contribute significantly to the refractive index at frequencies small enough to be comparable to the ionic gyro-frequency. Now the gyro-frequency for ions of oxygen or nitrogen is quite small in the ionosphere (less than 60 c./sec.), but for hydrogen ions it lies well up in the audible range; the proton gyro-frequency at F-layer height varies from about 900 c./sec. at the geomagnetic poles to 450 c./sec. at the equator. This fact encourages the hope that the hydrogen ions may be detectable through their effects on the low-frequency end of the dispersion law of whistlers.

There are two reasons for expecting such effects to be easier to detect on whistlers observed at low rather than at high magnetic latitudes. Firstly, while ionization all along the path contributes to the complete dispersion curve, the departures sought for arise chiefly in the parts nearest the earth's surface at the two ends, where the ionic gyro-frequency is highest: hence they should be more marked at low latitudes, where a greater proportion of the path lies at relatively low heights. Secondly, the departures from the $f^{-\frac{1}{2}}$–t law at low frequencies can be detected only by comparison with an extrapolation of measurements made at higher frequencies; but at high frequencies there are also departures owing to the wave frequency becoming comparable with the electron gyro-frequency. These arise chiefly at the top of the path, where the electron gyro-frequency is least, and hence will be less marked at low latitudes.

In this paper theoretical dispersion curves are calculated for whistlers occurring at two magnetic latitudes, 45° and 55°. The calculations cover the frequency range from 20 kc./sec. to 50 c./sec., and both sources of departure from the simple law are taken into account. First, a number of assumptions required in the calculation are listed in Section 2. Next, the general method of calculation is described in Section 3. In Sections 4 and 5 expressions are derived for corrections to the simple dispersion law applicable at low and high frequencies respectively. The results of the calculations are presented in Section 6, and are discussed finally in Section 7.

2. ASSUMPTIONS

Before the complete dispersion law can be calculated some assumptions have to be made about the shape of the ray path which the whistlers follow through the outer atmosphere, and also about the variation of the magnetic field strength and the electron density along the path. These assumptions are listed below:

(*a*) *Ray Path*

It will be assumed that everywhere along the path the propagation is longitudinal, that is to say, the mean wave normal direction is parallel to the magnetic field. In this case the ray path follows a magnetic line of force exactly.

(*b*) *Geomagnetic Field*

The geomagnetic field will be represented in the usual way as being due to a dipole situated at the center of the earth. A line of force then has the equation

$$r/r_0 = \cos^2 L/\cos^2 L_0$$

where r is the distance from the center of the earth, L is the magnetic latitude, and r_0, L_0 are the corresponding coordinates for the point where the line intersects the earth's surface.

The electron gyro-frequency f_H, which is directly proportional to the field strength, varies with position according to the law

$$f_H = f_e(r_0/r)^3(1 + 3\sin^2 L)^{\frac{1}{2}}$$

where f_e ($\simeq$0.8 Mc./sec.) is its value at ground level on the geomagnetic equator. The corresponding frequency for the positive ions is smaller in the ratio of the mass of the ion to the mass of an electron; for protons this ratio is 1836, and f_e is therefore about 440 c./sec.

(*c*) *Distribution of Ionization*

Following Dungey (1954*a*, 1955), the outer atmosphere will be assumed to consist of fully ionized hydrogen at a temperature of 1500° K., in thermal and hydrostatic equilibrium under gravity and in dynamical equilibrium with the ionization in interplanetary space. The critical frequency for the ionization is proportional to the square root of the electron density, which on the above assumptions is distributed according to the law

$$N = N_s \exp(r_0^2/rH_0)$$

where N_s is the density in free space far from the earth. A value of 600 cm.$^{-3}$ will be adopted for this density, following Siedentopf, Behr, and Elsasser (1953); it corresponds to a critical frequency of about 220 kc./sec. The quantity H_0 is the scale height of the ionization at the given temperature and at the value of gravity which is found at the earth's surface: for ionized hydrogen at 1500° K., $r_0/H_0 \simeq 2.5$.

The hydrogen will be assumed to begin at a height of 300 km. The main ionospheric layers, in which the simple whistler dispersion law is obeyed closely, will be assumed to contribute 6 sec.$^{\frac{1}{2}}$ to the total dispersion (see below).

3. METHOD OF CALCULATION

The group delay t experienced by a wave packet of mean frequency f in travelling through a dispersive, anisotropic medium is given by

$$t(f) = \frac{1}{c}\int M'(f)\, ds$$

where c is the velocity of light, ds an element of the ray path, and M' the group-ray refractive index (i.e. the refractive index corresponding to the velocity with which the packet travels in the ray direction). When the propagation is longitudinal this latter quantity is equal to the group refractive index μ', which as normally defined corresponds to the component of velocity parallel to the wave normal. At audio frequencies the group refractive index for the longitudinal extraordinary mode is given quite closely by the expression

$$\mu'(f) \simeq \tfrac{1}{2}f_0/(ff_H)^{\frac{1}{2}} \tag{1}$$

where f_0 is the critical frequency of the medium and f_H is the gyro-frequency for electrons. This approximation, which has been much used in earlier work

on whistlers, is valid if the wave frequency is small compared to f_0 and f_H, and large compared to f_i, the gyro-frequency for the positive ions. It leads to a dispersion law of the form

$$t f^{\frac{1}{2}} = \frac{1}{2c} \int \frac{f_0}{f_H^{\frac{1}{2}}} ds = D \tag{2}$$

where the quantity D, which is a constant for any one path, is termed the 'dispersion' of the whistler.

The present paper is concerned with situations in which the group refractive index is not represented adequately by Eq. 1. In most cases, however, the difference will be slight and it is conveniently taken into account by adding a small correction term as follows:

$$\mu'(f) = \tfrac{1}{2}[f_0/(f f_H)^{\frac{1}{2}}]\,[1+\delta(f)]\,. \tag{3}$$

The corrected dispersion law will then be

$$t f^{\frac{1}{2}} = D + \frac{1}{2c} \int \frac{f_0}{f_H^{\frac{1}{2}}} \delta\, ds. \tag{4}$$

The integral is to be taken over the complete ray path, i.e. a single traverse of the line of force in the case of a 'short' whistler, and a double traverse for a 'long' whistler. The correction δ is to be determined by more exact application of the magnetoionic theory, and expressions appropriate to low and high audio frequencies are derived in the next two sections.

4. MODIFICATIONS TO THE DISPERSION LAW AT LOW AUDIO FREQUENCIES

A number of authors, notably Aström (1950), Ginsburg (1951), Hines (1953), and Dungey (1954 *b*, *c*) have studied the behavior of the magnetoionic modes of propagation at frequencies low enough for the motion of the positive ions to be significant. In the present paper chief use has been made of the work of Aström and Hines.

At frequencies not large compared with the gyro-frequency of the positive ions, the wave refractive indices for the two modes, when propagated directly along the magnetic field, are given by the approximate expression

$$\mu^2 \simeq f_0^2/[f_H(f_i \pm f)]\,. \tag{5}$$

The upper sign in the denominator refers to the extraordinary (right-hand circularly polarized) mode and the lower one to the ordinary (left-handed) mode. The approximation is close when the indicated values of μ^2 are much greater than unity. Collisions have been ignored, since they are almost certainly too infrequent in the outer atmosphere to affect the refractive indices or cause appreciable absorption.

The corresponding velocities for the two modes are plotted as functions of frequency in the solid lines of Fig. 1; the broken lines are the asymptotes to the two curves. The ordinary mode (lower curve) does not propagate freely above the ionic gyro-frequency; of the two modes it is the more strongly affected by the ions because the sense of rotation of its electric vector is such as to assist the natural gyration of positive ions around the lines of force. The extraordinary mode (upper curve) propagates freely over the whole range of

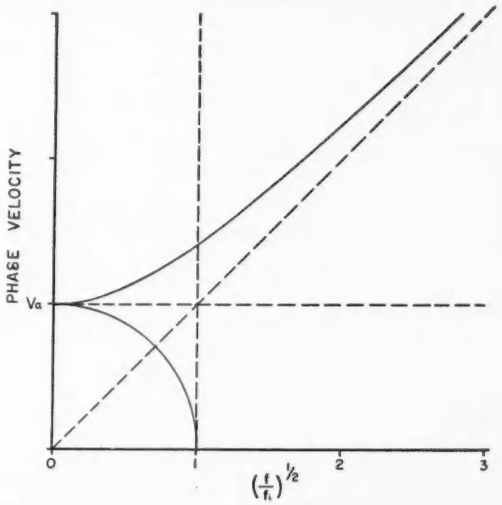

FIG. 1. Velocities of longitudinal propagation for the magnetoionic modes at very low frequency. Upper curve—extraordinary mode. Lower curve—ordinary mode.

frequencies considered; as the frequency is lowered it exhibits a continuous transition from dispersive behavior at audio frequencies to the non-dispersive behavior at frequencies well below the ionic gyro-frequency, which is characteristic of hydromagnetic waves. The limit V_a, to which the velocities of both modes tend as the frequency approaches zero, is given by

$$V_a = c(f_H f_i)^{\frac{1}{2}}/f_0 = H(\mu_0/\rho)^{\frac{1}{2}}.$$

The expression on the right, in which ρ is the mass density of the medium and μ_0 the magnetic permittivity of free space, is the form due to Alfvén (1942); it can readily be shown equivalent to the other.

Our present concern is with the dispersive properties of the extraordinary mode. The group refractive index for this mode can be derived in the usual way from the wave refractive index of Eq. 5, and the result is

$$\mu' = \frac{1}{2}\frac{f_0}{(ff_H)^{\frac{1}{2}}}\left[\frac{1+2f_i/f}{(1+f_i/f)^{3/2}}\right]. \tag{6}$$

The first factor on the right-hand side of this equation is the approximate expression of Eq. 1 obtained by ignoring the ions, while the factor in brackets takes their effect into account. This factor is plotted as a function of frequency in the full curve of Fig. 2; the broken straight lines are the asymptotes to the curve at high and low frequencies.

The following points should be noted: Firstly, the ions do not alter the group refractive index very much until the frequency becomes less than about one quarter of the ionic gyro-frequency. Secondly, their effects are opposite at high and low frequencies; over a range of frequencies extending up to several

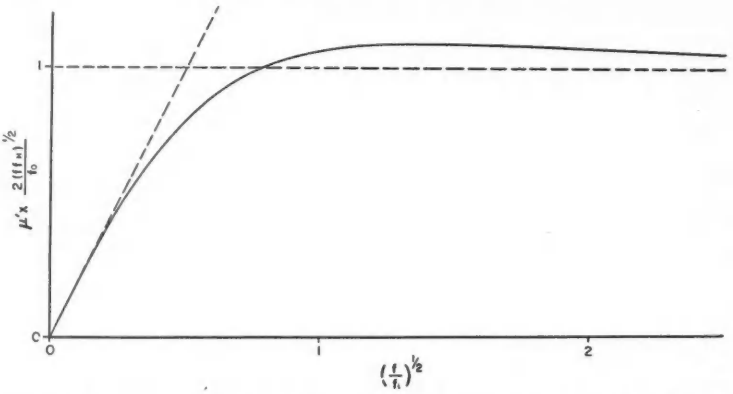

FIG. 2. Ratio of group refractive index for extraordinary mode to value obtained when the positive ions are ignored.

times f_i the ions cause the group refractive index to be slightly larger than that calculated from the simple expression, while at frequencies much less than f_i they make it smaller. Hence when these effects are integrated along the entire ray path to yield the total correction to the dispersion law, as in Eq. 4, the contributions from the upper and lower portions will cancel each other to some extent at frequencies intermediate between the values of f_i at the summit of the path and at ground level. These considerations imply that the ions will be rather difficult to detect.

The correction factor δ, required for the integral of Eq. 4, is equal to the difference between the full curve and the broken horizontal line in Fig. 2. Algebraically, it is obtained by writing Eq. 6 in the form of Eq. 3, giving

$$\delta = \frac{1+2f_i/f}{(1+f_i/f)^{3/2}} - 1$$

$$\simeq \tfrac{1}{2}f_i/f \text{ when } f \gg f_i.$$

It is positive at frequencies greater than 0.618 f_i and negative at lower frequencies, tending to values of zero and -1 in the limits of very high and very low frequencies respectively. It takes its maximum positive value of 0.0887 at $f = 2f_i$.

5. MODIFICATIONS TO THE DISPERSION LAW AT HIGH AUDIO FREQUENCIES

Departures from Eq. 1 also occur at high audio frequencies, for in deriving this equation it was assumed that both the critical frequency and the electron gyro-frequency were much greater than the frequency of the wave. As the wave frequency is raised one or other of these assumptions must eventually fail, and this failure will clearly begin at the highest point of the path, where it crosses the geomagnetic equator, as here the values of both f_0 and f_H are least.

To ascertain which assumption breaks down first, the values of f_0 and f_H at this point must be compared. Making use of the distributions described in

Section 2, it is found that the path starting from magnetic latitude 45° crosses over the equator at a height of one earth radius, at which point $f_0 = 420$ kc./sec. and $f_H = 100$ kc./sec., while the path from magnetic latitude 55° reaches a height of two earth radii where $f_0 = 330$ kc./sec. and $f_H = 29$ kc./sec. Evidently in both cases the departures from Eq. 1 at high frequencies will arise primarily through the wave frequency becoming comparable to the electron gyro-frequency.

In a recent paper Helliwell, Crary, Pope, and Smith (1956) have given an approximate expression for the group refractive index which applies under the present circumstances, where the wave frequency is small compared with f_0 but not small compared with f_H. For the particular case of longitudinal propagation it reads

$$\mu' \simeq \frac{1}{2}\frac{f_0 f_H}{f^{\frac{1}{2}}(f_H - f)^{3/2}}$$

$$= \frac{1}{2}\frac{f_0}{(f f_H)^{\frac{1}{2}}}\left(\frac{1}{1-f/f_H}\right)^{3/2}. \tag{7}$$

The correction factor to be used in Eq. 3 at high audio frequencies is therefore

$$\delta = (1-f/f_H)^{-3/2} - 1. \tag{8}$$

If the wave frequency f does not approach f_H too closely anywhere along the path, the labor of computing the integral of Eq. 4 can be eased by approximating to δ with the first few terms of the power series obtained by expanding the bracketed term in Eq. 8 in ascending powers of f/f_H. Thus

$$\delta = \sum_1^\infty A_n (f/f_H)^n$$

where

$$A_n = (2n+1)!/(2^n n!)^2.$$

This series converges for all $f < f_H$. The present calculations were made using only the first two terms, viz.

$$\delta \simeq 1.5(f/f_H) + 1.875(f/f_H)^2.$$

6. THE COMPLETE DISPERSION LAW

The complete dispersion law for a whistler may now be calculated following the methods described in the preceding paragraphs. This has been done here for short whistlers originating at 45° and 55° magnetic latitude, the integrations being performed numerically from values of the functions computed at intervals of 5°; for long whistlers the calculated delay times should be doubled. The general shape of the curve relating instantaneous frequency and delay time is shown in the full line of Fig. 3, which applies to 45° magnetic latitude. The part between 20 kc./sec. and 50 c./sec. has been plotted from the computed points, and the remainder has been filled in schematically according to the behavior suggested by Eqs. 6 and 7.

The broken line is a plot of the elementary dispersion law of Eq. 2. It agrees tolerably well with the exact law between 5 kc./sec. and 50 c./sec. but outside these limits there are marked disagreements. Thus, at low frequencies, the

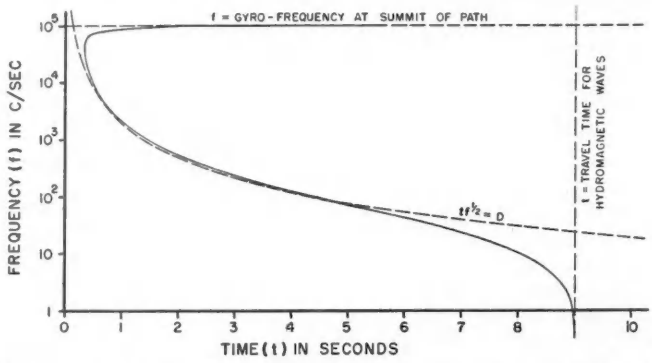

FIG. 3. The complete dispersion law for a whistler occurring at magnetic latitude 45°.

elementary law predicts a delay time tending to infinity as the frequency tends to zero but, in fact, the delay tends to a finite limit which is the travel time for hydromagnetic waves of very low frequency. Again, at high frequencies the elementary law predicts a delay which tends to zero as the frequency is raised, but in the exact law the delay attains a minimum value at a certain frequency (the 'nose frequency') and thereafter it increases rapidly, becoming infinite at an upper limiting frequency equal to the electron gyro-frequency at the summit of the path (Helliwell *et al.* 1956). All higher frequencies are unable to traverse the complete path, and so do not appear in the whistler; the fate of these waves is not quite certain, but theory suggests that when they reach the level in the outer atmosphere where their refractive indices become infinite they are absorbed without reflection in the manner described by Budden (1955).

The small discrepancies between the approximate and exact dispersion laws at audio frequencies are revealed better by plotting the product $tf^{\frac{1}{2}}$ against frequency (see Eq. 4) since, according to the former, this quantity should be independent of frequency and equal to the dispersion constant. Fig. 4 shows the results plotted in this way. The upper set of these curves refers to magnetic latitude 55°, and the central set to 45°. In each case the horizontal broken line A is drawn at the level $tf^{\frac{1}{2}} = D$; the broken curve B is the value obtained with only the high-frequency corrections due to electron gyro-resonance, and the full curve C shows the complete dispersion law with the effect of the hydrogen ions included.

The main features of the complete curves are as follows. At high frequencies $tf^{\frac{1}{2}}$ is much greater than D. It falls as the frequency is lowered and would continue to do so smoothly, tending to D as a limit, were it not for the ions. At medium audio frequencies their contribution to $tf^{\frac{1}{2}}$ is positive, but when the low audio frequencies are reached it reverses sign, as the frequency-dependence of the correction factor δ would suggest (see Fig. 2). In consequence the total value of $tf^{\frac{1}{2}}$ has a minimum at a medium audio frequency, then rises to a maximum at some lower frequency, and finally decreases fast as the frequency is lowered further. The difference between the maximum and

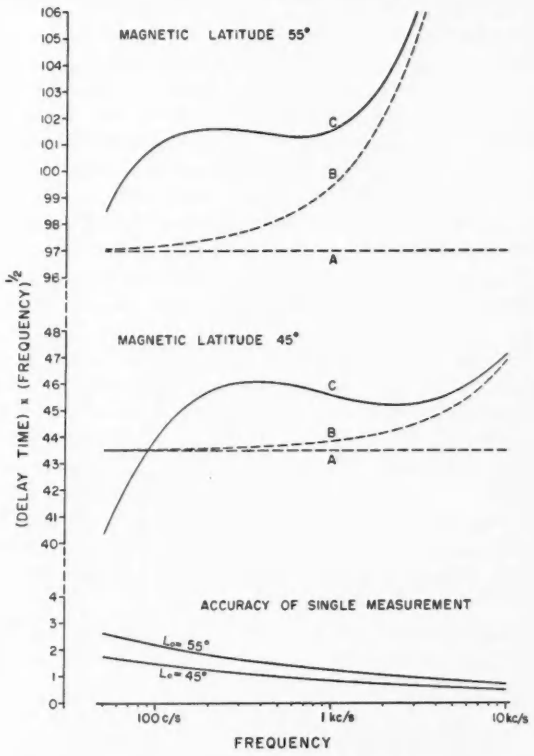

FIG. 4. Comparison between exact and approximate dispersion laws.

minimum values of $tf^{\frac{1}{2}}$ is less at 55° than at 45°, so it is clear that at some still higher latitude these stationary points would disappear from the curve altogether and be replaced simply by a broad region of reduced slope.

Table I below gives the numerical values of some of the parameters of the complete dispersion curves of Figs. 3 and 4.

TABLE I

PARAMETERS OF DISPERSION CURVES

	Magnetic latitude 45°	Magnetic latitude 55°
Dispersion constant D	43.5 sec.$^{\frac{1}{2}}$	97 sec.$^{\frac{1}{2}}$
Electron gyro-frequency at summit of path	100 kc./sec.	29 kc./sec.
Nose frequency	~50 kc./sec.	~15 kc./sec.
Frequency of minimum $tf^{\frac{1}{2}}$	~2 kc./sec.	~700 c./sec.
Frequency of maximum $tf^{\frac{1}{2}}$	~350 c./sec.	~200 c./sec.
Travel time for zero frequency	9 sec.	32 sec.

7. DISCUSSION

The graphs of Fig. 4 demonstrate how the dispersion law of whistlers should be affected at low audio frequencies by the positive ions in the outer atmosphere, if these are mainly protons. These graphs show that in a whistler originating at 45° magnetic latitude the protons are already beginning to make themselves felt at about 2 kc./sec. If, on the other hand, the ions were of relatively large atomic weight, such as oxygen-16 or nitrogen-14, their effects would be qualitatively similar but would set in at a proportionately lower frequency, probably at one too low to be observable. The presence or absence of the predicted effects in the low audio range therefore provides a criterion to determine whether or not the outer atmosphere consists mainly of ionized hydrogen. It remains to discuss whether these effects are likely to be measurable.

The dispersion law of a whistler is most readily determined by playing back a recording of it (accompanied inevitably by much extraneous atmospheric noise) through a frequency analyzer consisting of a number of narrow-band filters connected in parallel and tuned to various selected frequencies. The time at which the response of each filter attains a maximum measures, after slight correction, the time at which the instantaneous frequency of the tone is equal to the resonant frequency of the filter. For the best possible output signal-to-noise ratio the bandwidth of the filter should be set at a value which depends, not very critically, on the rate of change of frequency in the whistler, and is of the order of $|\, df/dt \,|^{\frac{1}{2}}$.

If the whistler is a more or less pure tone, if the bandwidth of the filter is set correctly, and if the peak signal-to-noise ratio after filtering is of order unity, then the accuracy of a single time measurement will be about

$$\Delta t \simeq |\, dt/df \,|^{\frac{1}{2}}$$

$$\simeq (D/2)^{\frac{1}{2}} f^{-3/4} \qquad \text{from Eq. 2.}$$

A single measurement of the quantity $tf^{\frac{1}{2}}$ therefore has an accuracy

$$\Delta(tf^{\frac{1}{2}}) \simeq (D/2)^{\frac{1}{2}} f^{-1/4}.$$

In the lowermost set of curves in Fig. 4 this quantity is plotted as a function of frequency for the two whistlers considered. It is not to be compared directly with the difference (due to the ions) between the values of $tf^{\frac{1}{2}}$ on the graphs B and C, as only C is measured, and the rising portion of this graph at the high frequencies could be fitted to a curve of type B (with no ion effects) by modifying slightly the assumptions of Section 2. It is therefore to be compared with the amount by which the ions cause the graph C to deviate at low frequencies from the ordinates obtained by extrapolating its high-frequency portion on the assumption that it is part of a curve of type B. At 45° latitude the deviation due to the ions exceeds the error of measurement at frequencies below about 2 kc./sec., while at 55° it does so below about 700 c./sec.

If the peak signal-to-noise ratio is greater than assumed, then the measurements could be made more accurately. If, however, as is often the case, the whistler is of the noisy 'swish' type rather than a pure tone, then the accuracy

will be worse than calculated. In either event, since $tf^{\frac{1}{2}}$ varies only slowly with frequency, its value at any one frequency could be determined more accurately by averaging many independent measurements made at nearby frequencies separated by the minimum interval $|df/dt|^{\frac{1}{2}}$.

It seems reasonable to conclude that the hydrogen ions in the outer atmosphere, if such they be, have effects on the dispersion law of a whistler occurring at 45° magnetic latitude which are probably on the threshold of detectability at frequencies below about 2 kc./sec. A single good record, in which these frequencies happened to be strong, might suffice to decide the issue of the composition of the outer atmosphere, so the effort that would be required to obtain such a record appears well worth while.

ACKNOWLEDGMENTS

The author wishes to acknowledge the value of discussions with Dr. C. O. Hines.

REFERENCES

ALFVÉN, H. 1942. Nature, **150**: 405.
ASTRÖM, E. 1950. Arkiv Fysik, **2**: 443.
BUDDEN, K. G. 1955. The physics of the ionosphere. The Physical Society, London. p. 320.
DUNGEY, J. W. 1954*a*. Penn. State Univ. Sci. Rept. No. 69.
——— 1954*b*. Penn State Univ. Sci. Rept. No. 57.
——— 1954*c*. J. Geophys. Research, **59**: 323.
——— 1955. The physics of the ionosphere. The Physical Society, London. p. 229.
GINSBURG, V. L. 1951. Zhur. Eksptl. i. Teoret. Fiz. **21**: 788.
HELLIWELL, R. A., CRARY, J. H., POPE, J. H., and SMITH, R. L. 1956. J. Geophys. Research, **61**: 139.
HINES, C. O. 1953. Proc. Cambridge Phil. Soc. **49**: 299.
SIEDENTOPF, H., BEHR, A., and ELSASSER, H. 1953. Nature, **171**: 1066.
STOREY, L. R. O. 1953. Trans. Roy. Soc. (London), **246**: 113.

NOTES

MAGNETIC SUSCEPTIBILITY OF RUBIDIUM AND THE ELECTRICAL RESISTANCE ANOMALY*

By F. T. Hedgcock†

In the study of the magnetic susceptibility of the alkali metals down to liquid helium temperatures at present underway in this laboratory, some interesting results have already been found and it is the purpose of this note to report briefly on the susceptibility of rubidium down to liquid nitrogen temperatures.

Experiments on the electrical resistivity by MacDonald (1952) showed an anomalous change in the resistivity–temperature curve at approximately 180° K. Calculations of the characteristic temperature, Θ,‡ based on the resistive data below 180° K. gave a normal variation of Θ with temperature while those based on the data above 180° K. gave unintelligible results. It was suggested at the time that a change in the crystallographic or electronic configuration might occur at this temperature. An investigation by Kelly and Pearson (1955) proved that the transition was not crystallographic and probably not electronic. The electronic transition tentatively suggested (MacDonald 1952) was some change in the relative density of $5s$ to $4d$ electrons in the conduction process on proceeding to lower temperatures, perhaps somewhat similar to that suggested for chromium by Söchtig (1940). If we assume some such process then presumably the additional probability of s–d band scattering would result in an increase in the resistivity above 180° K. Since the magnetic susceptibility is proportional to the density of states at the Fermi level, one would expect an increase in the paramagnetic contribution to the total susceptibility at temperatures above 180° K. where the electronic s–d band transition has been suggested to take place. It was with this in mind that the magnetic susceptibility was measured from room temperature to 100° K.

EXPERIMENTAL ARRANGEMENTS

All of the specimens were long enough to allow the Gouy method to be used and the magnetic susceptibility balance was evacuated immediately after the specimen was placed in position.

Specimen 1.—The susceptibility of this sample was determined by taking the difference in the susceptibility of a quartz tube before and after filling the tube with rubidium. To avoid changing the mass of the quartz container the tube was not sealed. A subsequent resistive study of the sample showed no anomaly at 180° K. On continuing to heat the sample the resistance rose

*Issued as N.R.C. No. 4107.

†N.R.C. Laboratory Postdoctorate Fellow, Division of Pure Physics, National Research Council, Ottawa, Canada. Now at Department of Physics, University of Ottawa, Ottawa, Canada.

‡For methods of calculating Θ from resistive data see Kelly and MacDonald (1953).

sharply at about 280° K. We interpreted this as indicating the melting of the eutectic mixture of oxygen and rubidium at this temperature (compare the behavior of cesium as measured by Brauer (1947)). From this and similar experimental results obtained by Dugdale (private communication) it appears that large amounts of oxygen in rubidium destroy the anomalous resistive behavior.

Specimen 2.—A long thin-walled quartz tube was chosen and its position in the magnetic field adjusted until it experienced no magnetic force when the magnetic field was switched on. The tube was then half filled with rubidium, sealed, and placed in the same position in the magnetic field. This method gave the susceptibility of rubidium directly and reduced to a minimum the oxide formed in the fabrication and mounting of the specimen.

The results for both the specimens studied are shown in Fig. 1.

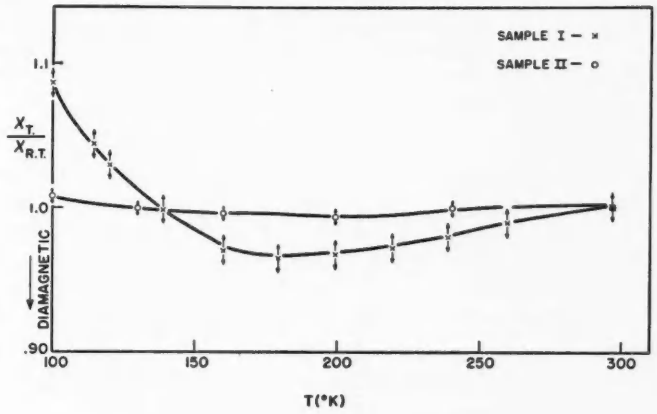

FIG. 1.

MAGNETIC EFFECTS OF OXYGEN

The only oxide of rubidium whose magnetic properties have been determined is RbO_2 which Helms and Klemm (1939) determined to be paramagnetic at room temperature, the paramagnetism increasing as one goes to low temperatures. Although there is no mention in the literature of the magnetic susceptibility of the lower oxides, from structural considerations they would be expected to be diamagnetic (cf. Sidgwick 1950). The low temperature end of the susceptibility curve for specimen I is noticeably more paramagnetic than specimen II. This may be due to the presence of RbO_2. Using the results of Helms and Klemm (1939), the amount of RbO_2 needed to explain the present results would be in excess of 30% of the total mass of the specimen. A visual examination of specimen I showed no large amounts of oxide so that it is extremely unlikely that this amount of oxide was present.

In sample II, which has least oxygen, the general shape of the curve is

maintained but the low temperature paramagnetism is markedly decreased. Excluding the unlikely possibility of the presence of RbO_2 this might mean that the oxygen present in sample I is in solution and gives rise to an appreciable temperature dependent paramagnetism, while the most probably formed lower oxides are diamagnetic and show a slight temperature dependence. If this is so it is probably fortuitous that the diamagnetic and paramagnetic effects give rise to a change in slope at 180° K. A T^{-1} plot of the paramagnetism for sample I in excess of that for sample II, and using a Curie constant for molecular oxygen, yields an oxygen content of approximately 0.2%, which is probably reasonable.

That the oxygen present should have a Curie constant at least of the same order of magnitude as molecular oxygen seems surprising. This result may be compared to some recent measurements on the CuO–O_2 system (Perakis and Serres 1955) where the oxide is diamagnetic and an excess of oxygen gave rise to a large paramagnetism which obeyed a Curie law and whose Curie constant was equal to that for molecular oxygen. Henry (private communication) determined the effect of dissolved oxygen on the magnetic susceptibility of pure silver at room temperature and found a large paramagnetic contribution of the same order of magnitude as that for molecular oxygen.

CONCLUSION

An examination of the susceptibility results shows that in neither the pure nor the impure samples is there any evidence of an appreciable paramagnetism above 180° K., as would be expected if a $5s$–$4d$ transition were taking place.* We may summarize the evidence so far available regarding the resistive transition as follows:

(*a*) It is not due to a crystallographic change (see Kelly and Pearson 1955).

(*b*) From the present measurements and the work of Kelly and Pearson (1955) it is not an electronic transition of the type originally suggested by MacDonald (1952).

(*c*) Apart from what has already been said above there is a great deal of evidence that small amounts of oxygen can markedly affect the properties of rubidium (see, e.g., Dauphinee, Martin, and Preston-Thomas 1955).

From this, one can only conclude at present that small amounts of oxygen are possibly the cause of the resistive anomaly in rubidium. It must however be pointed out that the resistive anomaly is still found (according to measurements made in this laboratory) in even the purest samples of rubidium available to us.

*McGarvey and Gutowsky (1953) reported a peak in the rubidium resonance shift occurring at 254° K. and evidence of another peak at 225° K. If the peaks in the Knight shift are, as suggested, due to a possible change in the density of conduction electrons near the Fermi level one would expect peaks in the susceptibility curve at these temperatures. No evidence of the peaks was found in the present measurements although this may be due to the relatively large temperature intervals at which the measurements were made (approx. every 20° C.).

ACKNOWLEDGMENTS

The author would like to thank Dr. D. K. C. MacDonald for suggesting the investigation and Dr. S. Dugdale and Dr. W. Pearson for interesting discussions.

BRAUER, G. 1947. Z. anorg. Chem. **101**: 255.
DAUPHINEE, T. M., MARTIN, D. L., and PRESTON-THOMAS, H. 1955. Proc. Roy Soc., A, **233**: 214.
HELMS, A. and KLEMM, W. 1939. Z. anorg. Chem. **97**: 241.
KELLY, F. M. and MACDONALD, D. K. C. 1953. Can. J. Phys. **31**: 147.
KELLY, F. M. and PEARSON, W. B. 1955. Can. J. Phys. **33**: 17.
MACDONALD, D. K. C. 1952. Phil. Mag. **43**: 479.
MCGARVEY, B. R. and GUTOWSKY, H. S. 1953. J. Chem. Phys. **21**: 2114.
PERAKIS, N. and SERRES, A. 1955. J. phys. radium, **16**: 387.
SIDGWICK, N. V. 1950. The chemical elements and their compounds. Oxford University Press, London. p. 90.
SÖCHTIG, H. 1940. Ann. Physik, **38**: 97.

RECEIVED AUGUST 13, 1956.
DIVISION OF PURE PHYSICS,
NATIONAL RESEARCH COUNCIL,
OTTAWA, CANADA.

THE HALF-LIFE OF MERCURY-203*

BY G. G. EICHHOLZ AND J. V. KRZYZEWSKI

In the course of some recent experiments involving the use of the isotope Hg-203 it was necessary to use a precise value for the half-life of the isotope. However, it was found that there were considerable discrepancies in the values published so far, which are listed in Table I. For this reason a careful redetermination of the half-life has been carried out.

TABLE I

DATA ON THE HALF-LIFE OF Hg-203

Author	Date	Value, days
Sherr *et al.*	1941	50
Friedlander and Wu	1943	51
Saxon	1948	43.5±0.5
Lyon	1951	46.5
Cork *et al.*	1952	47.9±0.2

Measurements were carried out on a small sealed source of mercury which had been mounted in a permanent framework. Gamma radiation from the source was detected by means of an argon-filled pressure ionization chamber and a vibrating-reed electrometer. This system was known to be very stable

*Published by permission of the Deputy Minister, Department of Mines and Technical Surveys, Ottawa, Ontario.

and has been used in previous determinations of this type (e.g. Eichholz and Ficko 1952), and its linearity had been well established (Horwood and McMahon 1950). A sealed uranium source was run at the same time as the mercury source to check the sensitivity of the instrument, which was found to vary by less than 1% over the period of the experiment, with no indication of systematic drift.

The mercury source consisted of 35 gm. of triple-distilled mercury which had been activated in the Chalk River pile and had been allowed to decay for seven months before it was used for these measurements. This ensured the decay of any short-lived impurities. The purity of the gamma spectrum was further checked by means of a gamma-ray spectrometer. The initial intensity of the source was such as to give a discharge rate 16 times that of background.

Readings were taken once a week over a period of 213 days, nearly five half-lives. The decay curve was plotted and the half-life obtained from it by a least-squares calculation. The resultant value for the half-life of mercury-203 was 46.91 ± 0.14 days, close to the other more recent determinations.

CORK, J. M., MARTIN, D. W., LEBLANC, J. M., and BRANYAN, C. E. 1952. Phys. Rev. **85**: 386.
EICHHOLZ, G. G. and FICKO, L. A. 1952. Phys. Rev. **86**: 794.
FRIEDLANDER, G. and WU, C. S. 1943. Phys. Rev. **63**: 227.
HORWOOD, J. L. and MCMAHON, C. 1950. Can. Mining J. **71** (4): 56.
LYON, W. S. 1951. Phys. Rev. **82**: 276.
SAXON, D. 1948. Phys. Rev. **74**: 849.
SHERR, R., BAINBRIDGE, K. T., and ANDERSON, H. H. 1941. Phys. Rev. **60**: 473.

RECEIVED JULY 10, 1956.
RADIOACTIVITY DIVISION,
DEPARTMENT OF MINES AND TECHNICAL SURVEYS,
MINES BRANCH,
OTTAWA, ONTARIO.

Under this heading brief reports of important discoveries in physics may be published. These reports should not exceed 600 words and, for any issue, should be submitted not later than six weeks previous to the first day of the month of issue. No proof will be sent to the authors.

The Nuclear Magnetic Resonance Spectrum of Na^{23} in $NaH_2PO_4 \cdot 2H_2O$

As a first step in a study of the effects of temperature changes on electric field gradients existing at nuclear sites in crystals, a complete investigation has been made of the Na^{23} nuclear quadrupole interaction in a single crystal of $NaH_2PO_4 \cdot 2H_2O$ at room temperature.

A selected crystal of $NaH_2PO_4 \cdot 2H_2O$, grown by us from an aqueous solution, was mounted in the magnet gap in such a way that it could be rotated about an axis perpendicular to $\mathbf{H}_0$, the magnetic field. The Na^{23} nuclear magnetic resonance spectrum was observed using a spectrometer of the Pound and Knight type (1950). The complete spectrum consisted of 12 lines centered about 6.538 Mc./sec., ($\mathbf{H}_0 = 5800$ gauss), whose frequencies depended on the crystal orientation with respect to $\mathbf{H}_0$. However with any one of the a, b, c crystallographic axes perpendicular to $\mathbf{H}_0$, only six lines appeared and with any two of the a, b, c axes simultaneously perpendicular to $\mathbf{H}_0$, only three lines were observed. The frequencies of the lines were measured at 30° intervals for a rotation about each of the a, b, and c axes.

Since for Na^{23} the spin, I, equals 3/2, the spectrum for a particular sodium site in the unit cell should consist of three lines, corresponding to the three allowed transitions between the four magnetic levels. The 12-line spectrum, observed in $NaH_2PO_4 \cdot 2H_2O$, is therefore a superposition of four "simple" three-line spectra corresponding to four sodium sites at which the electric field gradients must differ in some respect. The reduced six-line and three-line spectra have been interpreted by making use of the fact that if two sites are related by a twofold rotation axis, the electric field gradient tensors at the two sites must have identical eigenvalues and differ only in the orientation of their principal axes, although they must be symmetrically inclined with respect to the twofold rotation axis. If the crystal is mounted so that this axis is either perpendicular or parallel to $\mathbf{H}_0$ the two symmetrically inclined tensors are equivalent from the point of view of the perturbation they cause and they then give rise to identical spectra. On this basis it can be shown that the four sodium sites must be related by three mutually perpendicular twofold rotation axes parallel to the a, b, and c axes. Therefore the electric field gradient tensors at the four sites have identical eigenvalues and differ only in the orientation of their principal axes.

The mathematical procedures developed by Bersohn (1952) and Volkoff (1953) have been used to analyze the results. Because the a, b, and c axes, about which the crystal rotations were performed, are each parallel to a twofold rotation axis we were able to obtain, from a study of the frequency differences between the lines corresponding to the transitions $m = \pm 3/2 \rightleftharpoons \pm 1/2$, the magnitudes but not the relative signs of the tensor components in the a, b, c coordinate system. Luckily second-order shifts of the "centers of gravity" of the lines, although small, were measurable and revealed the relative signs. The four tensors in the a, b, c system were then diagonalized in the ordinary way to yield the eigenvalues.

TABLE I

QUADRUPOLE COUPLING CONSTANT AND ASYMMETRY PARAMETER FOR Na^{23} NUCLEI IN $NaH_2PO_4 \cdot 2H_2O$ (AVERAGED OVER THE FOUR SITES RELATED BY THE THREE TWOFOLD ROTATION AXES)

Quadrupole coupling constant $= \frac{Qe^2}{h}\frac{\partial E_z}{\partial z}$	1178.6 ± 0.5 kc./sec.
Asymmetry parameter $= \left(\frac{\partial E_x}{\partial x} - \frac{\partial E_y}{\partial y}\right) \Big/ \frac{\partial E_z}{\partial z}$	0.467 ± 0.002

This work makes available information about the sodium sites in $NaH_2PO_4 \cdot 2H_2O$, namely, the quadrupole coupling constant and the asymmetry parameter, Table I, and the principal axes of the electric field gradient tensors as shown in Table II. It confirms the existence of the three mutually perpendicular twofold rotation axes coinciding with the three crystallographic axes as suggested by morphological data and shows that the sodium ions are situated in general positions if the space group is P_{222}. Substituting the value of 0.100 ± 0.003 barns for the nuclear quadrupole moment of Na^{23} (Lew 1949) into our experimental value for the quadrupole

TABLE II

DIRECTION COSINES OF THE FIELD GRADIENT TENSOR PRINCIPAL AXES (x, y, z) WITH RESPECT TO THE CRYSTALLOGRAPHIC a, b, c AXES AT THE Na^{23} SITES IN $NaH_2PO_4 \cdot 2H_2O$ (THE FOUR SETS OF RELATIVE SIGNS REFER TO THE FOUR SITES RELATED BY THE THREE TWOFOLD ROTATION AXES AND THE MAGNITUDES OF THE COSINES ARE THEIR AVERAGE VALUES)

Axes	x	y	z
a	$\begin{matrix}+\\+\\-\\-\end{matrix}$ 0.0787 ± 0.003	$\begin{matrix}+\\+\\-\\-\end{matrix}$ 0.937 ± 0.02	$\begin{matrix}+\\+\\-\\-\end{matrix}$ 0.3265 ± 0.001
b	$\begin{matrix}+\\-\\+\\-\end{matrix}$ 0.1956 ± 0.003	$\begin{matrix}-\\+\\-\\+\end{matrix}$ 0.345 ± 0.02	$\begin{matrix}+\\-\\+\\-\end{matrix}$ 0.9215 ± 0.001
c	$\begin{matrix}-\\+\\+\\-\end{matrix}$ 0.9778 ± 0.003	$\begin{matrix}+\\-\\-\\+\end{matrix}$ 0.057 ± 0.02	$\begin{matrix}+\\-\\-\\+\end{matrix}$ 0.2102 ± 0.001

coupling constant gives a value of 1.6×10^{14} e.s.u./cm.^{2} for the electric field gradient along the z principal axis. This value is of the order of magnitude that one would expect for ionic bonds (Townes and Dailey 1952). Further work is in progress with $NaH_2PO_4 \cdot 2H_2O$ at the temperature of liquid air.

This work was supported by the Defence Research Board. One of the authors (F. Holuj) wishes to acknowledge the award of a Cominco Fellowship by the Consolidated Mining and Smelting Company of Canada.

BERSOHN, R. 1952. J. Chem. Phys. **20**: 1505.
LEW, H. 1949. Phys. Rev. **76**: 1086.
POUND, R. V. and KNIGHT, W. D. 1950. Rev. Sci. Instr. **21**: 219.
TOWNES, C. H. and DAILEY, B. P. 1952. J. Chem. Phys. **20**: 35.
VOLKOFF, G. M. 1953. Can. J. Phys. **31**: 820.

RECEIVED AUGUST 13, 1956.
F. HOLUJ
H. E. PETCH
DEPARTMENT OF PHYSICS,
HAMILTON COLLEGE, MCMASTER UNIVERSITY,
HAMILTON, ONTARIO.

CANADIAN JOURNAL OF PHYSICS

Notes to Contributors

Manuscripts

(i) ***General.*** Manuscripts, in English or French, should be typewritten, double spaced, on paper 8½ × 11 in. **The original and one copy are to be submitted.** Tables and captions for the figures should be placed at the end of the manuscript. Every sheet of the manuscript should be numbered.

Style, arrangement, spelling, and abbreviations should conform to the usage of this journal. Names of all simple compounds, rather than their formulas, should be used in the text. Greek letters or unusual signs should be written plainly or explained by marginal notes. Superscripts and subscripts must be legible and carefully placed.

Manuscripts and illustrations should be carefully checked before they are submitted. Authors will be charged for unnecessary deviations from the usual format and for changes made in the proof that are considered excessive or unnecessary.

(ii) ***Abstract.*** An abstract of not more than about 200 words, indicating the scope of the work and the principal findings, is required, except in Notes.

(iii) ***References.*** References should be listed **alphabetically by authors' names,** unnumbered, and typed after the text. The form of the citations should be that used in issues of this journal published in 1956; in references to papers in periodicals, titles should not be given and only initial page numbers are required. The names of periodicals should be abbreviated in the form given in the most recent *List of Periodicals Abstracted by Chemical Abstracts*. All citations should be checked with the original articles and each one referred to in the text by the authors' names and the year.

(iv) ***Tables.*** Tables should be numbered in roman numerals and each table referred to in the text. Titles should always be given but should be brief; column headings should be brief and descriptive matter in the tables confined to a minimum. Vertical rules should be used only when they are essential. Numerous small tables should be avoided.

Illustrations

(i) ***General.*** All figures (including each figure of the plates) should be numbered consecutively from 1 up, in arabic numerals, and each figure referred to in the text. The author's name, title of the paper, and figure number should be written in the lower left corner of the sheets on which the illustrations appear. Captions should not be written on the illustrations (see Manuscripts (i)).

(ii) ***Line Drawings.*** Drawings should be carefully made with India ink on white drawing paper, blue tracing linen, or co-ordinate paper ruled in blue only; any co-ordinate lines that are to appear in the reproduction should be ruled in black ink. Paper ruled in green, yellow, or red should not be used unless it is desired to have all the co-ordinate lines show. All lines should be of sufficient thickness to reproduce well. Decimal points, periods, and stippled dots should be solid black circles large enough to be reduced if necessary. Letters and numerals should be neatly made, preferably with a stencil (**do NOT use typewriting**) and be of such size that the smallest lettering will be not less than 1 mm. high when reproduced in a cut 3 in. wide.

Many drawings are made too large; originals should not be more than 2 or 3 times the size of the desired reproduction. In large drawings or groups of drawings the ratio of height to width should conform to that of a journal page but the height should be adjusted to make allowance for the caption.

The original drawings and one set of clear copies (e.g. small photographs) are to be submitted.

(iii) ***Photographs.*** Prints should be made on glossy paper, with strong contrasts. They should be trimmed so that essential features only are shown and mounted carefully, with rubber cement, on white cardboard with no space or only a **very** small space (less than 1 mm.) between them. In mounting, full use of the space available should be made (to reduce the number of cuts required) and the ratio of height to width should correspond to that of a journal page (4¾ × 7½ in.); however, allowance must be made for the captions. Photographs or groups of photographs should not be more than 2 or 3 times the size of the desired reproduction.

Photographs are to be submitted in duplicate; if they are to be reproduced in groups one set should be mounted, the duplicate set unmounted.

Reprints

A total of 50 reprints of each paper, without covers, are supplied free. Additional reprints, with or without covers, may be purchased.

Charges for reprints are based on the number of printed pages, which may be calculated approximately by multiplying by 0.6 the number of manuscript pages (double-spaced typewritten sheets, 8½ × 11 in.) and including the space occupied by illustrations. An additional charge is made for illustrations that appear as coated inserts. The cost per page is given on the reprint requisition which accompanies the galley.

Any reprints required in addition to those requested on the author's reprint requisition form must be ordered officially as soon as the paper has been accepted for publication.

Contents

Printed in Canada *by* University of Toronto Press